2004

Modeling and Simulation of an Industrial Furnace with Flue Gas Recirculation for NOx Control

Qing Jiang
Western University

Modeling and Simulation of an Industrial Furnace with Flue Gas Recirculation for NOx Control

By

Qing Jiang

Department of Mechanical and Materials Engineering
Faculty of Engineering

Submitted in partial fulfillment of
the requirements of the degree of
Master of Engineering Science

Faculty of Graduate Studies
The University of Western Ontario
London, Ontario
January 2004

ABSTRACT

This thesis reports research work carried out to construct on-line real-time dynamic feedback controllers that will reduce the NOx emission in an industrial furnace. The work began with a detailed analysis of the mechanisms for NOx formation. Based on the knowledge gained, a low NOx furnace was designed using CFD modeling techniques to optimize the furnace configurations. The arrangement of the mixing box for recirculated flue gas and fresh air has been determined using numerical simulations. The research has shown that flue gas recirculation (FGR) is an effective way to reduce NOx.

To gain a better understanding of the dynamic characteristics of the furnace, the sensitivity of the furnace to the variations of different furnace inputs has been evaluated in the frequency domain by superimposing sinusoidal signals onto the following three furnace inputs: combustion air flow rate, combustion air temperature, and the pressure head of the recirculation fan. The furnace outputs considered were the mole fraction of NOx and the mass fraction of oxygen.

Frequency domain based system identification techniques have been used to convert the frequency responses to a set of transfer function representations in an effort to facilitate the control system design. Four transfer functions have been constructed and the accuracy of these transfer functions are further evaluated by means of CFD simulations. It was concluded that these transfer functions can indeed provide an accurate representation of the dynamic behaviours of the furnace around given operating conditions.

To ensure that the furnace operates around the designed operating conditions most favourable to NOx minimization under various disturbances or uncertainties, possible regulation of the furnace inputs through feedback control has been investigated. Based on the knowledge gained of the dynamic relationships between the furnace inputs and outputs, a control system composed of one PID and two PI controllers has been synthesized by using nonlinear optimization techniques. The performance of the closed-loop control system has been evaluated based on both the linear models and full-scope nonlinear CFD models. In both cases, satisfactory results have been obtained. The main contribution of the thesis was to develop a methodology for the design and analysis of feedback control based NOx reduction technologies for industrial furnaces.

ACKNOWLEDGEMENTS

The author wishes to express his appreciation to professors Chao Zhang and Jin Jiang for their guidance and support during his graduate study. Their patience, encouragement, and continued guidance were very important for the author.

Appreciation is also extended to Dr. Youmin Zhang for his suggestions and helpful discussions on the control model.

The author would like to express his sincere appreciation to the Imperial Oil Research Foundation for the financial support that made the work reported in this thesis possible.

TABLE OF CONTENTS

LIST OF FIGURES

LIST OF TABLES

NOMENCLATURE

Symbol	Description
A , A_i	Constant
a_0 , a_1 ,a_2 ,a_3, a_4 , a_5 , a_6	Coefficients
B , B_i	Constant
b_0 ,b_1 , b_2 , b_3 , b_4 , b_4 ,b_6	Coefficients
C_1	Constant in turbulent model
C_2	Constant in turbulent model
C_d	Constant in turbulent model
C_g	Constant in turbulent model
C_μ	Constant in turbulent model
E_1	Accumulated error of the input of oxygen concentration
E_2	Accumulated error of the input of NOx emission
e_1	Transient error of the input of oxygen concentration
e_2	Transient error of the input of NOx emission
f	Mixture fraction
f_{O2}	Mass fraction of O_2 at the outlet of the furnace
$\bar{f}$	Mean mixture fraction
$\bar{f'^2}$	Mean mixture fraction variance
G	Gain to build transfer function

G_k	Generation of turbulence kinetic energy due to mean velocity gradients
$G(s)_{air\ mass}$	Transfer function from mass flux of combustion air to NOx
$G(s)_{air\ temp}$	Transfer function from the temperature of combustion air to NOx
$G(s)_{fan}$	Transfer function from the pressure head of the fan to NOx
$G(s)_{O2}$	Transfer function from mass flux of combustion air to O_2
h	Convective heat transfer coefficient, [$W/m^2.K$]
h	Static enthalpy, [J/kg]
k	Turbulence kinetic energy
k_i	Chemical reaction constant of i spice, [$m^3 mol^{-1} s^{-1}$]
m_{air}	Air mass flux sinusoidal shift, [$kg/m^2.s$]
m_{fuel}	Mass flow of fuel, [kg/s]
$(m_{air})_{inlet}$	Air mass flux inlet, [$kg/m^2.s$]
PID_1	The controller of oxygen to air mass flux
PI_2	The controller of NOx to air temperature
PI_3	The controller of NOx to pressure head of FGR fan
P_{fan}	Pressure head sinusoidal shift, [Pa]
(P_{fan})	Pressure head of the FGR fan, [Pa]
S_h	Sources of enthalpy due to chemical reaction and radiation, [J/kg]
T	Gas local temperature, [K]
T_{air}	Air temperature sinusoidal shift, [K]

$(T_{air})_{inlet}$	Air temperature inlet, [K]
t	Time, [s]
u_i , u_j	Mean gases velocity components, [m/s]
u_i' , u_j'	Fluctuating air velocity components, [m/s]
u_{max}	Maximum input variable
u_{min}	Minimum input variable
u_o	Input variable at steady operating point
x_i	Coordinate in x, y, z directions, [m]
Y_{NO}	NO mass fraction
y_{max}	Maximum output variable
y_{min}	Minimum output variable
y_{NO}	NOx mole fraction at the outlet of the FGR furnace, [ppm]
y_o	Output variable at steady state operating point
Z_k	Elemental mass fraction for some element, *k*
Z_{kO}	The mass fraction of element *k* at oxidizer inlet
Z_{kf}	The mass fraction of element *k* at fuel inlet

Greek Alphabet

α	Gas absorption coefficient
ε	Dissipation rate of k

ε	Gas radiation emissivity
ω	Frequency, [Rad/s]
μ	Kinematic coefficient of viscosity, [m^2/s]
μ_t	Turbulent viscosity, [m^2/s]
ρ	Density of gases, [kg/m^3]
$\sigma_k, \sigma_\varepsilon, \sigma_h, \sigma_t$	Turbulent Prandtl numbers

CHAPTER ONE

Introduction

1.1 Background and Motivation

Air pollution is a serious problem in modern society. Environmental protection has become a societal responsibility. NOx emission, which is a collective name for NO and NO_2, is a major air pollution source. NOx not only causes nitric acid rain, but also forms ground-level ozone in the stratosphere. It is estimated that over 95 percent of all man-made NOx is produced by the combustion of various fuels in the industrial process [1]. The degeneration of air quality prompts the governments of many countries to establish stricter standards to limit the amount of NOx released without penalty. According to the Canadian Environment Quality Guidelines [2], the release of NOx should not exceed the following limits for a furnace or boiler.

Less than 400-1000 $\mu g/m^3$ (NOx/Flue gas) in a consecutive hour;

Less than 200-300 $\mu g/m^3$ (NOx/Flue gas) in 24 consecutive hours;

Less than 60-100$\mu g/m^3$ (NOx/Flue gas) in a consecutive year.

The development of effective ways to reduce NOx emission in combustion processes in order to meet the strict limitations placed on industry has become extremely important. Flue gas recirculation (FGR) is an effective way to reduce NOx emission for standard industrial furnaces. However, FGR furnaces work at a low excess oxygen concentration. A slight drift from the operating point could result in a significant increase in the amount of NOx emission. Therefore, it is necessary to develop an effective control system for FGR furnaces to provide tight control on the operating conditions.

The main objective of this thesis is to use a novel approach to develop a real time feedback control system for a FGR industrial furnace to reduce NOx emission. Although many emission monitor systems have been developed to monitor the combustion process in industrial furnaces, few studies have been published on the use of information from an emission monitor system for real-time NOx emission control. The reason for this situation is that the significant time delay exists in NOx measurement. Recently, new sensitive NOx analyzers have been developed and the dead time has been reduced to less than one second. This thesis reports on pioneering research in the development of real-time feedback and online NOx emission controllers for FGR furnaces.

In order to achieve the main objective, a set of sub-objectives has been completed in the following chapters. A simplified FGR furnace is designed and optimized in Chapter 2 by the results of CFD simulation at an operating point. The input/output relationships of the FGR furnace have been investigated by superimposing sinusoidal signals of different frequencies on the furnace inputs. In Chapter 3, a set of dynamic models in the form of transfer functions has been constructed and validated based on the data acquired in Chapter 2. Finally, the PI and PID controllers for the FGR furnace have been designed and optimized by using the nonlinear least squares method in Chapter 4.

1.2 Literature Review

1.2.1 The mechanism of NOx formation

The formation of NOx can be classified into three distinct chemical kinetic processes: thermal NOx, prompt NOx, and fuel NOx. Thermal NOx is formed by oxidation of nitrogen in the combustion air at a relatively high temperature in a fuel-lean environment. It strongly depends on the flame temperature. Prompt NOx is produced by a high-speed reaction at the flame front, and fuel NOx is produced by oxidation of nitrogen contained in the fuel. Since the amount of nitrogen in liquid or gas fuels is very minimal, the prompt NOx is very low [3]. Therefore, only thermal NOx is considered in this research.

NOx includes the mixture of NO and NO_2. Both NO and NO_2 are formed during a combustion process. Generally, NO_2 concentration is negligible compared with NO concentration. It is usually considered as a transient intermediate species that exists only at flame conditions, and it can subsequently be converted back to NO in the post-flame region. Therefore, the research of thermal NOx formation usually refers to the thermal NO formation.

The original formation and verification of the thermal NOx mechanism is attributed to Zeldovich [4, 5], who studied the explosion of gases within a combustion bomb. Hanson and Salimian [6] suggested the use of the extended Zeldovich mechanism to determine the formation of thermal NOx. Thermal NOx comes from the oxidation of molecular nitrogen in the combustion air. The concentration of O atoms in flames grows with temperature due to the dissociation processes of oxygen. If the temperature is high enough, O atoms attack N-N chemical bonds in the direct high activation energy process.

$$O + N_2 \overset{k_{\pm 1}}{\leftrightarrow} N + NO \tag{1.1}$$

The N atoms react quickly with O_2 to regenerate O atoms by:

$$N + O_2 \overset{k_{\pm 2}}{\leftrightarrow} O + NO \tag{1.2}$$

This reaction is known as the Zeldovich mechanism. The concentration of NO is further increased by a radical-radical reaction:

$$N + OH \overset{k_{\pm 3}}{\leftrightarrow} H + NO \tag{1.3}$$

in which the rate constants are given by:

$$k_1 = 1.8 \times 10^8 \exp(\frac{-38370}{T})$$
$$k_{-1} = 3.8 \times 10^7 \exp(\frac{-425}{T})$$
$$k_2 = 1.8 \times 10^4 T \exp(\frac{-4680}{T})$$
$$k_{-2} = 3.8 \times 10^3 T \exp(\frac{-20820}{T})$$
$$k_3 = 7.1 \times 10^7 \exp(\frac{-450}{T})$$
$$k_{-3} = 1.7 \times 10^8 \exp(\frac{-24560}{T})$$

The unit of all the rate constants is $m^3 mol^{-1} s^{-1}$. The rate of the NO formation in these reactions is very sensitive to temperature and radical concentrations. Thus, the thermal NO is formed mostly in the flame regions with higher temperatures. The actual thermal NO usually is a little higher than the calculated one if radical concentrations exceed their equilibrium values, which often happens in flame fronts. More thermal NO can be formed under fuel-lean conditions because oxygen concentration affects thermal NO formation.

Based on the quasi-steady state assumption for N concentration, the net rate of NO formation via the above reactions can be determined by

$$\frac{d[NO]_T}{dt} = 2[O][N_2]\left[1-\frac{k_{-1}k_{-2}[NO]^2}{k_1k_2[N_2][O_2]}\right]\Big/\left[1+\frac{k_{-1}[NO]}{k_2[O_2]+k_3[OH]}\right] \quad \text{mol m}^{-3}\text{ s}^{-1} \qquad (1.4)$$

where $k_{\pm i} = A_i T^{B_i} \exp(-C_i/T)$. The reaction constants A_i, B_i, and C_i are taken from Hanson and Salimian [6].

The concentration of OH in the third reaction in the extended Zeldovich mechanism is given by [7, 8]:

$$[OH]=2.129\times10^{2}T^{-0.57}exp(-4595/T)[O]^{0.5}[H_2O]^{0.5} \quad \text{mol/m}^3 \qquad (1.5)$$

To determine the O radical concentration, a partial equilibrium approach [9] is used:

$$[O] = AT^B[O_2]^{1/2}\exp(-C/T) \quad \text{mol/m}^3 \qquad (1.6)$$

where $A=36.64$, $B=0.5$ and $C=27123$.

1.2.2 Methods to reduce NOx formation

According to the Zeldovich mechanism, the formation of thermal NOx is sensitive to flame temperature and concentration of O_2 in the flame envelope. Therefore, a number of combustion control techniques used to reduce thermal NOx emissions are based on the following three general principles: (1) lower temperature, (2) lower oxygen concentration in the flame envelope, and (3) reduced residence time at peak temperature. Recently developed techniques to achieve the above conditions are described as [10]:

(1) Flue gas recirculation (FGR): Relatively cool flue gases are recirculated back into the flame envelope. Relative to the combustion flame in the furnace, flue gases are cooler. Recirculation of these gases back into the flame dilutes the concentration of O_2 in the flame envelope, enlarges the flame envelope, and reduces the peak flame temperature.

(2) High excess air ratio: The furnace operates at a high excess air ratio to reduce the peak flame temperature. However, this also reduces furnace efficiency.

(3) Staged air injection: Combustion air is injected into the furnace at different stages. Approximately 60 to 70% of the theoretically required combustion air is injected into the first zone in which all the fuel is partially combusted. This fuel-rich combustion reduces NOx because of the low oxygen concentration. The rest of the combustion air is injected into the second zone to oxidize the residual fuels. Peak flame temperatures are lowered in both zones, which in turn reduce the NOx emission.

(4) Staged fuel injection: A portion of the fuel is injected into the combustion air and burned in the first combustion zone. The NOx generation rate is low at lower flame temperatures. The remainder of the fuel is injected downstream from the first zone. NOx emission from the secondary combustion zone is suppressed due to the diluted oxygen concentration.

Generally speaking, an air-staged low NOx burner can reduce NOx emission by approximately 30 to 50% compared to a conventional burner. A fuel-staged low NOx burner can lower NOx emission to one third of that generated by a conventional burner. Some high excess air burners can achieve even better results [10]. However, the high level of excess air reduces the efficiency of the furnace. Also, air and fuel staged low NOx burners tend to have longer and narrower flames than standard burners. This will have impact on the size of the furnace.

A common method used to reduce thermal NOx emission in a combustion system is flue gas recirculation (FGR) [10]. This technique shows that a portion of the flue gases is fed back by a circulation fan and mixed with the fresh combustion air before entering the furnace. A heat recovery device is commonly used to cool down the flue gases. Otherwise, the temperature of the flue gases would be too high for the fan. With FGR, NOx formation is suppressed due to the two mechanisms. First, the peak flame temperature is reduced due to the larger mass of gases to be heated. Second, the oxygen concentration in the flame envelope is lowered due to the low oxygen concentration in the recirculated flue gases. Lowering the peak flame temperature has a dominant effect on NOx reduction. The amount of the flue gas recirculation is limited by the combustion stability of the burner at the low oxygen concentration condition. If the rate of flue gas recirculation reaches 30%, the NOx output will be at a very low level. However, it will cause flame instability and limit the performance of the furnace and boiler [11]. FGR is usually limited to 20% for natural gas and from 10 to 12% for oil-fired furnaces [12]. NOx reduction can vary from 45 to 80% at the high recirculation rates. FGR can be achieved by performing external or internal recirculation of flue gases. The internal recirculation of flue gases takes place at the burner where intensive air-swirling occurs. The rate of flue gas recirculation depends on the combustion air swirl number. The internal recirculation in jet flames has been realized by the low NOx burners of FLOX (flame lose oxidation) and GAFT (gas dynamic abated flame temperature) [13]. An external fan and a damper can be used to control the amount of flue gas recirculation to achieve external recirculation. Moloney [14] reported that FGR could reduce the particulate emissions and improve the evaporation rate of an industrial boiler. It is demonstrated that the NOx reductions are achieved by FGR without detrimental combustion effects to the furnace with regards to load, pulsation, vibration, or excessive temperatures [15]. Potentially, FGR also offers an inexpensive alternative compared with other more costly approaches, such as selective catalytic and non-catalytic reduction methods. It was also found that the use of FGR could reduce the CO emission from a furnace [11]. Clearly, FGR is an effective way to reduce NOx emission.

In this work, only an external flue gas recirculation scheme is considered since most of industrial furnaces are still equipped with conventional burners, and it would be easier to retrofit an existing furnace with an external recirculation mechanism.

1.2.3 Active combustion control

FGR furnaces work only at a low excess oxygen concentration. A small drift from the original operating point could cause a significant increase in NOx emission. Figure 1.1 shows that the output of thermal NOx triples while the concentration of O_2 in the flue gas varies from 1.5% to 5% [10]. The flow rate of recirculating flue gases is also sensitive to the fluctuations of combustion airflow rate [11]. Therefore, monitoring systems have been developed to monitor different types of combustion processes, including continuous emission monitors (CEMS) and predictive emission monitors (PEMS) [16, 17, 18, 19].

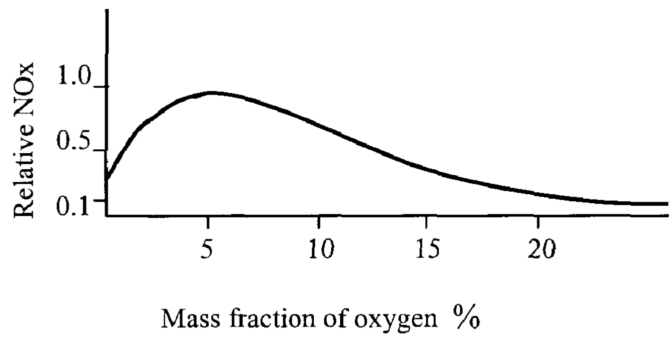

Fig. 1.1 Excess oxygen concentration vs relative NOx emission [10]

However, these monitoring schemes have not been used effectively for real-time closed-loop control purposes. One of the reasons for this is the lack of knowledge of dynamic relationships between a furnace's inputs and its emissions. Recently, stronger efforts have been made to gain a better understanding as to how a furnace behaves in a dynamic environment. A combustion process is a very complicated nonlinear process. It is almost impossible to deduce the relationships between input variables and output variables mathematically based on fluid flow, heat transfer and combustion models. Among existing published work, Matsumura [20] built a multi-input and multi-output model to describe the relationship between the NOx concentration in the flue gases and the furnace input variables. This model was obtained through a recursive least squares method.

Another obstacle the real-time control encounters is the time delay associated with the NOx measurement. A control system with a feed forward term was adopted to overcome this problem [21]. The precise prediction of this measurement delay is a prerequisite for such a control system as it is based on the prediction of the current NOx concentration. In recent years, the measurement delay seems to have become less of a problem due to advances in sensor technology [22]. Several manufacturers have announced that they have successfully developed sensitive NOx analyzers using the chemiluminescent method. The measurement delay could be reduced to less than one second and the minimum detectable concentration is as low as 0.02 ppm. This is encouraging news for control engineers, and now is the right time to develop an effective real-time combustion control system for combustion processes.

Preliminary studies have concluded that real-time feedback control is particularly desirable for optimizing combustion processes, alleviating combustion instabilities, and most of all, reducing the emission of pollutants such as NOx, CO, etc. [23]. The basic approach of Active combustion control (ACC) is to measure the appropriate furnace variables in real-time and feed such information back to controllers to regulate the furnace inputs accordingly. Depending on the dynamic properties of the combustion processes, the combustion control system can adjust its outputs automatically to meet the desired furnace performance requirements. The performance may include such items as flame stability, range of temperature variations, fuel efficiency, and emission levels. In the current study, the emphasis is placed on the reduction of NOx emission. Comprehensive coverage of NOx control techniques can be found in three excellent survey papers [24, 25, 26].

1.2.4 Computational fluid dynamics (CFD) simulations

CFD modeling has found increasing use in the design and evaluation of utility furnaces, combustion optimization and NOx reduction technologies [27, 28, 29, 30, 31]. This procedure has the following merits: (1) there is no need to build an experimental furnace at an early stage of investigation; (2) it is easy to test different furnace configurations; (3) it is easy to change the input variables; (4) it is easy to realize some particular combustion process that is difficult in the form of practical experiments.

1.3 Methodology

The relationships between the furnace inputs and outputs need to be established to design an effective control system. Once such relationships exist, the desirable feedback control law can be developed to achieve the specified system performance. Detailed relationships between the furnace inputs and outputs will be built and optimal control system can be designed for an industrial furnace with flue gas recirculation (FGR).

Instead of experimental measurement, a CFD simulation is conducted for the combustion process in the FGR furnace. CFD plays two major roles in the current investigation: (1) it provides detailed input and output data based on which the linearized furnace control model can be constructed; and (2) it validates the performance of the designed controller under a realistic nonlinear furnace operating conditions. The FGR model furnace created in this study is a simplified FGR furnace that has the characteristics of flow and combustion of a furnace. The model furnace is optimized according to the numerical results acquired at steady operating conditions.

The transient input and output data at different frequencies are used to determine the gain and time delay. A least squares method is employed to optimize the frequency response transfer functions between the inputs and outputs. A nonlinear optimization method is used to design the PI (Proportional-Integral) and PID (Proportional-Integral-Derivative) controllers. To verify the validity of these dynamic models and controllers, the responses generated from these dynamic models and controllers are compared with those obtained from the numerical solutions by CFD simulations.

1.4 Outline of This Thesis

This thesis is divided into five chapters. Chapter 1 describes the motivation, methodology, research background and literature review, as well as highlights of the contributions. Chapters 2, 3, 4 are composed of three papers submitted to journals. In Chapter 2, a simplified FGR model furnace is obtained based on CFD simulations. Numerical simulations are conducted for the furnace. The NOx emission and combustion profiles at the steady state are acquired. Finally, the transient relationships between the NOx emissions and the furnace input variables, such as the inlet combustion air mass flow rate, inlet combustion air temperature, and the pressure head of the FGR fan, are investigated. Chapter 3 concentrates mainly on the development of dynamic models based on frequency response tests, which are suitable for online and real-time feedback control to reduce NOx emissions from FGR furnaces. These models are verified by comparing the responses generated from these models with those obtained from the numerical solutions using CFD. In Chapter 4, the control strategy for NOx reduction is discussed. The controllers are designed using the nonlinear optimization method. In order to verify the performance of the controllers, the signal just behind the PID controller is extracted as an input boundary condition for the model furnace in CFD simulations. The transient NOx output is then compared with the solutions in the simulation of dynamic reactions. Chapter 5 contains the conclusions of this thesis work.

1.5 Contributions of This Thesis

The research reported in this thesis contains some pioneering work across the disciplines of fluid dynamics, combustion and linear control system technologies. The main contributions can be summarized as follows:

1. A FGR furnace has been designed. Its NOx emission is only 17% of the standard furnace. An optimal arrangement of the mixing box and the optimal direction of fuel injection are suggested.
2. The sensitivity of the furnace has been investigated using frequency response technologies.
3. The transfer functions representing the furnace input and output relationships are obtained.
4. The optimal design of furnace controllers has been carried out. The performance of the controllers has been validated using CFD simulation studies.

References

1. Hayhurst, A. N. and Vince, I. M., "Nitric Oxide Formation From Nitrogen Flames", Progress in Energy and Combustion Science, vol. 6(1), pp. 35-51, 1980.
2. Page 7, Canadian Environment Quality Guidelines www.ccme.ca, 2003.
3. Ishii, T., Zhang, C. and Sugiyama, S., "Effects of NO Models on the Prediction of NO Formation in a Regenerative Furnace", ASME Trans. Journal of Energy Resources Technology, Vol.122, pp.224-228, 2000.
4. Zeldovich Ya. B., Sadovnikov, P. Ya. and Frank-Kamenetski, D. A., The oxidation of Nitrogen during combustion, Izd-vo AN SSSR, 1974.
5. William C. Gardiner, Jr., Combustion Chemistry, Springer-Verlag. 1984.
6. Hanson, R. K. and Salimian, S., "Survey of Rate Constants in H/N/O System", Combustion Chemistry, 1984.
7. D.L. Baulch; Cobos, C. J.; Cox, R. A.; Frank, P.; Just, T.; Kerr, J. A.; Philling, M. J.; Froe, J., "Evaluated Kinetic Data for Combustion Modeling", J. Physical and Chemical Reference Data, 21(3), pp.411-734, 1992.
8. C. Westbrook and F. Dryer, "Chemical Kinetic Modeling of Hydrocarbon Combustion". Progress in Energy and Combustion Science. Vol. 10, No. 1, pp. 11-19, 1984.
9. Warnatz, J., "NOx Formation in High Temperature Processes", Proc. European Gas Conference, pp. 303-320, 1991.
10. Lewandowski D. A., Design of Thermal Oxidation System for Volatile Organic Compounds. Lewis Publishers. 2000.

11. Dehann T. E., "Cost, Safety and Performance Issues Associated with Ultra Low NOx Burners", Proceedings of 1996 International Joint Power Generation Conference, vol. 30, pp. 823-824, 1996.

12. Tompkins G., "Flue-gas Recirculation Works for Packaged Boilers", Power, vol. 134, pp. 11-12, April 1990.

13. Jomeczek, J.; Goral, J. and B., Gradon, "The GAFT Burner for Reducing NOx in Gas-fired High-temperature Industrial Furnaces", Journal of the Institute of Energy, 58, pp. 178-183, 1995.

14. Maloney, K. L., "Flue Gas Recirculation for Stoker Boiler", Industrial Power on the Rebound. Presented at the 1986 Industrial Power Conference, vol. 1, pp. 77-82, 1986.

15. Bell, Colin T. F. and Warren S., "Experience With Burner NOx Reduction", Hydrocarbon Processing, vol. 62, no. 9, pp. 145-147, 1983.

16. Chakravarthy, S. S. S.; Vohra, A. K. and Gill, B. S., "Predictive Emission Monitors (PEMS) for NOx Generation in Process Heaters", Computers and Chemical Engineering, vol. 23, pp. 1649-1659, 2000.

17. Cooper, D. A. and Andreasson, K., "Predictive NOx Emission Monitoring on Board a Passenger Ferry", Atmospheric Environment, vol. 33, pp. 4637-4650, 1999.

18. Croy, R. L., Simpson, C. W., Tipton, D. B., Sinha, P., Lashier, M. E., "NOx PEMS Experience on Operating Ethylene Furnaces", Environmental Progress, vol. 16, No. 4, 1997.

19. Cheng, A. M. and Hagen, G. F., "An Accurate Predictive Emissions Monitoring System (PEMS) for an Ethylene Furnace", Environmental Progress, vol. 15, No. 1, 1996.

20. Matsumura, S.; Ogata, K.; Fujii, S.; Shioya, H. and Nakamura, H., Modeling and DeNOx Control System for Fossil-fuel-fired Power Plants, IFAC Control of Power Plants and Power Systems, pp. 19-24, Cancun, Mexico, 1995.

21. Henrike C. Krijnsen, Wijnand E. J. van Kooten, Hans Peter A. Calis and Cor M. van den Bleek, "Reductant Flow Control for NOx Removal From Lean Exhaust Gases", The Canadian Journal of Chemical Engineering, vol. 79, pp. 3-17, 2001.

22. www.k2bw.com, 2003.

23. Delabroy, O., Haile, E., Lacas, F., Candel, S., Pollard, A, Sobiesiak, A., and Becker, H. A., "Passive and Active Control of NOx in Industrial Burners", Experimental Thermal and Fluid Science, 16, pp. 64-75, 1998.

24. Docquier, N. and Candel, S., "Combustion Control and Sensors: A Review", Progress in Energy and Combustion Science, 28, pp. 107-150, 2002.

25. Muzio, L. J. and Quartucy, G. C., "Implementation NOx Control: Research to Application", Progress in Energy and Combustion Science, 23, pp. 233-266, 1997.

26. Krijnsen, H. C.; Wijnand, E. J. van Kooten; Hans, Peter, A. Calis and Cor, M. Van den Bleek, "Reductant Flow Control for NOx Removal From Lean Exhaust Gases", The Canadian Journal of Chemical Engineering, vol. 79, pp. 3-17, 2001.

27. Falcitelli, M.; Pasini, S.; Tognotti, L., "Modelling Practical Combustion Systems and Predicting NOx Emissions with an Integrated CFD Based Approach", Computers and Chemical Engineering, vol. 26, NO. 9, pp. 1171-1183, 2002.

28. Adams, B.; Cremer, M.; Valentine, J.; Bhamidipati, V.; O'Connor, D.; Vierstra, S.; Letcavits, J.J., "Use of CFD Modeling for Design of NOx Reduction Systems in Utility Boilers", Proceedings of the 2002 International Joint Power Generation Conference, pp. 695-702, 2002.

29. Ilbas, M., Bowen, P., O'Doherty, T., and Syred, N., "CFD Modelling of a Low NOx Combustor Fired by Natural Gas and Gas-oil", Proc. of Conference on Combustion & Emission Control, London, UK, pp. 189- 198, 1995.

30. Fiveland, W. A. and Laitham, C. E., "Use of Numerical Modeling in the Design of a Low-NOx Burner for Utility Boilers", Proc. of Combustion Technologies for a Clean Environment (ed. By Maria da Graça Carvalho), pp. 111-130, 1995.

31. Zhang, C., Ishii, T., Hino, Y. and Sugiyama, S., "The Numerical and Experimental Study of Non-premixed Combustion Flames in Regenerative Furnaces", ASME Trans. Journal of Heat Transfer, 122, pp. 287-293, 2000.

CHAPTER TWO[1]

An Investigation of the Correlations of Inputs/Outputs of a FGR Industrial Furnace with CFD Simulation Method

2.1 Introduction

The emission of NO and NO_2, collectively known as NOx, is known to be one of the leading causes of a variety of health-related problems. The emission of NOx from combustion processes in industrial furnaces and boilers is a major pollutant source in our environment. It is estimated that over 95 percent of all man-made NOx that enters the atmosphere is produced by combustion of various fuels [1]. Due to stringent environmental laws and a sense of responsibility to future generations, it becomes increasingly important to find new ways to cut down on combustion-generated NOx emissions. According to the Canadian Environment Quality Guidelines [2], the release of NOx should not exceed the following limits for a furnace or a boiler: 400-1000 $\mu g/m^3$ (NOx/Flue gas) in an occasional hour, 200-300 $\mu g/m^3$ (NOx/Flue gas) in 24 consecutive hours and 60-100$\mu g/m^3$ (NOx/Flue gas) in one consecutive year. One solution to reduce NOx emission is to use innovative technology to optimize furnace operating conditions.

Both NO and NO_2 are formed during a combustion process. Generally, NO_2 concentration is negligible compared with NO concentration. It is usually considered as a transient intermediate species existing only at flame conditions that is subsequently converted back into NO in the post-flame region. In gas- or oil-fired industrial furnaces,

[1] Work contained in this chapter was submitted to ASME J. of Energy Resources Technology in August, 2003.

the major portion of NO generated is the thermal NO. The prompt NO and reburning NO are usually in a very small quantity [3]. Thus, only the thermal NO is considered in this work. It is well known that the formation of the thermal NO can be determined by the extended Zeldovich mechanism [4], which indicates that the formation of NO depends strongly on the flame temperature and the concentration of oxygen (O_2) in the flame envelope. A number of combustion control strategies based on this knowledge have been developed to reduce the thermal NO emission by limiting the following variables: (1) the peak temperature of the flame envelope; (2) the oxygen concentration in the flame envelope; and (3) the residence time at the peak temperature [5]. An effective technique to reduce the thermal NO formation is to use FGR, where a portion of the exhaust gases at the furnace outlet is fed back to the furnace inlet to mix with the fresh combustion air before entering the furnace. A heat recovery device is commonly used to cool down the flue gases before this mixing process befins. The main effects of such flue gas recirculation are to dilute the O_2 concentration in the flame envelope, enlarge the flame envelope, and reduce the peak flame temperature. Lowering the peak flame temperature has a major effect on the amount of NO formed. The amount of flue gas recirculation is limited by the combustion stability of the burner at low oxygen concentration conditions. Typically, it is limited to 20% for gas-fired furnaces and 10~12% for oil-fired ones. NO can be reduced by 45% to 80% at high recirculation rates. Clearly, FGR is an effective NO emission reduction technique. Potentially, it offers an inexpensive alternative to other more costly approaches such as selective catalytic reduction, non-catalytic reduction, etc. Tompkins [6] also reported that the use of the FGR could also reduce the CO emission from a furnace.

The FGR can be achieved through either external or internal recirculation of flue gases. Internal recirculation of flue gases occurs at burners where intensive air swirling exists. The rate of internal flue gas recirculation depends on the combustion air swirl number. Successful applications of the internal recirculation were realized by the flame loss oxidation and gas-dynamic abated flame temperature burners [7]. To achieve external recirculation, an external fan and a damper could be used to control the amount of flue gas recirculation. Only an external flue gas recirculation scheme is considered in this paper since most industrial furnaces are still equipped with conventional burners, and it would be easier to retrofit an existing furnace with an external recirculation mechanism.

The FGR is an effective way to reduce NO emission. The NO emission is also sensitive to other furnace input variables, especially the combustion air mass flow rate. In practice, FGR furnaces usually operate at a low excess oxygen concentration. A slight variation in the operating conditions could result in a significant change for NOx emission. The flow rate of the recirculated flue gases is also sensitive to the fluctuation of the inlet combustion air mass flow rate [6]. Therefore, it is imperative to have accurate knowledge about how NO is affected by all the controllable furnace inputs before any active combustion control system can be designed. Such relationships are generally dynamic in nature and are best represented in the frequency domain. The objective here is to determine such relationships through numerical simulations guided by clear physical intuition.

The study concludes that the combustion air mass flux is the most sensitive variable for NOx emission. Particular attention should be paid in the design of the combustion control system. Other input variables, the temperature of the combustion air and the pressure head of the FGR fan have relatively fewer effects. The results of this investigation are of significant value to the understanding of the dynamic relationships between furnace input variables and NOx emission at the furnace output, and they also provide important information for combustion control system design.

This chapter is organized as follows: In Section 2.2, a brief description of the furnace and its operating conditions is provided. Mathematical modeling of the combustion process as well as NOx model is covered in Section 2.3. The procedure for numerical solutions is given in Section 2.4. The numerical results under normal operating conditions of the furnace are summarized in Section 2.5. The relationships between the NO emission and perturbations of the respective furnace inputs are shown in Section 2.6 and are followed by the conclusions.

2.2 Configuration and Operating Conditions of the FGR Furnace

The configuration of the FGR furnace used in this study is illustrated in Fig. 2.1. Its dimensions and the arrangement of the mixing box have been optimized based on the numerical simulation results. The dimensions of the furnace are $3.75\times1.4\times1.4$ m^3. The burner is located at the center of the left-hand sidewall and the exhaust outlet is at the center of the right-hand sidewall as shown in Fig. 2.1. A flue gas recirculation pipe 0.15 m in diameter is used to recirculate the flue gases back to the inlet of the furnace. The recirculation flue gases are extracted from the center of the top-right side of the furnace as shown in the figure. The dimensions of the mixing box at the inlet of the furnace are $0.3\times0.3\times0.8$ m^3. The combustion air and the recirculation flue gases enter the mixing box in the same direction so that the flue gases and the combustion air can be mixed symmetrically before entering the furnace to avoid any potential deviation of the flame in a particular direction inside the furnace. The stabilizer at the center of the right-hand side wall of the mixing box is simplified as a round plate 0.07 m in diameter based on the data given by Vahnati [8]. A diffuser with an inlet diameter 0.2 m and exit diameter of 0.35 m is used between the mixing box and the furnace as shown in Fig. 2.1. The fuel and gases are injected into the diffuser through a concentric pipe with an inner diameter of 0.07 m and outer diameter of 0.2 m. The fuel is injected through the center pipe and gases are injected through the annular area between the two pipes. Therefore, this is a non-premixed combustion process.

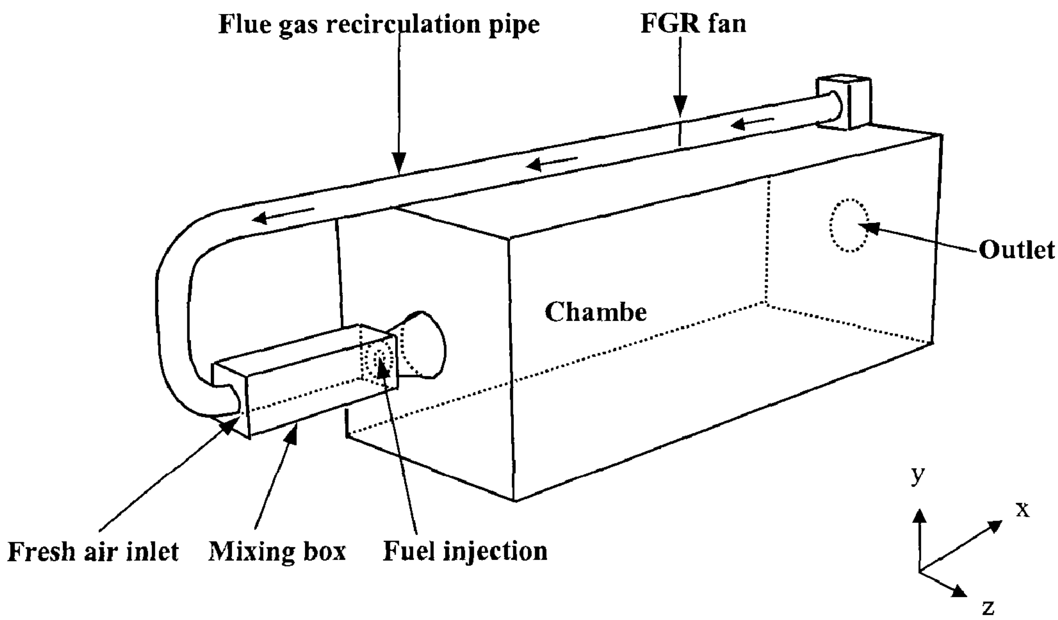

Figure 2.1 Configuration of the FGR furnace

Liquid propane is used as the fuel in the current study. The heat input to the furnace from the fuel is 345 kW. Other parameters under normal operating conditions are shown in Table 2.1. This is a reheating furnace where the bottom wall of the furnace is kept at a constant temperature of 1100 K. The heat output of the furnace is mainly through the bottom wall. Under normal operating conditions, the combustion air is preheated to 700 K before it enters to the furnace and the FGR mass flow rate is about 8.2% of the total gas mass flow rate entering the furnace. This value is less than the recommended one (10~12%) for liquid fuel. Therefore, a slight positive drift of the pressure head in the FGR fan will not blow away the flame from the stabilizer.

Table 2.1 Operating conditions of the furnace

Fuel (propane, C_3H_8)	Flow rate	0.0075 kg/s
	Temperature	300 K
	Heating value	345 kW
Input combustion air	Flow rate	0.135 kg/s (or 1.849 kg/m^2·s)
	Temperature	700 K (or 426.85°C)
Heat output	190 kW from the bottom of the furnace	
Pressure head of the FGR fan	33.8 Pa	
Flue gas recirculation rate	0.012 kg/s	
Temperature at the bottom wall	1100 K	
Temperature at the FGR pipe	700K	

2.3 Mathematical Models of the Combustion Process

2.3.1 Turbulent combustion model

For turbulent non-premixed combustion, if the chemical reaction is sufficiently fast and all species and enthalpy have equal diffusion coefficients, the instantaneous thermochemical state of the mixture will be a function of the instantaneous mixture fraction, f, which is defined as

$$f = \frac{Z_k - Z_{kO}}{Z_{kF} - Z_{kO}} \tag{2.1}$$

where Z_k is the element mass fraction for the element k. Subscripts O and F represent the values at the oxidizer and the fuel stream inlet, respectively.

In order to take into account of the dissociation that is important near stoichiometric conditions and intermediate species, the present combustion model is derived based on the assumption that the chemical reactions occur much faster with respect to the turbulent mixing time scale. Therefore, an instantaneous chemical equilibrium always exists. The instantaneous thermochemical state can be determined by minimizing the Gibbs free energy. Temporal fluctuations can be modeled by a PDF (possibility density function). The β-PDF [9, 10] is used in this work.

The turbulent combustion model includes the conservation equations of mass, momentum, energy, turbulence kinetic energy, dissipation rate of turbulent kinetic energy, mixture fraction and its variance. Density-weighted (Favre) averaging is utilized to account for the effects of density changes. The transient three-dimensional Favre-averaged conservation equations in Cartesian coordinates can be expressed as [9, 10]:

Continuity

$$\frac{\partial \rho}{\partial t} + \frac{\partial}{\partial x_i}\left(\tilde{\rho}\overline{u_i}\right) = 0 \tag{2.2}$$

where is ρ the density, x_i is the position vector, and u_i is the velocity vector. The variables with a bar are the Favre-averaged values. The variable with a tilde represents the Reynolds-averaged value.

Momentum

$$\frac{\partial}{\partial t}\left(\tilde{\rho}\overline{u_i}\right) + \frac{\partial}{\partial x_j}\left(\tilde{\rho}\overline{u_i}\,\overline{u_j}\right) = \frac{\partial}{\partial x_j}\left[\mu_e\left(\frac{\partial \overline{u_i}}{\partial x_j} + \frac{\partial \overline{u_j}}{\partial x_i}\right) - \left(\frac{2}{3}\delta_{i,j}\mu_e\frac{\partial \overline{u_l}}{\partial x_l}\right)\right] - \frac{\partial \tilde{P}}{\partial x_i} \tag{2.3}$$

where $\mu_e = \mu + \mu_t$, $\mu_t = \tilde{\rho} C_\mu \frac{k^2}{\varepsilon}$ and $C_\mu = 0.09$. P is the pressure, μ the molecular viscosity, and μ_t the turbulent viscosity. k and ε represent the turbulent kinetic energy and its dispassion rate, respectively.

Enthalpy

$$\frac{\partial}{\partial t}\left(\tilde{\rho}\bar{h}\right)+\frac{\partial}{\partial x_i}\left(\tilde{\rho}\overline{u_i h}\right)=\frac{\partial}{\partial x_i}\left(\frac{\mu_t}{\sigma_h}\frac{\partial \bar{h}}{\partial x_i}\right)+\overline{S_h} \tag{2.4}$$

where h is the static enthalpy and σ_h is the turbulent Prandtl number. S_h consists of sources of enthalpy due to chemical reaction and radiation, and $\sigma_h = 0.7$.

Turbulent kinetic energy and its dispassion rate

$$\frac{\partial}{\partial t}(\tilde{\rho}k)+\frac{\partial}{\partial x_i}\left(\tilde{\rho}\overline{u_i}k\right)=\frac{\partial}{\partial x_i}\left(\frac{\mu_t}{\sigma_k}\frac{\partial k}{\partial x_i}\right)+G_k-\tilde{\rho}\varepsilon \tag{2.5}$$

$$\frac{\partial}{\partial t}(\tilde{\rho}\varepsilon)+\frac{\partial}{\partial x_i}\left(\tilde{\rho}\overline{u_i}\varepsilon\right)=\frac{\partial}{\partial x_i}\left(\frac{\mu_t}{\sigma_\varepsilon}\frac{\partial \varepsilon}{\partial x_i}\right)+C_1\frac{\varepsilon}{k}G_k-C_2\tilde{\rho}\frac{\varepsilon^2}{k} \tag{2.6}$$

where

$G_k = \mu_t\left(\frac{\partial \overline{u_j}}{\partial x_i}+\frac{\partial \overline{u_i}}{\partial x_j}\right)\frac{\partial \overline{u_i}}{\partial x_i}$, $C_1 = 1.44$, $C_2 = 1.92$, $\sigma_k = 1.0$ and $\sigma_\varepsilon = 1.3$.

Mixture fraction and its variance

$$\frac{\partial}{\partial t}(\tilde{\rho}\bar{f})+\frac{\partial}{\partial x_i}\left(\tilde{\rho}\overline{u_i}\bar{f}\right)=\frac{\partial}{\partial x_i}\left(\frac{\mu_t}{\sigma_t}\frac{\partial \bar{f}}{\partial x_i}\right) \tag{2.7}$$

$$\frac{\partial}{\partial t}(\tilde{\rho}\overline{f'^2})+\frac{\partial}{\partial x_i}\left(\tilde{\rho}\overline{u_i}\overline{f'^2}\right)=\frac{\partial}{\partial x_i}\left(\frac{\mu_t}{\sigma_t}\frac{\partial \overline{f'^2}}{\partial x_i}\right)+C_g\mu_t\left(\frac{\partial \bar{f}}{\partial x_i}\right)^2-C_d\tilde{\rho}\frac{\varepsilon}{k}\overline{f'^2} \tag{2.8}$$

where $\overline{f'^2}$ is the variance of the mixture fraction, f, and $\sigma_t = 0.7, C_g = 2.86$ and $C_d = 2.0$.

As near wall boundary conditions, the values of k and ε at the first grid node are obtained using standard wall functions [11]. The discrete transfer radiation model [12, 13], which is relatively simple and can be applied to a wide range of optical thickness, is employed to calculate the radiation heat transfer. The assumption of gray radiation is acceptable for all inner surfaces of the furnace. The weighted-sum-of-gray-gases model [14, 15] is used to calculate the absorption coefficient.

The liquid fuel injection is modeled by a discrete phase model. The turbulent dispersion of liquid fuel droplets and other forces on the liquid fuel phase have been neglected because the liquid fuel droplets only last for a short period of time and exist only in a small region near the inlet of the furnace.

2.3.2 NO model

The rate of NO formation is much slower than the rate of main hydrocarbon oxidation. Therefore, it is reasonable to assume that the reactions involved in the NO chemistry can be separated from the main combustion reaction mechanism. The NO formation rates and NO concentrations can be calculated using a post processor based on previously calculated velocity, turbulence, temperature, and chemistry fields. The mean NO concentration is obtained by solving the transport equation based on the flow field and the combustion solution. The effect of residence time in NO mechanisms, a Lagrangian reference frame concept, is included through the convection terms in the governing equation represented in the Eulerian reference frame.

$$\frac{\partial}{\partial t}(\overline{\tilde{\rho} Y_{NO}}) + \frac{\partial}{\partial x_i}(\overline{\tilde{\rho} u_i Y_{NO}}) = \frac{\partial}{\partial x_i}\left(\tilde{\rho} D \frac{\partial \overline{Y_{NO}}}{\partial x_i}\right) + \overline{S_{NO}} \tag{2.9}$$

where Y_{NO} is the NO mass fraction and the source term, S_{NO}, is determined from different NO formation mechanisms. The thermal NO is considered in this study. The formation of thermal NO can be determined by the extended Zeldovich mechanism [4], i.e.

$$\begin{aligned} & O+N_2 \overset{k_{\pm1}}{\leftrightarrow} N+NO \\ & N+O_2 \overset{k_{\pm2}}{\leftrightarrow} O+NO \\ & N+OH \overset{k\pm3}{\leftrightarrow} H+NO \end{aligned} \tag{2.10}$$

Based on the quasi-steady state assumption for N concentration, the net rate of NO formation via the above reactions can be determined by

$$\frac{d[NO]_T}{dt} = 2[O][N_2]\left(1-\frac{k_{-1}k_{-2}[NO]^2}{k_1[N_2]k_2[O_2]}\right) \Big/ \left(1+\frac{k_{-1}[NO]}{k_2[O_2]+k_3[OH]}\right) \tag{2.11}$$

where $k_{\pm i}=A_i T^{B_i} exp\left(\frac{-C_i}{T}\right)$

The NO source term can be calculated from

$$S_{NO}=M_{NO}\left\{\frac{d[NO]_T}{dt}\right\} \tag{2.12}$$

where M_{NO} is the molecular weight of NO. In order to calculate the mean NO formation rate, $\overline{S}_{NO}$, which is required in the mean NO transport equation, the temperature PDF approach [16] is used to include the effect of turbulence on the NO formation. The mean NO formation rate can be determined by

$$\overline{S}_{NO}=\int S_{NO}(T)P(T)dT \tag{2.13}$$

where T is the temperature and $P(T)$ is the PDF. The shape of PDF is assumed to be in the form of a β- function.

2.4 Numerical Procedure

The fluid flow, heat transfer, combustion, and NOx formation processes in the furnace are simulated using a commercial software package FLUENT [17]. The control volume approach [18] is used in which a nonstaggered grid arrangement is employed to discretize the governing differential equations, Eqs. (2.2) to (2.8). The velocity and pressure fields are linked by the SIMPLE algorithm [18].

The convergence criteria are set at 6×10^{-7} for the residual of the energy equation and 4×10^{-5} for other equations. A grid independence test is carried out using non-uniform grid sizes 119,963 and 175,119. It is found that the results from these two grid sizes are very close. For example, the difference in the peak temperature is only 0.5%. Therefore, the grid 119,963 is selected for the numerical simulations.

The boundary conditions are specified based on the furnace operating condition listed in Table 2.1. The heat loss through the furnace walls excluding the bottom wall is assumed to be negligible.

2.5 Results Under the Furnace Normal Operating Conditions

Since the NOx emission from the furnace is very sensitive to how the fuel is injected into the furnace, the numerical simulations are performed for the furnace with different fuel injection angles under operating parameters specified in Table 2.1. The results of the analysis are shown in Table 2.2.

Table 2.2 Effect of the fuel injection angle

Case	Fuel injection angle (θ)	Peak flame temp. (K)	NOx (ppm)	O_2 Mass fraction	CO (ppm)	Heat output (kW)
0	0.0°	1976.0	74.9	0.0267	<1	190.0
1	5.7°	1980.7	79.9	0.0267	<1	190.2
2	11.3°	1996.7	101.2	0.0267	<1	190.7
3	16.7°	2064.9	202.5	0.0267	<1	196.1

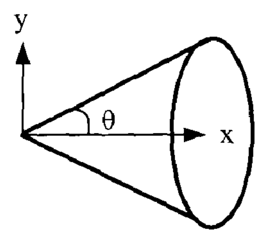

Figure 2.2 The cone angle of fuel injection

Cone injection is used to maintain a symmetrical flame in the furnace. The injection angle listed in Table 2.2 represents half the cone angle shown in Figure 2.2. The injection angle of 0° means that the fuel is injected into the furnace in the horizontal direction. It is noticed that the NO emission from the furnace increases as the fuel injection angle increases. This is because the chemical reactions are very fast and the turbulent dispersion becomes the dominant factor for the flame shape and volume. A divergent fuel injection, i.e. larger fuel injection angle, results in a quicker mix of the combustion air and the fuel. Consequently, a smaller and more intense flame envelope is created in the furnace, which results in a higher peak flame temperature and leads to a higher NO formation in the furnace. When the fuel injection angle changes from 0° to 16.7°, the peak flame temperature increases from 1976 K to 2065 K and the NO emission from the furnace is almost tripled as indicated in Table 2.2. The results in Table 2.2 clearly illustrate that the NO emission is very sensitive to the peak flame temperature. Furthermore, the results also indicate that the fuel injection angle does not affect the O_2 concentration at the furnace outlet. The CO concentrations are less than 1 ppm for all cases. Additionally, the heat output from the furnace increases slightly (<0.4%) when the fuel injection angle increases except for Case 3 where the heat output increases by 3%. A fuel injection angle of 0° is chosen for the rest of this work since the NOx emission is minimal at this fuel injection angle.

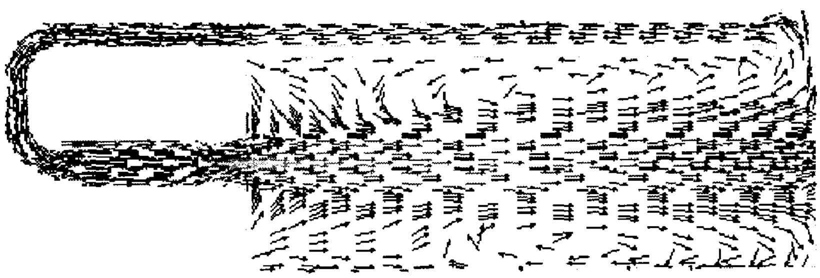

Figure 2.3 Velocity vector on the plane at z=0 m

The flow field on the horizontal plane at z = 0 m, which cuts through the center of the air and fuel injection pipes is presented in Fig. 2.3. It can be seen from the figure that the velocity distribution in the furnace is almost symmetrical along the central axis, x. This means that the extraction of a small amount of flue gases from the top-right side of the furnace has little effect on the main flow field. The air is injected into the furnace at a high velocity in the x-direction. Therefore, the main flow is in the x-direction. The velocity is very low outside of the main flow region. The figure shows that there are two recirculation zones located on each side of the central x axis in the furnace.

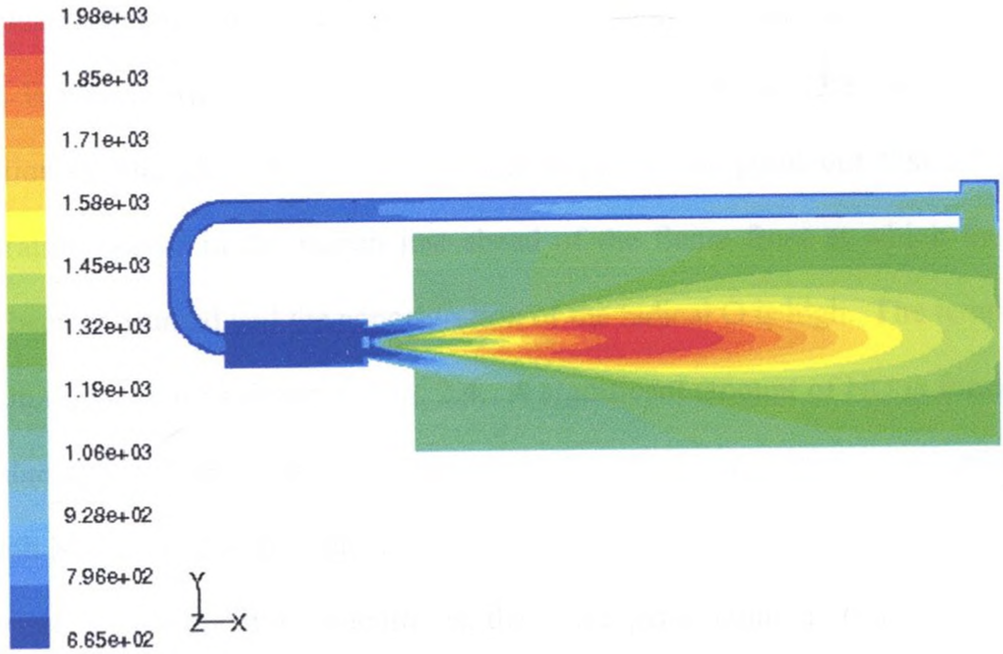

Figure 2.4 Temperature contour (K) on the plane at z=0 m

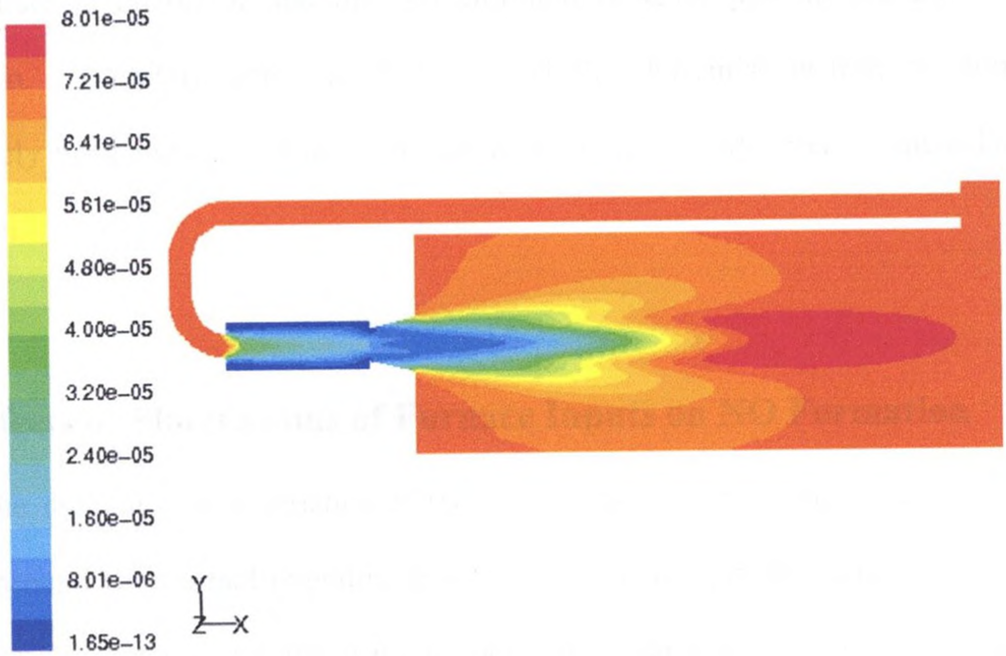

Figure 2.5 NO contour (mole fraction) on the plane at z=0 m

Figure 2.4 shows the temperature distribution on the same plane (z = 0 m). This figure clearly shows that the main reaction zone, which is located in the centre of the furnace, is characterized by a high temperature profile. Figure 2.5 illustrates the NO distribution on the plane at z = 0 m. It is important to point out that a higher NO concentration occurs in the region just ahead of the flame front at which the fuel has already been consumed and the concentration of the radical O is high. The temperature is highest in this region as shown in Fig. 2.4. A significant amount of NO is formed in this region due to the high temperature and high O radical concentration according to the Zeldovich NO formation mechanism.

Under normal operating conditions, the flame peak temperature is 1976 K and the NO emission is 75 ppm. For purpose of comparison, a numerical simulation is also conducted for the furnace shown in Fig. 2.1 but without the FGR. The flame peak temperature is 2070.7 K and the NO emission is 427.0 ppm at the same operating condition. Therefore, using the FGR method, the NO emission from the furnace has effectively been reduced by 82%. Clearly, the FGR is very effective in reducing NO emission.

2.6 Effects of Fluctuations of Furnace Inputs on NO Formation

The dynamic characteristics of the furnace are examined by varying the furnace inputs around the normal operating conditions to investigate the sensitivity of the NO formation to changes of furnace input controllable parameters. The three main inputs: mass flux (mass flow rate per unit flow area) of the combustion air, the temperature of the combustion air and the pressure head of the FGR fan, are disturbed individually by adding low amplitude sinusoidal signals of different frequencies. The amplitudes of these signals are selected based on maximum allowable perturbations with practical constraints and the stability limits of the combustion process. The output variable considered herein is the mole fraction of NO at the furnace outlet.

2.6.1 Effect of the fluctuation in the combustion air mass flux

The mass flux of the combustion air at the furnace inlet is perturbed by 10% around the furnace normal operating conditions. The resulting mass flux can be represented as:

$$m_{air} = 1.8490 + 0.1849\sin(\omega t) \quad [kg/m^2.s] \tag{2.14}$$

where ω is the frequency in rad/s. The simulations are carried out for the following frequencies: $\omega = 2\pi/150,\ 2\pi/36,\ 2\pi/12,\ 2\pi/3.6,\ 2\pi/2.1,\ 2\pi/1.2,\ 2\pi/0.78,$ and $2\pi/0.48$ (rad/s). The results under the frequencies of $2\pi/150,\ 2\pi/1.2,$ and $2\pi/0.48$ are shown in Fig. 2.6. The results show that the variation in NO is dramatic when the input air flow fluctuates at a low frequency. The level of NO emission reaches 210 ppm at $\omega = 2\pi/150$ as shown in Fig. 2.6 (c), which is almost triple the value at the normal operating point. It is important to emphasize that, at a low frequency ($\omega = 2\pi/150$) the NOx emission almost tripled while the mass flow rate of the combustion air has only changed 10% in the positive drift direction from the normal operating point. At a high frequency ($\omega = 2\pi/0.48$), the maximum NO is 90 ppm, which is only about 20% higher than that at the normal operating point. From Fig. 2.6, it can also be seen that the NO fluctuates at the same frequency as that of the input signal.

An increase in the flow rate of the combustion air increases the amount of oxygen available for the reaction with nitrogen, resulting in an increase in NO formation. A decrease in the flow rate of the combustion air will decrease the NO formation. Therefore, at low frequencies, the input signal fluctuation and the output NO variation are in-phase as shown in Fig. 2.6 (b) and (c). However, the phase shift increases as the frequency of the perturbation increases. For example, At a high frequency with $\omega = 2\pi/0.48$, the input signal fluctuation and the output NO variation are out of phase as shown in Fig. 2.6 (a). However, the amplitude of the variation in output NO at a high frequency is much smaller than that at a low frequency as shown in Fig. 2.6. In fact, such information is very important as far as the real-time control system is concerned because it represents the dynamic nature of the furnace. The detailed numerical simulation results at $\omega = 2\pi/150$ are summarized in Table 2.3. It can be seen from the table that when the NO emission is 210 ppm (at t = 37.5 s), the O_2 mass fraction at the outlet of the furnace is 0.0405, which is 52% higher than the value of 0.0267 at the normal operating point. Furthermore, the FGR flow rate drops to 0.0052 kg/s, which is less than half the value of 0.012 kg/s at the normal operating point. The increase in O_2 concentration and the decrease in the flow rate of the flue gas recirculation cause the NO emission to increase. When the mass flow rate of the combustion air changes by 10% in negative drift (at t = 112.5 s) from the normal operating point, the flow rate of the flue gas recirculation increases to 0.0178 kg/s, which is about 14% of the total gas mass flow entering the furnace. This is slightly higher than the recommended value (< 12%). The flame may be blown off from the stabilizer. Therefore, low frequency drift must be avoided. The results in Table 2.3 also reveal that the fluctuation of the inlet combustion air mass flux does not affect the CO concentration at the furnace outlet. However, the heat output from the furnace does change when the inlet combustion air mass flux fluctuates as shown in Table 2.3. The amplitude of the heat output fluctuation is less than 4% of the value at the furnace normal operating point.

Table 2.3 Effect of the combustion air mass flux for $\omega=2\pi/150$

Time (sec)	Air mass flux ($kg/s.m^2$)	FGR (kg/s) $\times 10^4$	Peak/Outlet temperature (K)	NO (ppm)	O_2 Mass fraction $\times 10^2$	CO (ppm)	Heat output (kW)
0	1.8490	121	1976/1367	74.9	2.67	<1	190
12.5	1.9141	90.1	2009/1366	112	3.10	<1	187
25	2.0091	63.5	2041/1367	169	3.66	<1	185
37.5	2.0339	52.0	2056/1366	210	4.05	<1	183
50	2.0091	61.2	2055/1366	204	4.12	<1	183
62.5	1.9414	87.0	2032/1368	159	3.85	<1	185
75	1.8490	120	1994/1369	99.3	3.28	<1	189
87.5	1.7566	150.6	1953/1369	57.2	2.55	<1	192
100	1.6889	171.1	1923/1367	32.8	1.86	<1	193
112.5	1.6641	178.4	1905/1365	23.4	1.40	<1	193
125	1.6889	172.7	1905/1363	22.6	1.27	<1	193
137.5	1.7566	152.6	1926/1363	31.0	1.50	<1	192
150	1.8490	123	1956/1365	54.0	2.00	<1	191
162.5	1.9141	90.6	2000/1365	95.7	2.75	<1	188
175	2.0091	63.8	2035/1366	155.6	3.44	<1	185
187.5	2.0339	52.0	2054/1366	199.7	3.92	<1	183
200	2.0091	61.0	2052/1367	199	4.05	<1	183
212.5	1.9414	86.8	2031/1368	155.9	3.81	<1	185
225	1.8490	119.8	1994/1369	98.3	3.26	<1	189
237.5	1.7566	150	1952/1369	56.8	2.54	<1	192
250	1.6889	171	1922/1367	32.6	1.86	<1	194
262.5	1.6641	178	1905/1365	23.3	1.40	<1	193
275	1.6889	172.8	1906/1363	22.6	1.27	<1	193
287.5	1.7566	152.8	1926/1365	30.8	1.50	<1	192
300	1.8490	123.5	1956/1365	53.8	2.00	<1	190

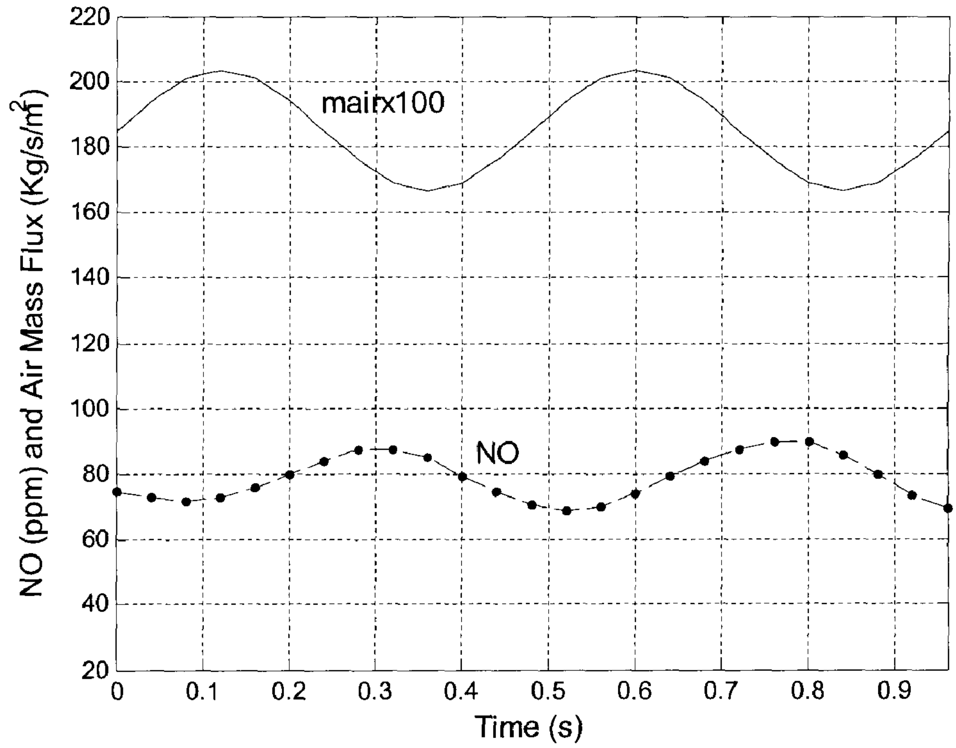

(a) $\omega=2\pi/0.48$

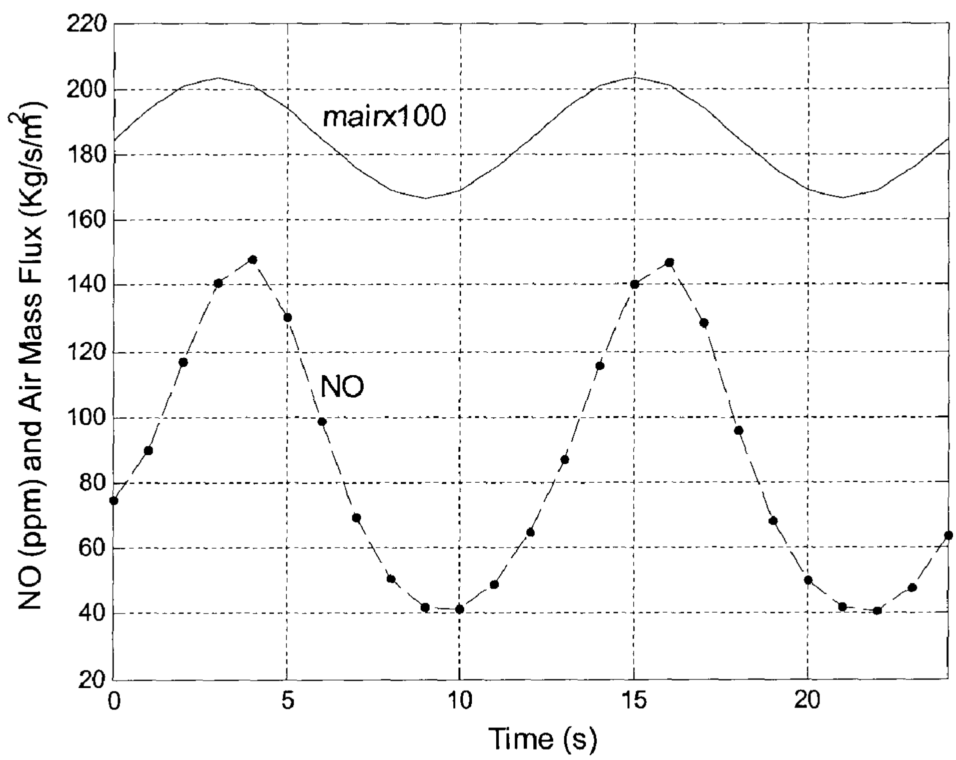

(b) $\omega=2\pi/12$

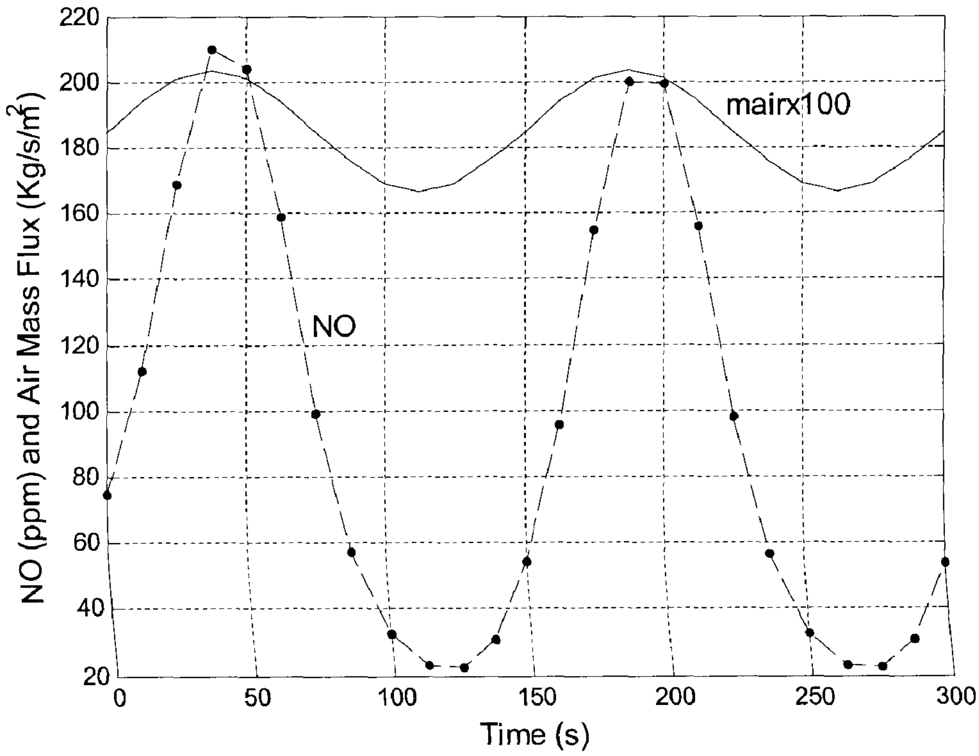

(c) ω=2π/150

Figure 2.6 NO emission as the combustion air mass flux is varied

2.6.2 Effect of the fluctuation in the combustion air temperature

The temperature of the combustion air is assumed to fluctuate sinusoidally around the normal operating conditions as governed by

$$T_{air} = 426.85 + 40\sin(\omega t)\ [^\circ C] \tag{2.15}$$

The following frequencies have been considered: ω = $2\pi/150$, $2\pi/36$, $2\pi/12$, $2\pi/3.6$, $2\pi/2.4$, $2\pi/1.2$, $2\pi/0.48$, and $2\pi/0.24$ (rad/s). The amplitude of the fluctuation is about 9.4% around the furnace normal operating point. Other input variables/parameters are kept at the furnace normal operating point.

The simulation results for three representative frequencies are shown in Fig. 2.7. The NO emission only fluctuates in the amplitude about 10% of the value at the furnace normal operating point at the high frequency ($\omega = 2\pi/0.48$) and about 30% at the low frequency ($\omega = 2\pi/150$). It can be seen that the NO emission is not very sensitive to the fluctuation of the combustion air temperature. This is due to the radiation heat transfer between the flame and the bottom furnace wall, which consumes most of the additional energy due to the temperature increase from the combustion air. Therefore, the flame peak temperature does not increase proportionally to the increase in combustion air temperature. It can also be concluded that the NO emission from the furnace is not sensitive to the fluctuation of the temperature of the recirculated flue gases because its flow rate is only about 10% that of the total flow rate of the combustion air. Thus, the effect of the fluctuation in temperature of the recirculated flue gases can be neglected in the control system analysis without too many adverse consequences in the prediction of NO emission from the furnace.

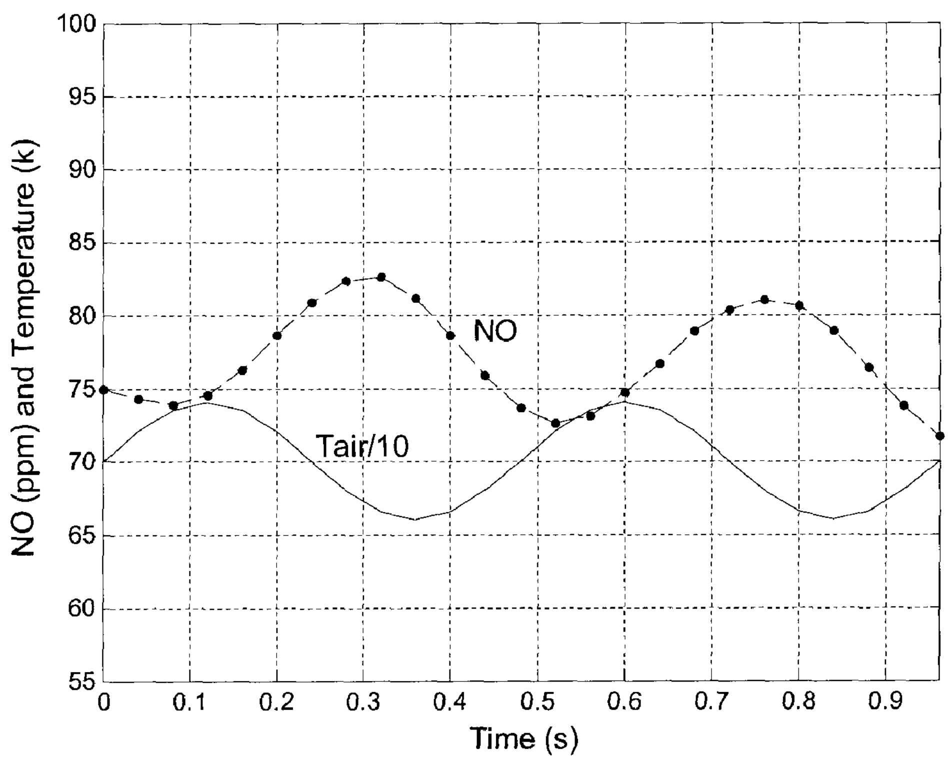

(a) ω**=2**π**/0.48**

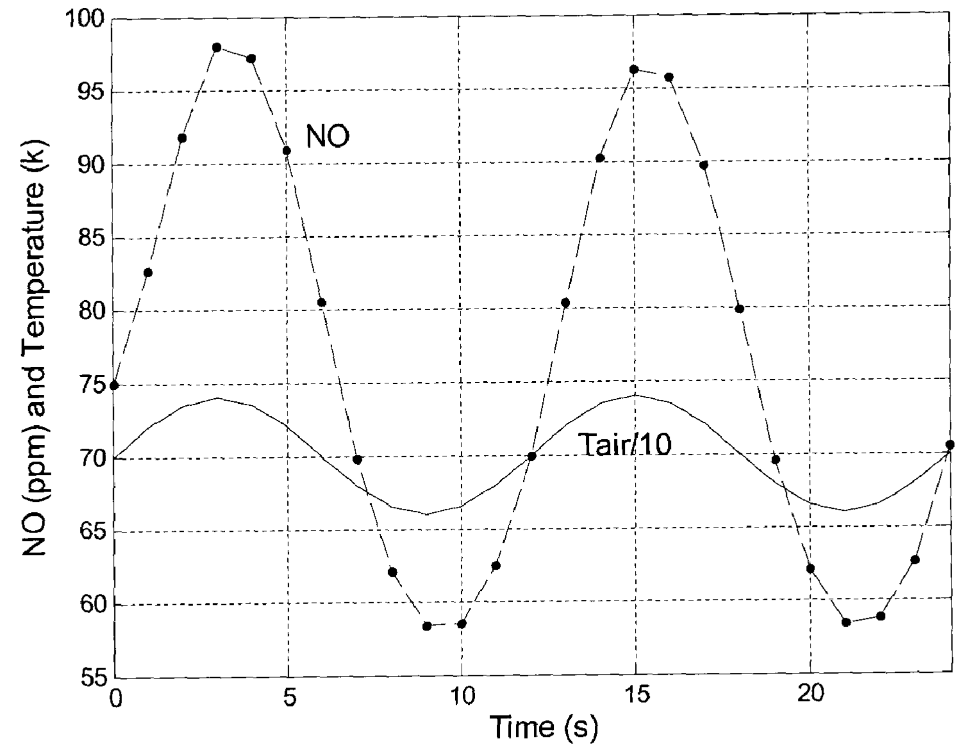

(b) $\omega=2\pi/12$

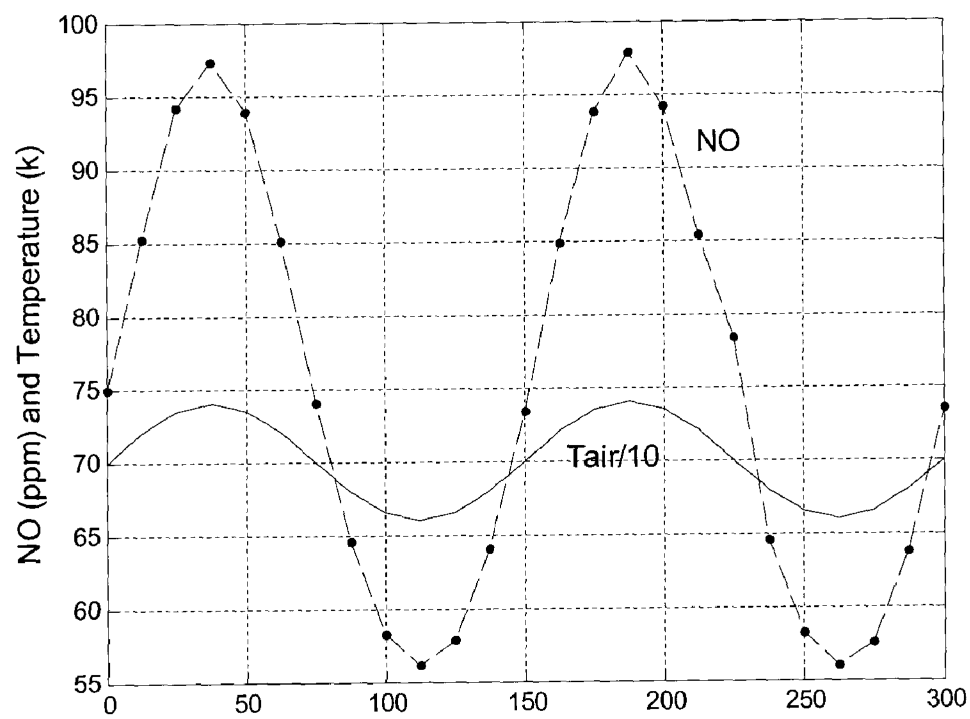

(c) $\omega=2\pi/150$

Figure 2.7 NO emission as the temperature of the combustion air is varied

From Fig. 2.7, it can be seen that the input signal fluctuation and the output NO variation are in phase at low frequencies as shown in Figs. 2.7 (b) and (c). This is because an increase in the combustion air temperature causes an increase in NO formation and a decrease in the combustion air temperature decreases the NO formation. However, the input signal fluctuation and the output NO variation are out of phase at high frequency as shown in Fig. 2.7 (a). Again, the amplitude of the NO variation at a high frequency is smaller than that at a low frequency as shown in Fig. 2.7.

2.6.3 Effect of the fluctuation in the pressure head of the FGR fan

The variation of the pressure head of the FGR fan can be represented by the following equation:

$$P_{fan} = 33.8 + 1.5\sin(\omega t) \quad [Pa] \tag{2.16}$$

where $\omega = 2\pi/150,\ 2\pi/36,\ 2\pi/12,\ 2\pi/3.6,\ 2\pi/2.4,$ and $2\pi/1.2$ (rad/s) have been chosen for the numerical simulations. The amplitude of the fluctuation is about 4.4% around the furnace normal operating point.

The simulation results at three testing frequencies are shown in Fig. 2.8. The maximum NO emission is less than 85 ppm at all frequencies, which is less than the 14% increase compared with the NO emission at the furnace normal operating point. Therefore, a slight drift in the pressure head of the FGR fan will have a minor effect on the NO emission. The pressure head of the FGR fan increases the flow rate of the recirculated flue gas, which in turn reduces the oxygen concentration. Therefore, the NO emission will be depressed. On the other hand, a decrease in the pressure head of the FGR fan will decrease the amount of flue gas recirculated, which will result in an increase in the NO emission. Hence, at low frequencies, the input signal fluctuation and the output NO variation are out of phase as shown in Figs. 2.8 (b) and (c). However, at a high frequency, for example, $\omega = 2\pi/1.2$, the input signal fluctuation and the output NO variation are in phase as shown in Fig. 2.8 (a). In fact, as most of physical systems do, the phase shift increases as the frequency of the perturbation increases.

The results shown in Figs. 2.6 to 2.8 indicate that the output NO varies at the same frequency as the input signal fluctuation. This implies that the furnace can be approximated by a linear system around the normal operating point. The higher the frequency, the more phase shift and the less the amplitude of NO fluctuation occur. This means that the furnace, like most of thc physical systems, has inertia and lowpass characteristics.

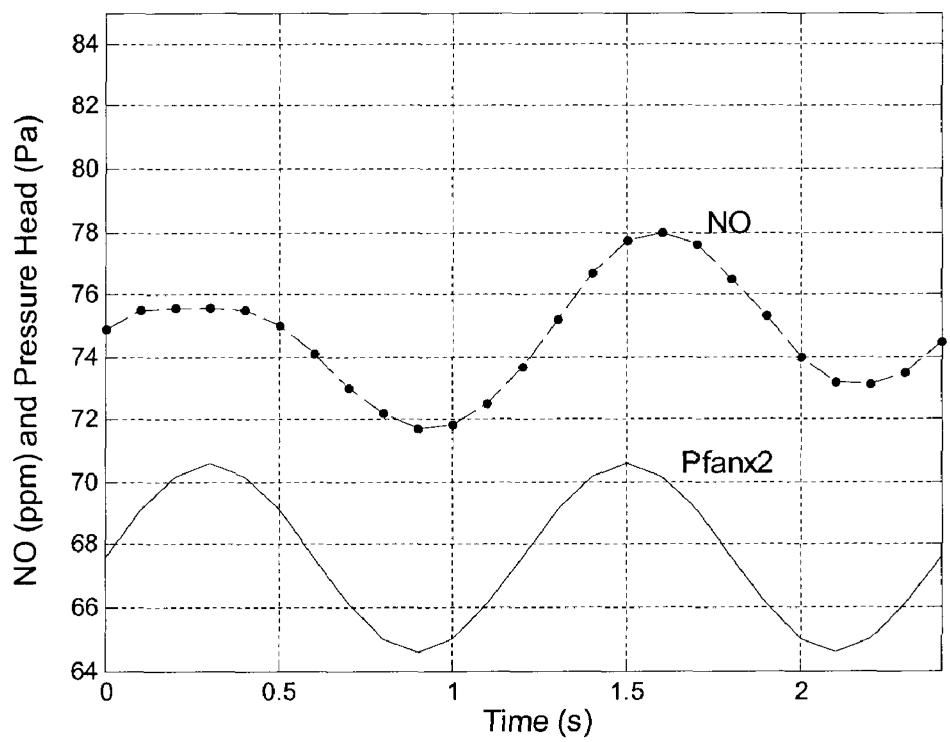

(a) $\boldsymbol{\omega=2\pi/1.2}$

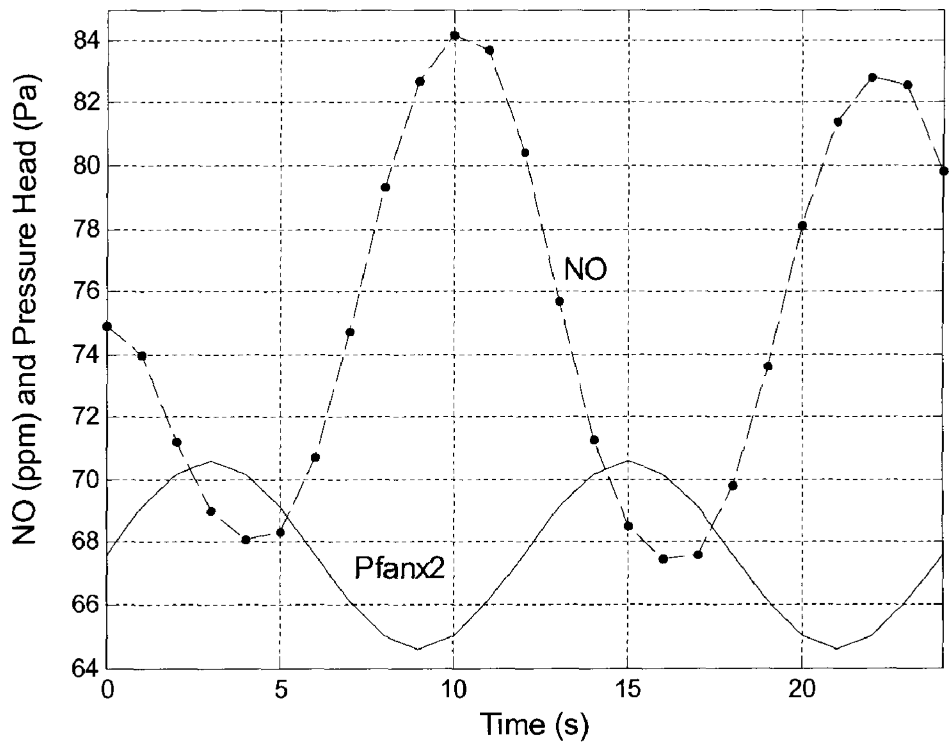

(b) $\omega=2\pi/12$

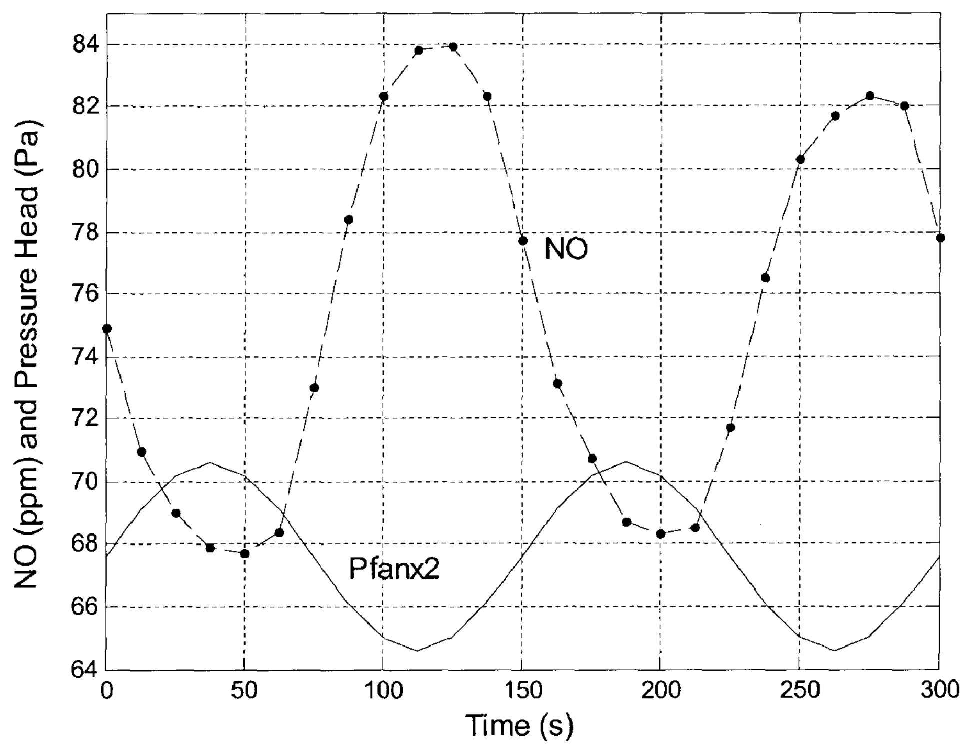

(c) $\omega=2\pi/150$

Figure 2.8 NO emission as the pressure head of the FGR fan is varied

2.7 Conclusions

A FGR furnace has been designed to study the sensitivity of the NOx emission to the fluctuation of the different furnace input variables. It was concluded that the extraction of a small amount of flue gases for recirculation from the top-right side of the furnace did not affect the main flow field. The use of the FGR can reduce the NOx emission by 82%. Furthermore, NOx emission was found to be very sensitive to the fuel injection angle and the fuel injection angle of 0° provides the lowest NOx emission.

Around the normal operating point, the sensitivity analysis indicates that the NOx fluctuates at the same frequency as the input variables, and the higher the frequency, the more phase shift and the less the amplitude of the NOx fluctuation. In other words, the furnace at normal operating conditions can be approximated by a linear system with low-pass frequency characteristics.

NOx changes drastically when the input combustion air mass flux fluctuates at a low frequency. The NOx emission is almost tripled when the mass flux of the combustion air makes only 10% positive drift from the normal operating point. Therefore, a stable combustion air mass flow rate is the key to achieve a low NOx emission furnace. However, it is also found that the NOx emission is not very sensitive to the temperature of the combustion air. The drift of the pressure head of the FGR fan has the least influence on the NOx emission.

Acknowledgement

The authors would like to express their sincere appreciation for the financial support received from the Imperial Oil Research Foundation for the work reported in this chapter.

References

[1] Hayhurst, A. N., and Vince, I. M., 1980, "Nitric Oxide Formation From Nitrogen Flames," Progress in Energy and Combustion Science, 6 (1), pp. 35-51.

[2] Canadian Environment Quality Guidelines, www.ccme.ca, 2003.

[3] Ishii, T., Zhang, C. and Sugiyama, S., 2000, "Effects of NO Models on the Prediction of NO Formation in a Regenerative Furnace," ASME Trans. Journal of Energy Resources Technology, 122, pp. 224-228.

[4] Hanson, R. K. and Salimian, S., 1984, "Survey of Rate Constants in H/N/O System", Combustion Chemistry (ed. W.C. Gardiner).

[5] Docquier, N. and Candel, S., 2002, "Combustion Control and Sensors: a Review", Progress in Energy and Combustion Science, 28, pp. 107-150.

[6] Tompkins, G., 1990, "Flue-gas Recirculation Works for Packaged Boilers", Power, 134, pp. 11-12.

[7] Jomeczek, J., Goral, J. and B., Gradon, 1995, "The GAFT Burner for Reducing NOx in Gas-fired High-temperature Industrial Furnaces", Journal of the Institute of Energy, 58, pp. 178-183.

[8] Vahnati, M. M. and O'nions, P., 2000, "Design and Development of a Low NOx Coanda Ejector Burner", Journal of the Institute of Energy, 73, pp. 12-17.

[9] Bilger, R. W., 1980, "Turbulent Flows with Non-premixed Reactants", Turbulent Reacting Flows, Springer-Verlag, Berlin.

[10] Jones W. P., and Whitelaw, J. H., 1982, "Calculation Methods for Reacting Turbulent Flows: A Review", Combustion Flame, 48, pp. 1-26.

[11] Launder, B. E. and Spalding, D. B., 1974, "The Numerical Computation of Turbulent Flow," Computer Methods in Applied Mechanics and Engineering, 3, pp. 269-289.

[12] Carvalho, M. G., Farias, T. and Fontes, P., 1991, "Predicting Radiative Heat Transfer in Absorbing, Emitting, and Scattering Media Using the Discrete Transfer Method", Fundamentals of Radiation Heat Transfer, ASME HTDS, 160, pp. 17-26.

[13] Shah, N. G., 1979, "A New Method of Computation of Radiant Heat Transfer in Combustion Chambers," Ph.D. Thesis, Imperial College of Science and Technology, London, England.

[14] Siegel, R. and Howell, J. R., 1992, Thermal Radiation Heat Transfer, Hemisphere, Washington D.C.

[15] Coppalle, A. and Vervisch, P., 1983, "The Total Emissivities of High-Temperature Flames", Combustion Flame, 49, pp. 101-108.

[16] Janicka, J. and Kollmann, W., 1982, "A Numerical Study of Oscillating Flow around a Circular Cylinder", Combustion and Flame, 44, pp. 319-336.

[17] Fluent 6 User's Guide, 2001, Fluent Inc., Lebanon, NH.

[18] Patankar, S. V., 1980, Numerical Heat Transfer and Fluid Flow, Hemisphere PublishingCo., Washington, DC.

CHAPTER THREE[1]

Dynamic Model Construction and Validation of the FGR Furnace for NOx Emission Control

3.1 Introduction

As more demanding air pollution standards are placed on combustion systems, there is an increased effort to apply advanced control technologies to meet the stringent demands. Preliminary studies have concluded that ACC (Active Combustion Control) is particularly desirable for optimizing combustion processes, alleviating combustion instabilities, and most of all, reducing the emissions such as NOx and CO [1].

The basic approach of ACC is to measure the appropriate furnace variables in real-time and feedback such information to regulate the controllable furnace inputs. Depending on the dynamic properties of the combustion process, the combustion control system will adjust the controller outputs automatically to meet the desired furnace performance requirements. The performance may include flame stability, a range of temperature variations, fuel efficiency, and emission levels. Emphasis is placed on the reduction of NOx emission in the current study. Comprehensive coverage of NOx control techniques can be found in two excellent survey papers [2, 3]. It is important to note that, in the design of a highly effective ACC system two types of information are essential. One is the knowledge of the dynamic behavior of the furnace, and in particular, the input and output characteristics; the other is the desirable feedback control law needed to

[1] The version of this chapter has been submitted to J. of Combustion Science and Technology in August, 2003

achieve the specified performance. The former is a modeling issue, and the latter is a control synthesis issue. This chapter concentrates on the former.

Since the combustion process in industrial furnaces is a complex process due to the interaction between turbulence and chemical reactions, the modeling usually starts from the conservation equations of mass, momentum and energy. These models are generally in the form of nonlinear partial differential equations [4]. CFD (Computational Fluid Dynamics) methods have been used to simulate the combustion process in industrial furnaces by solving these equations [5, 6]. The CFD methods have also proved to be useful in studying different burner configurations for furnace designs. However, from a real-time feedback control point of view, detailed CFD modeling has very limited use, as most of the control system synthesis techniques rely on input-output models described in terms of ordinary differential equations or transfer functions at a given furnace operating condition. In order to take full advantage of the vast amount of available feedback control techniques, it is highly desirable to model the furnace in terms of transfer functions for the purpose of furnace control. Unfortunately, little work has been done in this regard. The advantage of constructing a transfer function model from CFD simulation results is that it allows someone to study the operational aspects of the furnace without physically constructing it. By doing so, combustion engineers can refine the furnace design as well as its associated control systems.

The main objective of this work is to present a unique procedure to derive transfer function representations of an industrial reheating furnace with external flue gas recirculation. The procedure involves CFD solutions of fundamental equations that describe the fluid flow, heat transfer and chemical reactions in the furnace. The inputs to the furnace consist of superimposed low amplitude sinusoidal signals of different frequencies to the steady-state normal furnace inputs. The frequency domain information is then used to construct the dynamic representations among three independent furnace inputs: the flow rate of the combustion air, the temperature of the combustion air, and the pressure head of the flue gas recirculation fan and two outputs: NO and O_2 concentrations.

The advantage of having transfer function representations of the furnace is that they can be directly used with both modern and classical control system design techniques to improve the operational performance of the furnace. The contribution of this work lies in the fact that it provides a unique approach to furnace model construction based on CFD analysis and system identification techniques. The work reported herein provides a bridge between the traditional tools used in combustion process analysis, i.e. CFD, and transfer function representations common among the control system community. Such a bridge is extremely important in the future development of advanced control technologies for active combustion controls.

The emission of NOx, which is a collective name for NO and NO_2, from combustion processes in industrial furnaces or boilers is a major pollutant source. NOx not only causes nitric acid rain, but also depletes ozone in the stratosphere. It is estimated that over 95 percent of all man-made NOx that enters the atmosphere is produced by combustion of various fuels [7]. To protect the environment and future generations, the governments of many countries have established increasingly strict laws to limit the amount of NOx that can be released into the environment without a penalty. According to the Canadian Environment Quality Guidelines (2003) [8], the release of NOx must be within the following limits for a furnace or a boiler:

1 hour: 400-1000 $\mu g/m^3$ (NOx/Flue gas)

24 hours: 200-300 $\mu g/m^3$ (NOx/Flue gas)

1 year: 60-100 $\mu g/m^3$ (NOx/Flue gas)

Clearly, it is very important to develop effective ways to reduce NOx emission in combustion processes. One commonly used method to reduce the thermal NOx formation in the combustion process in a furnace is to use flue gas recirculation, in which a portion of the flue gases exhausted from the furnace is cooled down, pumped back to the inlet, and mixed with the fresh combustion air before entering the furnace. There are two main reasons why NOx formation can be reduced when the FGR is used. First, the peak flame temperature in the furnace can be lowered due to the increased amount of cold gas entering the furnace. Secondly, the oxygen concentration in the flame envelope can be diluted by the recirculated flue gases. In practice, the amount of the flue gases recirculated is limited by the combustion stability at low oxygen concentration. The FGR is usually limited to 20% for gas-fired furnaces and 10~12% for oil-fired furnaces. The reduction in NOx can be as high as 45% to 80% at the high recirculation rates. Therefore, the FGR is an effective way to reduce the NOx emissions. As well the FGR can be classified into two types based on how the flue gas recirculation is carried out - internal and external. Internal recirculation of flue gases requires intensive air swirling at the burner. External recirculation uses an external fan and a damper to control the amount of flue gases recirculated. This chapter focuses on the external flue gas recirculation since most industrial furnaces are still equipped with conventional burners and it is easier to retrofit an existing furnace with a damper and a recirculation fan. FGR furnaces usually operate at low excess oxygen concentration in practice. A small amount of drift from the normal operating point could cause significant change in NOx emission. Further, the flow rate of the recirculation flue gases is sensitive to fluctuations of the inlet airflow rate [9].

This chapter is organized as follows: the configuration of the furnace and its operating condition under investigation are described in the next section. The mathematical models that describe the fluid flow, heat transfer, and combustion process are summarized in Section 3.3. The control model structures and some CFD simulation results are presented in Sections 3.4 and 3.5, respectively. A set of transfer functions are constructed based on the CFD simulation data in Section 3.6 with model validation in Section 3.7.

3.2 Furnace Configuration

Figure 3.1 illustrates the configuration of the furnace used in this study. The dimensions of the furnace are $3.75\times1.4\times1.4$ m^3. The burner is located at the center of the left-side wall and the exhaust outlet is located at the center of the right-side wall of the furnace. A flue gas recirculation pipe 0.15 m in diameter is installed to recirculate the flue gases from the outlet back to the inlet of the furnace. The recirculation flue gases are extracted from the center of the top-right side of the furnace as shown in the figure. The dimensions of the mixing box at the inlet of the furnace are $0.3\times0.3\times0.8$ m^3. The combustion air and the recirculation flue gases enter the mixing box in the same direction so that they can be mixed symmetrically before entering the furnace to avoid any potential deviation of the flame in a particular direction inside the furnace. The stabilizer at the center of the right-side wall of the mixing box is simplified as a round plate of 0.07

m in diameter. A diffuser with the inlet diameter of 0.2 m and exit diameter of 0.35 m is used between the mixing box and the furnace as shown in Fig. 3.1. The fuel and gases are injected into the diffuser through a concentric pipe with an inner diameter 0.07 m and outer diameter of 0.2 m. The fuel is injected through the center pipe and gases are injected through the annular area between the two pipes. This is a non-premixed combustion process.

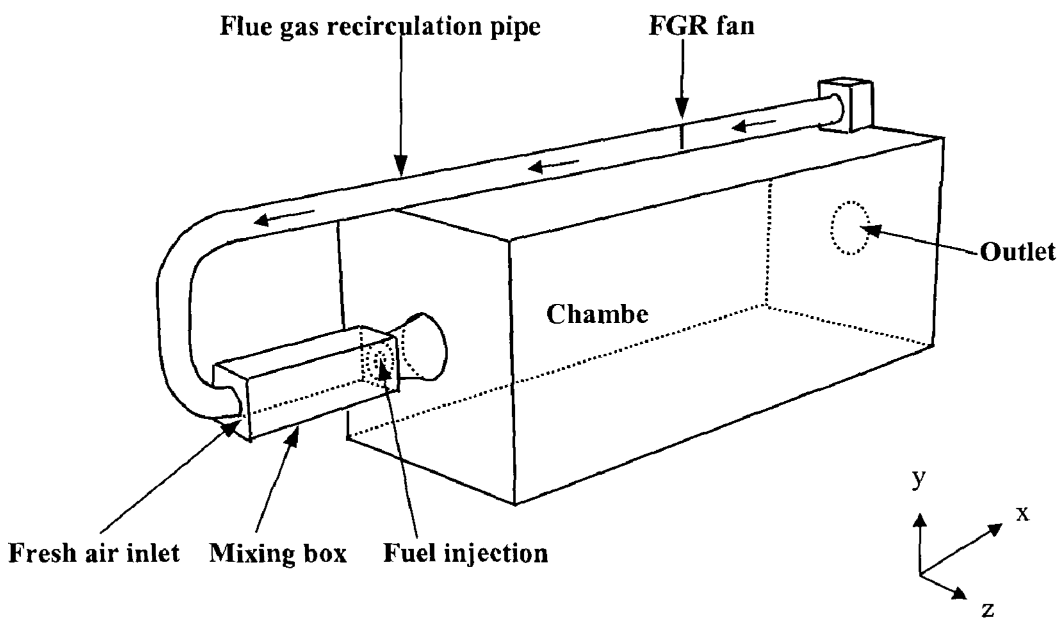

Figure 3.1 Configuration of the FGR furnace

The main operating parameters at the furnace operating point are given in Table 3.1. Liquid propane is used as the fuel. The heat input to the furnace from the fuel is 345 kW. The bottom furnace wall is set at a constant temperature of 1100 K and the rest of the walls are assumed to be insulated. The combustion air is preheated to a temperature of *700 K before it enters the furnace.*

Table 3.1 The normal furnace operating conditions

Fuel (propane, C_3H_8)	Flow rate	0.0075 kg/s
	Temperature	300 K
	Heating value	345 kW
Input combustion air	Flow rate	0.135 kg/s (or 1.849 kg/m^2·s)
	Temperature	700 K (or 426.85°C)
Heat output	190 kW from the bottom of the furnace	
Pressure head of the FGR fan	33.8 Pa	
Flue gas recirculation rate	0.012 kg/s	
Temperature at the bottom wall	1100 K	
Temperature at the FGR pipe	700K	

3.3 Mathematical Models

Instead of conducting experiments on the furnace itself, a numerical method is employed to simulate the fluid flow, heat transfer, and combustion process in the furnace based on the conservation equations of mass, momentum, and energy. The Favre-averaged conservation equations of mass, momentum and energy are given as [10, 11]:

$$\frac{\partial \rho}{\partial t}+\frac{\partial}{\partial x_i}\left(\tilde{\rho}\overline{u_i}\right)=0 \tag{3.1}$$

$$\frac{\partial}{\partial t}\left(\tilde{\rho}\overline{u_i}\right)+\frac{\partial}{\partial x_j}\left(\tilde{\rho}\overline{u_i}\,\overline{u_j}\right)=\frac{\partial}{\partial x_j}\left[\mu\left(\frac{\partial \overline{u_i}}{\partial x_j}+\frac{\partial \overline{u_j}}{\partial x_i}\right)-\left(\frac{2}{3}\delta_{ij}\mu\frac{\partial \overline{u_l}}{\partial x_l}\right)-\frac{\partial \tilde{P}}{\partial x_i}+\frac{\partial}{\partial x_j}\left(-\tilde{\rho}\overline{u_i' u_j'}\right)\right] \tag{3.2}$$

$$\frac{\partial}{\partial t}\left(\tilde{\rho}\bar{h}\right)+\frac{\partial}{\partial x_i}\left(\tilde{\rho}\overline{u_i h}\right)=\frac{\partial}{\partial x_i}\left(\frac{\mu_t}{\sigma_h}\frac{\partial \bar{h}}{\partial x_i}\right)+\overline{S_h} \tag{3.3}$$

where x_i is the position vector, u_i is velocity vector, ρ is density, P is pressure, μ is molecular viscosity, μ_t is turbulent viscosity, h is static enthalpy, and σ_h is the turbulent Prandtl number. The source term, S_h, in Eq. (3.3) consists of sources of enthalpy due to chemical reactions and radiation. The quantities with an overbar are the Favre-averaged values and the quantities with a tilde represent the Reynolds-averaged value. The prime denotes the fluctuation about the Favre average.

The Reynolds stresses, $-\tilde{\rho}\overline{u_i'u_j'}$, in Eq. (3.2) must be modeled in order to close Eq. (3.2). The Bousinesq hypothesis is used to relate the Reynolds stresses to the mean velocity gradients:

$$-\tilde{\rho}\overline{u_i'u_j'} = \mu_t\left(\frac{\partial \overline{u_i}}{\partial x_j} + \frac{\partial \overline{u_j}}{\partial x_i}\right) - \frac{2}{3}(\tilde{\rho}k + \mu_t\frac{\partial \overline{u_i}}{\partial x_i})\delta_{ij} \tag{3.4}$$

$$\mu_t = \tilde{\rho}C_\mu\frac{k^2}{\varepsilon} \tag{3.5}$$

where k and ε are the turbulent kinetic energy and its dispassion rate, respectively. The values of k and ε are obtained from the solution of their transport equations. For the standard k-ε model [12], k and ε transport equations are expressed as,

$$\frac{\partial}{\partial t}(\tilde{\rho}k) + \frac{\partial}{\partial x_i}(\tilde{\rho}\overline{u_i}k) = \frac{\partial}{\partial x_i}\left(\frac{\mu_t}{\sigma_k}\frac{\partial k}{\partial x_i}\right) + G_k - \tilde{\rho}\varepsilon \tag{3.6}$$

$$\frac{\partial}{\partial t}(\tilde{\rho}\varepsilon) + \frac{\partial}{\partial x_i}(\tilde{\rho}\overline{u_i}\varepsilon) = \frac{\partial}{\partial x_i}\left(\frac{\mu_t}{\sigma_\varepsilon}\frac{\partial \varepsilon}{\partial x_i}\right) + C_1\frac{\varepsilon}{k}G_k - C_2\tilde{\rho}\frac{\varepsilon^2}{k} \tag{3.7}$$

where $G_k = \mu_t\left(\frac{\partial \overline{u_j}}{\partial x_i} + \frac{\partial \overline{u_i}}{\partial x_j}\right)\frac{\partial \overline{u_i}}{\partial x_i}$, $C_1 = 1.44$, $C_2 = 1.92$, $C_\mu = 0.09$, $\sigma_k = 1.0$ and $\sigma_\varepsilon = 1.3$.

As near wall boundary conditions, values of k and ε at the first grid node are obtained using semi-empirical formulas known as standard wall functions [13]. Wall functions are used to bridge the viscosity-affected region between the wall and the fully turbulent region.

The effect of turbulent fluctuations on combustion is accounted for with an assumed-shape probability density function (PDF), the β-PDF [10, 14]. The P-1 model [15, 16] was used to calculate the radiation heat transfer at first. However, it did not provide a reasonable temperature distribution in the flue gas recirculation pipe due to the small local optical thickness in the pipe. Therefore, the discrete transfer radiation model (DTRM) [17, 18] is employed for the calculation of the radiation heat transfer. The DTRM is a relatively simple model and can be applied to a wide range of optical thicknesses. The assumption of gray radiation is acceptable for all inner surfaces of the furnace. The weighted-sum-of-gray-gases model [16, 19] is used to calculate the absorption coefficient. The chemistry model based on the chemical equilibrium concept, which assumes that the chemical reaction is rapid enough for chemical equilibrium to always exist at the molecular level, is employed to specify the instantaneous thermochemical state of the combustion mixture. The liquid fuel injection is modeled by a discrete phase model. The turbulent dispersion of liquid fuel droplets and other forces on the liquid fuel phase are neglected because the liquid fuel droplets last for a very short period of time and exist only in a very small region near the inlet of the furnace.

Both NO and NO_2 are formed during a combustion process. Generally, the concentration of NO_2 is negligible in comparison to NO concentration. It is usually considered as a transient intermediate species that exists only at flame conditions, and it is subsequently converted back into NO in the post-flame region. In gas- or oil-fired industrial furnaces, a major portion of the NO generated is the thermal NO. Thus, only the thermal NO is considered in this work. The mean NO concentration is obtained by solving its transport equation based on the flow field and combustion solution from the main combustion simulations. The temperature PDF approach [20] is used to account for the effect of turbulence on the NO formation. The CFD software FLUENT (2001) [21] is used for the CFD simulations.

3.4 Input and Output Representation of the Furnace

In order to construct a dynamic model suitable for real-time NO emission control, the frequency domain approach is employed to describe the variables that affect the NO formation in the furnace. As shown in Fig. 3.2, the input variables to the furnace are the fluctuation of mass flux (mass flow rate per unit flow area) of the combustion air, m_{air}, the fluctuation of temperature of the combustion air, T_{air}, and the fluctuation of pressure head of the FGR fan, P_{fan}. The output variables are the fluctuation of mole fraction of NO, y_{NO}, and the fluctuation of the mass fraction of O_2, f_{O2}, at the outlet of the furnace.

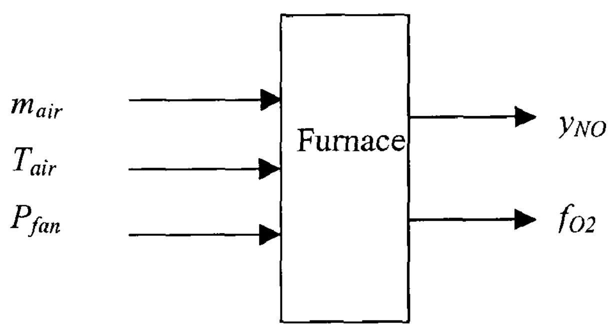

Figure 3.2 Dynamic model structure and input/output variables

The frequency domain model consists of frequency responses of the furnace at different operating conditions. The frequency responses are measured by adding sinusoidal signals of different frequencies onto the furnace input variables. These sinusoidal signals are expressed as:

$$m_{air} = 0.1849\, sin(\omega t) \quad [kg/m^2.sec]$$

$$T_{air} = 40\, sin(\omega t) \quad [K]$$

$$P_{fan} = 1.5\, sin(\omega t) \quad [Pa] \tag{3.8}$$

where ω is the frequency in rad/sec and t is time in seconds.

It is important to mention that the combustion in the furnace is a complex nonlinear process. Using the signals in Eq. (3.8), only a linear approximation is obtained. The constructed control models are only valid around given furnace operating conditions. This does not pose a problem for control system design if the control objective is to regulate the furnace around a given operating point.

3.5 CFD Simulation Results

The CFD simulations of the combustion process in the furnace are carried out by numerically solving the governing equations, Eqs. (3.1), (3.2), (3.3), (3.6), and (3.7), for the fluid flow and heat transfer under the following inlet conditions:

$$(m_{air})_{inlet} = 1.849 + 0.1849\, sin(\omega t) \quad [kg/m^2.sec]$$

$$(T_{air})_{inlet} = 700 + 40\, sin(\omega t) \quad [K]$$

$$(P_{fan})_{inlet} = 33.8 + 1.5\, sin(\omega t) \quad [Pa] \tag{3.9}$$

The constant terms in Eq. (3.9) correspond to the inputs at the furnace normal operating point.

CFD simulations are performed for six to eight different frequencies ranging from 0.04 to 26 rad/sec. The following two issues are considered when selecting these frequencies: (i) the bandwidth of the furnace; and (ii) the capability of the CFD models to handle rapidly changing signals. The range of frequencies for the input signals is selected based on a priori knowledge of the furnace.

Since the inlet conditions are time-dependent, CFD simulations are performed at each time step and the simulation results, including the concentrations of NO and O_2 at the furnace outlet, are recorded at every time step. It is important to point out that the concept of time step in CFD is different from that of the sampling interval in real-time control. The time step in CFD is the discretization time used to discretize the transient terms in the governing equations for fluid flow and heat transfer. It must be small enough to obtain an accurate numerical solution. On the other hand, the sampling interval in control system implementation is the discrete time step that the controller uses to take the measurement and generate the corresponding control signals. The CFD time step is much smaller than the sampling interval in most cases. Normally, there are several time steps within a single sampling interval.

The gain is defined as follows:

$$G = \frac{(y_{\max} - y_{\min}) / y_0}{(u_{\max} - u_{\min}) / u_0} \tag{3.10}$$

y_{max}, y_{min} are the maximum and minimum output variables, respectively; u_{max}, u_{min} are the maximum and minimum input variables, respectively and they are all in the same period.

y_0 and u_0 are the output and input variables at the steady original operating point respectively.

The gain and phase differences between the selected furnace input and the furnace output from the CFD simulations are calculated. The results for the mass fraction of O_2 at the furnace outlet are listed in Table 3.2.

Table 3.2 Gain and phase characteristics for O_2 at the furnace outlet

Input Variables	Frequency rad/s	Phase Delay (Dgree)	Gain
Combustion air mass flux	0.0419	10	5.200
	0.1745	35	2.507
	0.5236	60	1.496
	1.745	100	0.658
	2.992	157	0.416
	5.236	240	0.187

The mass fraction of O_2 at the furnace outlet is almost independent of the changes in the pressure head of the FGR fan and the combustion air temperature at the furnace inlet. Therefore, it can be considered as decoupled from these two inputs and only the results related to the combustion air mass flux are listed in Table 3.2. The frequency responses for the mole fraction of NO at the furnace outlet are listed in Table 3.3. It is observed from Tables 3.2 and 3.3 that the furnace outputs are sensitive to changes in the inputs in the frequency range of 0.04 – 13 rad/sec. When the frequency extends beyond

13 rad/sec, very few changes are observed at the outputs. This means that the furnace is a low-pass system.

Table 3.3 Gain and phase characteristics for NO at the furnace outlet

Input Variables	Frequency rad/s	Phase Delay (Dgree)	Gain
Combustion air mass flux	0.0419	12	11.812
	0.1745	20	8.058
	0.5236	30	7.044
	1.745	60	4.948
	2.992	103	3.542
	5.236	120	1.807
	8.055	120	0.940
	13.09	135	1.273
Combustion air temperature	0.0419	6	2.958
	0.1745	10	2.993
	0.5236	15	2.765
	1.745	40	2.457
	2.618	60	2.246
	5.236	105	1.334
	13.09	135	0.770
	26.18	180	0.804
Pressure head of the FGR fan	0.0419	12	2.346
	0.1745	20	2.663
	0.5236	45	2.512
	1.745	90	1.820
	2.618	120	1.414
	5.236	210	0.737

3.6 Construction of the Transfer Functions

Based on the frequency response information, it is concluded that the dynamic model of the furnace can be represented in terms of the following general transfer function structure:

$$G(s) = \frac{b_6 s^6 + b_5 s^5 + b_4 s^4 + b_3 s^3 + b_2 s^2 + b_1 s + b_0}{a_6 s^6 + a_5 s^5 + a_4 s^4 + a_3 s^3 + a_2 s^2 + a_1 s + a_0} \tag{3.11}$$

The constants, a and b, in Eq. (11) are then obtained using the least squares parameter estimation technique with appropriate dynamic compensations and the frequency responses given in Tables 3.2 and 3.3. The transfer function from the mass flux of the combustion air at the furnace inlet to the mass fraction of O_2 at the furnace outlet can be expressed as:

$$G(s)_{O2} = \frac{8.3875s^2 + 36.594s + 46.590}{s^5 + 3.1926s^4 + 27.868s^3 + 37.260s^2 + 78.147s + 10.000} \tag{3.12}$$

Similarly, the transfer function from the mass flux of the combustion air at the furnace inlet to the mole fraction of NO at the furnace outlet is found to be:

$$G(s)_{air\,mass} = \frac{-0.7532s^6 + 5.6356s^5 - 21.589s^4 + 423.76s^3 + 494.10s^2 + 2930.0s + 320.37}{s^6 + 4.3640s^5 + 62.070s^4 + 136.12s^3 + 402.91s^2 + 408.38s + 25.090}$$

(3.13)

The transfer function from the temperature of the combustion air at the furnace inlet to the mole fraction of NO at the furnace outlet can be represented by:

$$G(s)_{air\,temp} = \frac{-23.6270s^3 - 133.77s^2 + 2398.2s + 20890}{s^4 + 39.555s^3 + 900.74s^2 + 3972.1s + 7478.8} \tag{3.14}$$

Finally, the transfer function from the pressure head of the FGR fan to the mole fraction of NO at the furnace outlet is:

$$G(s)_{fan} = \frac{7.1681s - 63.801}{s^3 + 4.6133s^2 + 25.700s + 22.654} \tag{3.15}$$

Caution is advised when estimating the transfer functions as there could be multiple transfer functions with orders ranging from third to sixth, which could provide a satisfactory match for the recorded frequency response data. Effort has been made to ensure that (i) the transfer function obtained must correspond to a stable system, i.e. the real parts of all the poles must be negative and (ii) the frequency responses of the model must be in good agreement with the results obtained from the CFD simulations. All of the above four transfer functions satisfy these two conditions. The Bode plots of these transfer functions are shown in Appendix A.

Finally, the dynamic relationships between the furnace input and output variables can be represented by the following linear model:

$$\begin{bmatrix} y_{NO}/75.58 \\ f_{O2}/0.02674 \end{bmatrix} = \begin{bmatrix} G(s)_{air\,mass} & G(s)_{air\,temp} & G(s)_{fan} \\ G(s)_{O2} & 0 & 0 \end{bmatrix} \begin{bmatrix} m_{air}/1.849 \\ T_{air}/426.85 \\ P_{fan}/33.8 \end{bmatrix} \tag{3.16}$$

The constant terms in Eq. (3.16) correspond to the inputs and outputs at the furnace normal operating point.

3.7 Validation of the Dynamic Models

The comparison of the results obtained by the CFD simulations with those generated from the constructed dynamic models (Eqs. (3.12)-(3.15)) at different frequencies are presented in Figs. 3.3 to 3.6. The legends, "CFD" and "model", in the figures denote the results obtained by CFD simulations and those generated by the dynamic models, respectively. In all the figures, dotted lines represent the CFD simulation results and solid lines represent the results generated from the constructed dynamic models.

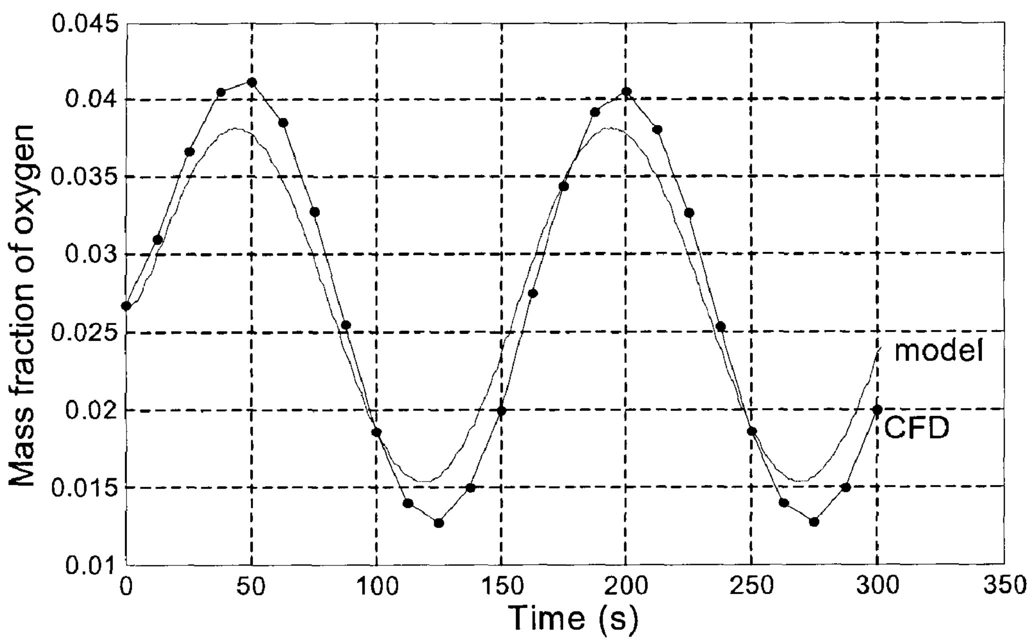

(a) $\omega=2\pi/150$

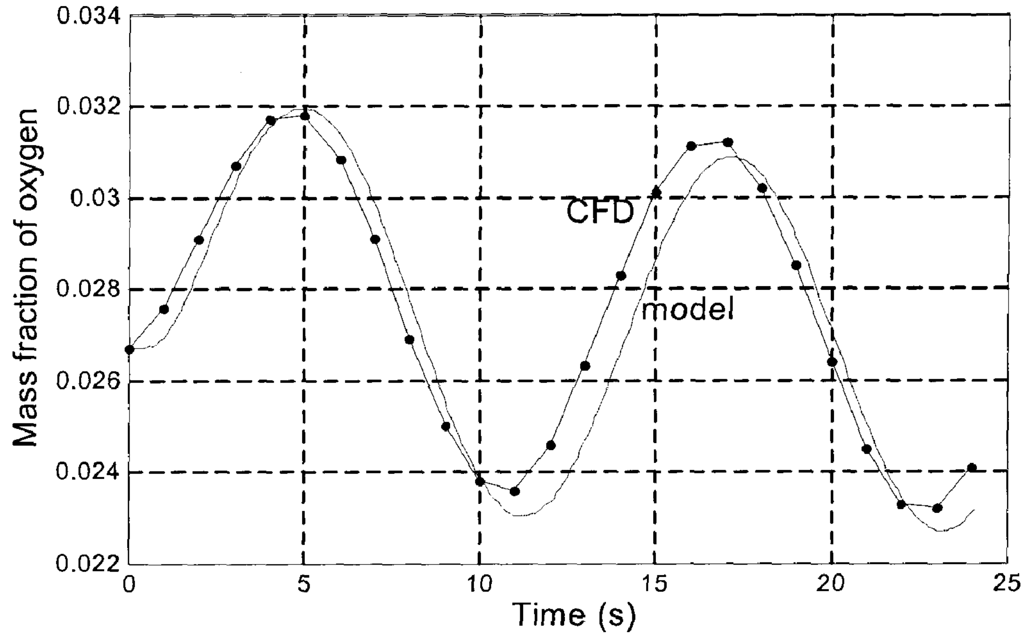

(b) ω=2π/12

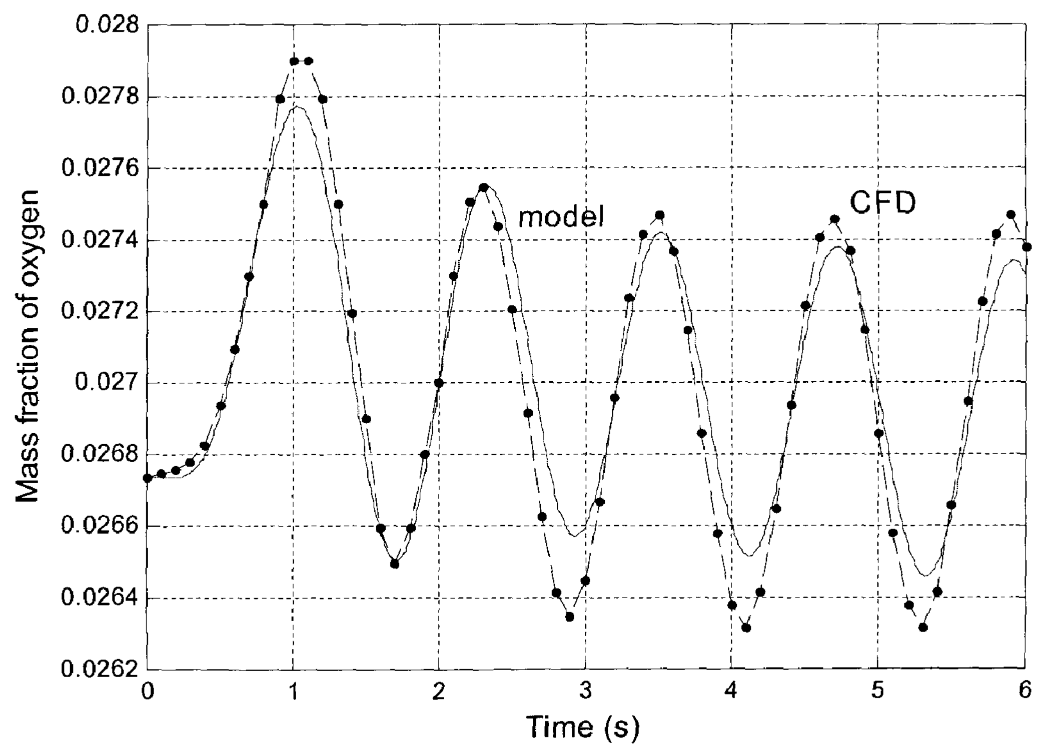

(c) ω=2π/1.2

Figure 3.3 Variation of O_2 at the furnace outlet relative to the combustion air mass flux

It can be seen from Fig. 3.3 that the estimation of the mass fraction of O_2 by the dynamic model is in an excellent agreement with the CFD simulations. The relative error in amplitudes is less than 9% and the difference in phase is very small at the low frequency ($\omega = 2\pi/150$). The phase shift increases slightly at the middle frequency ($\omega = 2\pi/12$). However, the maximum error which occurs at t=15 sec is still less than 5%. The model is very accurate at the high frequency ($\omega = 2\pi/1.2$) although more cycles are needed to get a stationary fluctuation due to the low pass dynamic nature of the furnace. These results show that the constructed dynamic model is reasonably accurate for the estimation of the mass fraction of O_2 at the furnace outlet.

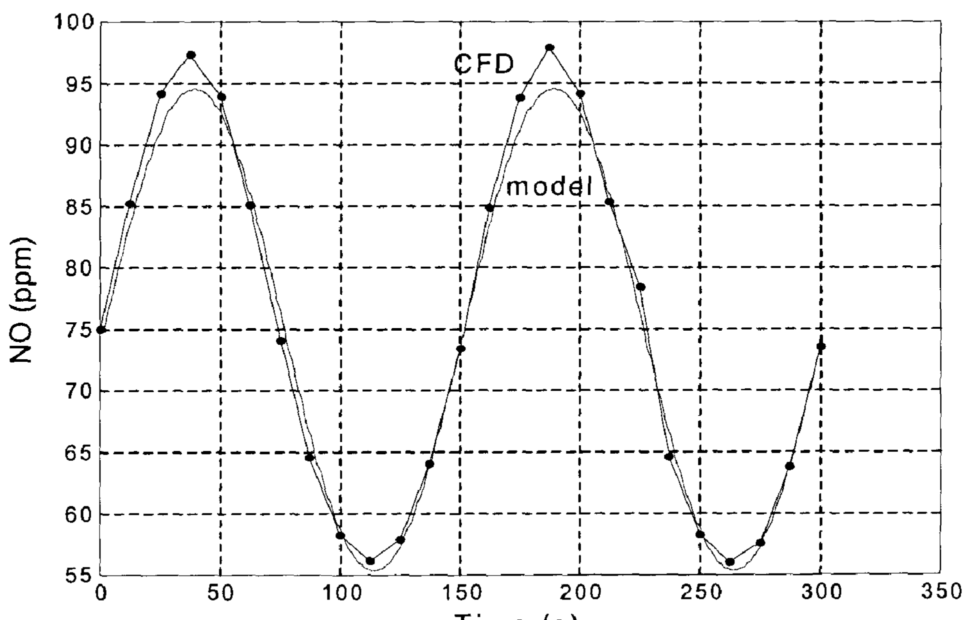

(a) ω=2π/150

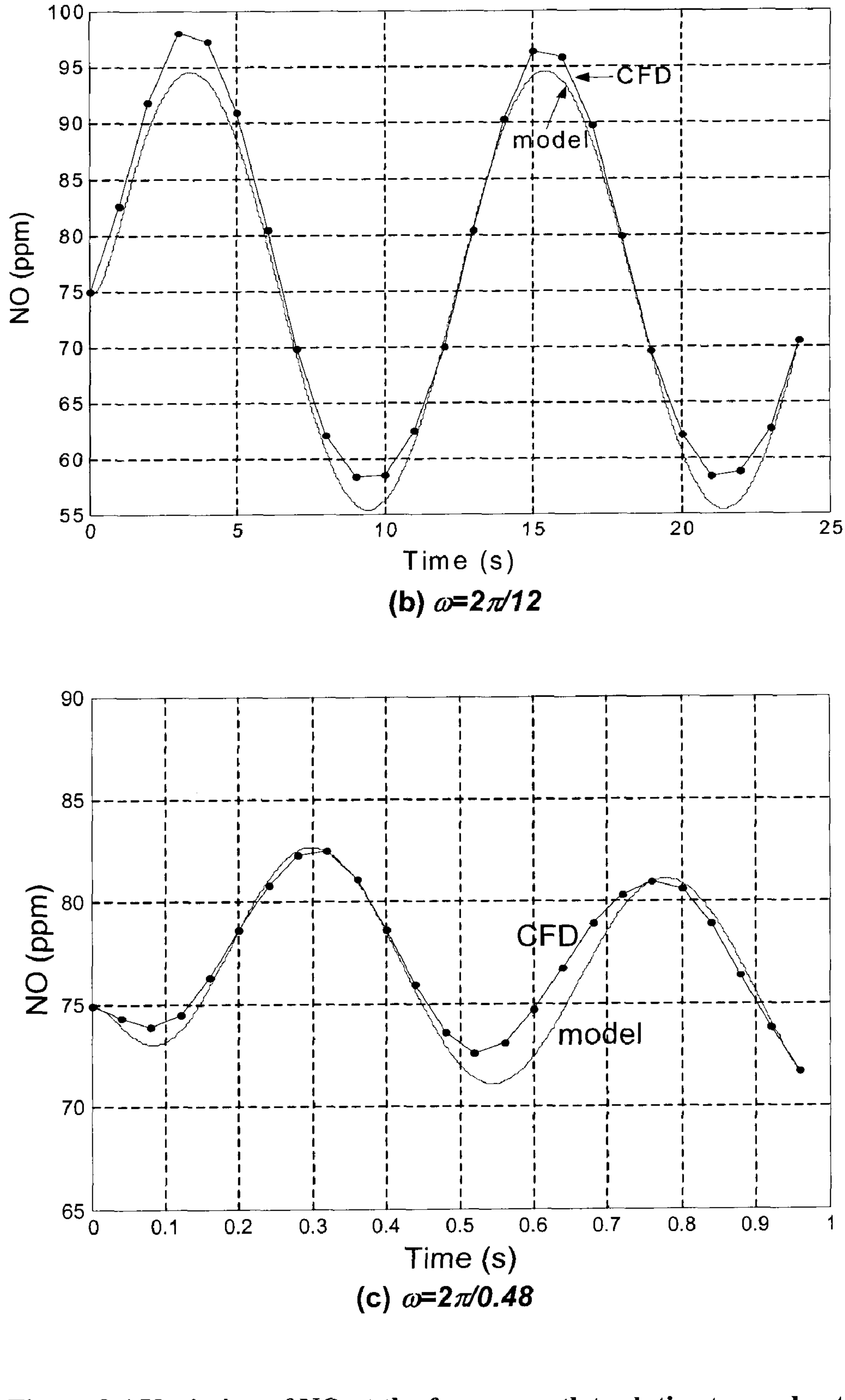

Figure 3.4 Variation of NO at the furnace outlet relative to combustion air temperature

Figure 3.4 shows the comparison of the NO emission predicted by the dynamic models and that obtained from the CFD simulations when the combustion air temperature at the furnace inlet fluctuates. The phase shift is very small and the maximum error in the amplitude is less than 4 ppm for all the frequencies considered. The predicted results from the dynamic model match almost perfectly with the results from the CFD simulations. Clearly, the constructed dynamic model is very accurate in this case.

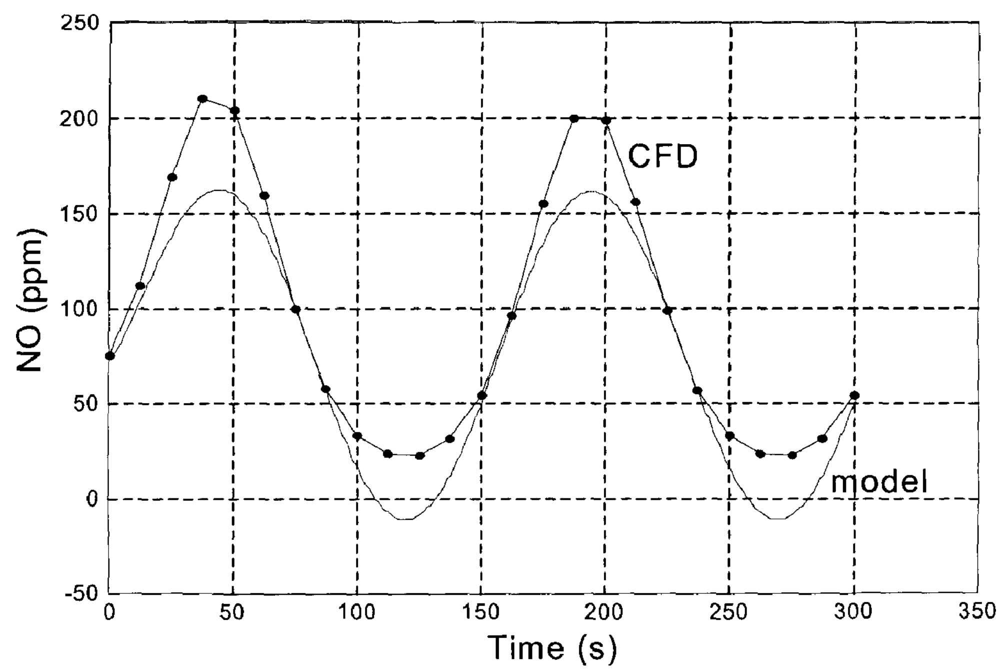

(a) ***ω=2π/150***

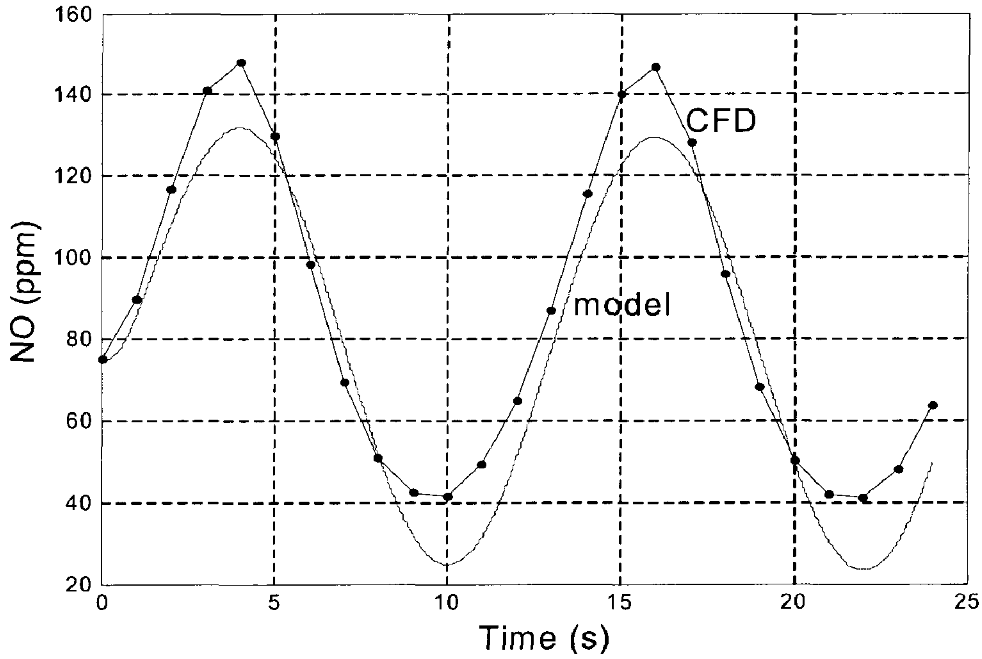

(b) ω=2π/12

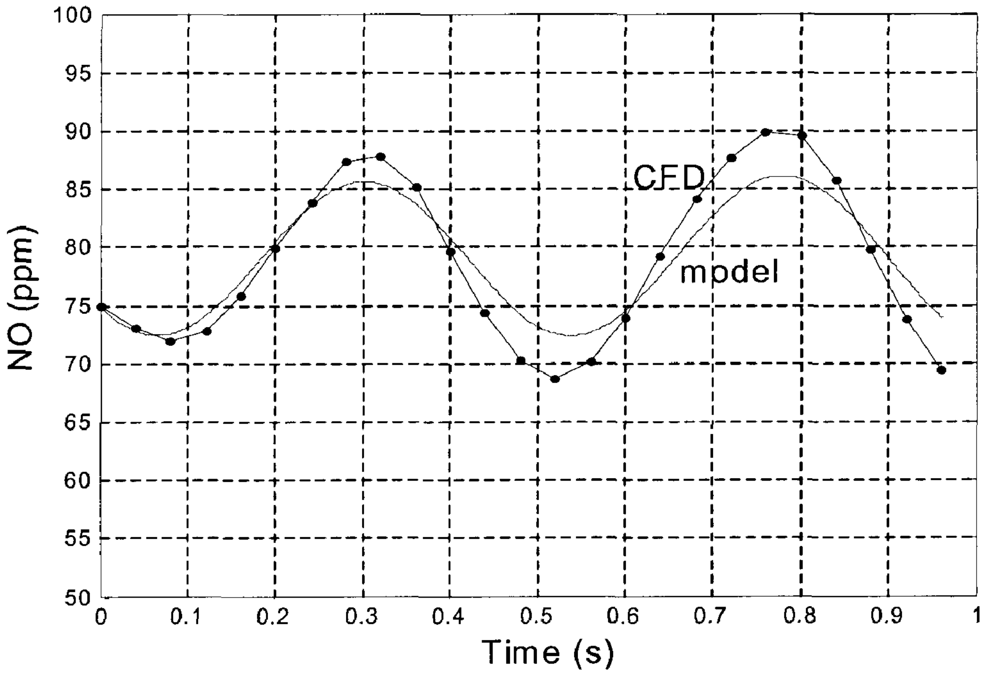

(c) ω=2π/0.48

Figure 3.5 Variation of NO at the furnace outlet relative to the combustion air mass flux

When analyzing the dynamic relationships between the NO formation and changes in the combustion air mass flux, some differences are observed between the CFD results and those generated from the dynamic model, as shown in Fig. 3.5. The error in the NO amplitude is more noticeable at low and middle frequency ranges. This may be due to the nonlinear characteristics between the NO formation and the combustion air mass flux. If, however, the level of NO control is limited to the range of 74.9 $\pm$ 10 ppm, this model can still provide satisfactory results. It is seen from Fig. 3.5 that the transfer function model can indeed capture the dynamics of the furnace for NO ranging between 60 and 100 ppm. Figure 3.5 shows that the fluctuation in the furnace input combustion air mass flux has a great effect on the NO formation. Figure 3.5 also shows that NO changes drastically when the input combustion air mass flux fluctuates at a low frequency.

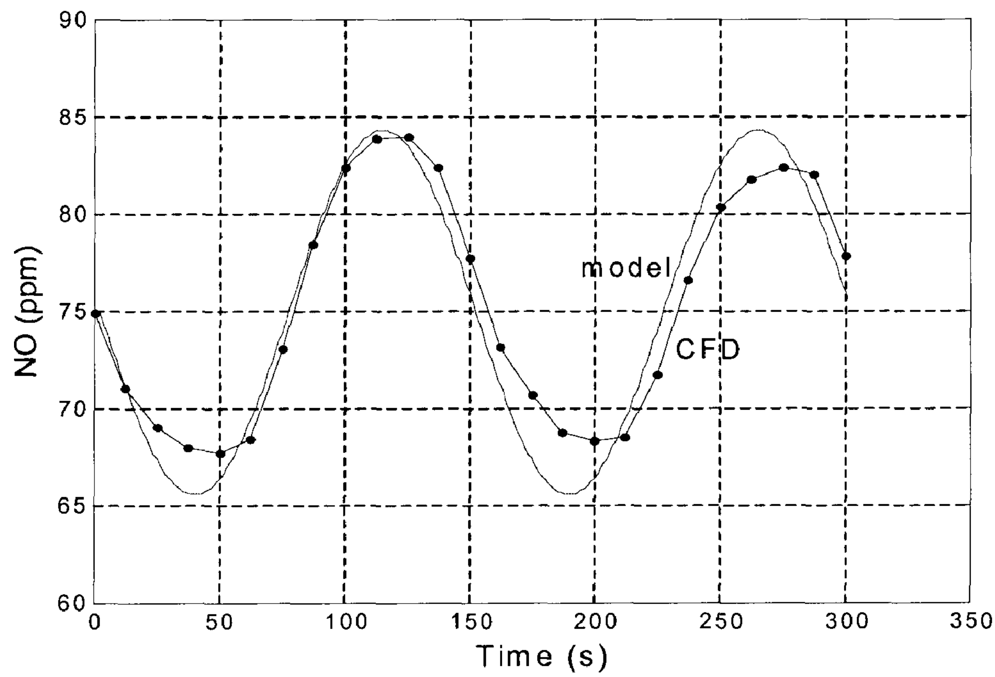

(a) ω**=2**π**/150**

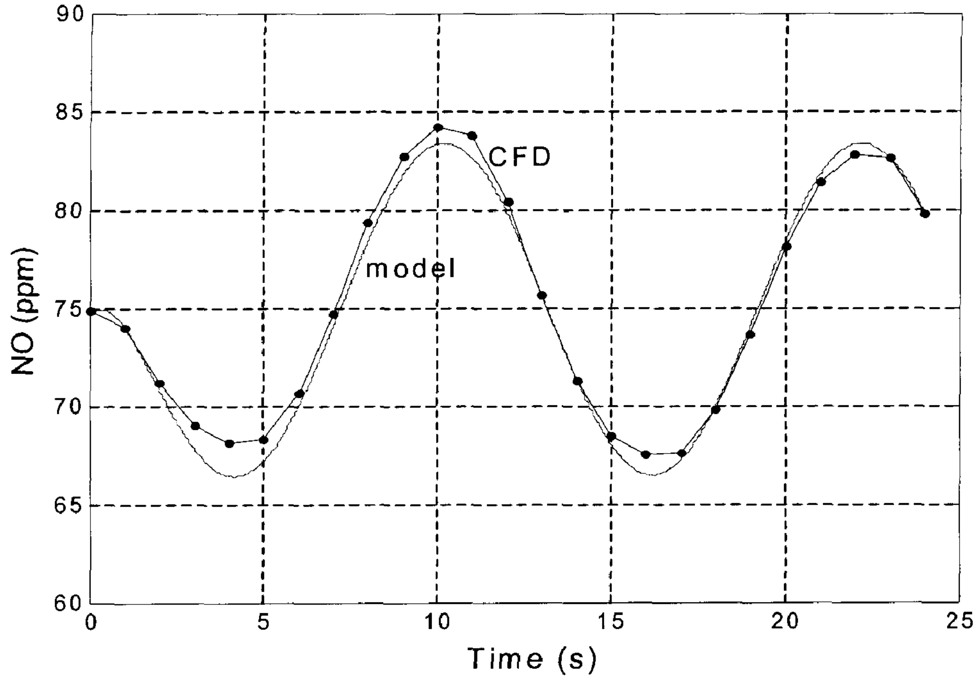

(b) $\omega = 2\pi/12$

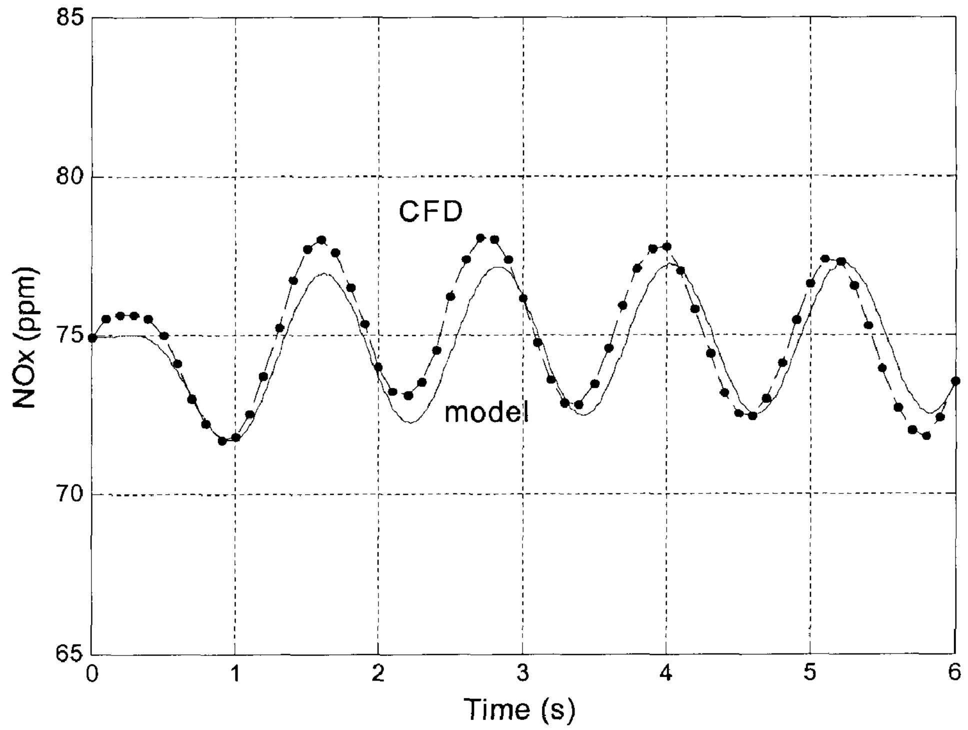

(c) $\omega = 2\pi/1.2$

Figure 3.6 Variation of NO at the furnace outlet relative to the pressure head of the FGR fan

Figure 3.6 shows the comparison of the NO emission predicted by the dynamic models and that obtained from the CFD simulations when the pressure head of the FGR fan fluctuates. The error in the NO amplitude is less than 2.5 ppm and a slight phase shift exists at low frequencies. When the frequency of the signal increases from $2\pi/150$ to $2\pi/12$ rad/sec, the error in the amplitude reduces and the phase difference disappears. When the frequency is increased beyond $2\pi/1.2$ rad/sec, the NO amplitude itself is only about 4 ppm. Figure 3.6(c) shows that there is a response delay due to the inertia of the furnace at high frequency. This transfer function is also an excellent representation between the pressure head of the FGR fan and the NO emission. It is observed from Fig. 3.6 that the change in the pressure head of the FGR fan has the least effect on the NO formation.

Based on the results obtained, it becomes clear that the combustion air mass flux is one of the most effective control inputs as far as the NO emission from the furnace is concerned. As discussed earlier, the combustion air mass flux not only has a strong influence on the NO emission but it also affects the O_2 concentration at the furnace outlet. With currently available oxygen sensors, it is worthwhile to investigate how to minimize NO emission by controlling the mass flux of the combustion air at the furnace inlet. If the mass fraction of excess air can be controlled in the range of 2.5% to 2.8%, the change of the NO emission caused by the change of the combustion air mass flux will be limited to the range from 60 to 100 ppm.

3.8 Conclusions

To optimize the operational aspects of industrial furnaces and to minimize NO emission through active combustion control, it is important to have some knowledge of the dynamic relationships between the furnace inputs and outputs. A set of dynamic models in terms of transfer functions has been constructed in this study for an industrial reheating furnace with flue gas recirculation. The inputs to these models are the mass flux of combustion air and the temperature of the combustion air at the furnace inlet, and the pressure head of the flue gas recirculation fan. The outputs are the NO concentration and the O_2 concentration at the furnace outlet. The study concludes that the NO emission is very sensitive to the change in the combustion air mass flux at the furnace inlet, and is relatively less sensitive to the variations in the other input variables.

To obtain the dynamic model for this multi-input and multi-output system, a CFD simulation is conducted to study the combustion process in the furnace based on the conservation equations of mass, momentum, and energy. Low amplitude sinusoidal signals at different frequencies have been superimposed to the nominal furnace operating input signals in the CFD simulation. The dynamic relationships between these inputs and outputs at each frequency are obtained in terms of the frequency responses. The frequency domain information is further converted to transfer function representations by means of a least squares based system identification technique. The order of the transfer functions ranges from third order to sixth order. These dynamic models are validated by comparing the full-scale CFD simulation results with those generated based on the constructed dynamic models and satisfactory results have been obtained. These models provide a good starting point for the design of real-time active combustion control systems to minimize NOx emissions. The control system design aspect of the work will be reported separately.

Acknowledgement

The authors would like to express their sincere appreciation for the financial support from the Imperial Oil Research Foundation for the work reported in this chapter.

References

1. Delabroy, O., Haile, E., Lacas, F., Candel, S., Pollard, A, Sobiesiak, A., and Becker, H. A., 1998, "Passive and Active Control of NOx in Industrial Burners", Experimental Thermal and Fluid Science, 16, pp. 64-75.
2. Docquier, N. and Candel, S., 2002, "Combustion Control and Sensors: A Review", Progress in Energy and Combustion Science, 28, pp. 107-150.
3. Muzio, L. J. and Quartucy, G. C., 1997, "Implementation NOx Control: Research to Application", Progress in Energy and Combustion Science, 23, pp. 233-266.
4. DeMarco, A. and Poncia, G., 1999, "A Model of Combustion Chambers, including Nitrogen Oxide Generation, in Thermal Power Plants", Control Engineering Practice, 7, pp. 483-492.
5. Ilbas, M., Bowen, P., O'Doherty, T., and Syred, N., 1995, "CFD Modelling of a Low NOx Combustor Fired by Natural Gas and Gas-oil", Proc. of Conference on Combustion & Emission Control, London, UK, pp. 189- 198.
6. Zhang, C., Ishii, T., Hino, Y. and Sugiyama, S., 2000, "The Numerical and Experimental Study of Non-premixed Combustion Flames in Regenerative Furnaces", ASME Trans. Journal of Heat Transfer, 122, pp. 287-293.

7. Hayhurst, A. N., and Vince, I. M., 1980, "Nitric Oxide Formation From Nitrogen Flames", Progress in Energy and Combustion Science, 6 (1), pp. 35-51.

8. Canadian Environment Quality Guidelines (2003) page 7, www.ccme.ca.

9. Tompkins, G., 1990, "Flue-gas Recirculation Works for Packaged Boilers", Power, 134, pp. 11-12.

10. Jones, W. P. and Whitelaw, J. H., 1982, "Calculation Methods for Reacting Turbulent Flows: A Review", Combustion and Flame, 48, pp.1-26.

11. Peters, A. A. F. and Weber, R., 1995, "Mathematical Modeling of a 2.25 MW_t Swirling Natural Gas Flame. Part1: Eddy Break-up Concept for Turbulent Combustion; Probability Density Function Approach for Nitric Oxide Formation", Combustion Science and Technology, 110-111, pp.67-101.

12. Launder, B. E. and Spalding, D. B., 1972, Lectures in Mathematical Models of Turbulence, Academic Press, London, England.

13. Launder, B. E. and Spalding, D. B., 1974, "The Numerical Computation of Turbulent Flow", Computer Methods in Applied Mechanics and Engineering, 3, pp. 269-289.

14. Bilger, R. W., 1980, Turbulent Reacting Flows, Springer-Verlag, Berlin.

15. Cheng, P., 1964, "Two-Dimensional Radiating Gas Flow by a Moment Method", AIAA Journal, 2, pp. 1662-1664.

16. Siegel, R. and Howell, J. R., 1992, Thermal Radiation Heat Transfer, Hemisphere, Washington D.C.

17. Carvalho, M. G., Farias, T. and Fontes, P., 1991, "Predicting Radiative Heat Transfer in Absorbing, Emitting, and Scattering Media Using the Discrete Transfer Method. Fundamentals of Radiation Heat Transfer", ASME HTDS, 160, pp. 17-26.

18. Shah, N. G., 1979, "A New Method of Computation of Radiant Heat Transfer in Combustion Chambers", Ph.D. Thesis, Imperial College of Science and Technology, London, England.

19. Coppalle, A. and Vervisch, P., 1983, "The Total Emissivities of High-Temperature Flames", Combustion Flame, 49, pp. 101-108.

20. Janicka, J. and Kollmann, W., 1982, "A Numerical Study of Oscillating Flow Around a Circular Cylinder", Combustion and Flame, 44, pp. 319-336.

21. Fluent 6 User's Guide, 2001. Fluent Inc., Lebanon, NH.

CHAPTER FOUR[1]

The Design and Validation of the Controllers for the FGR Furnace to Reduce NOx Emission

4.1 Introduction

NO and NO_2, collectively called NOx, are the key precursors to the formation of ground-level ozone, which is known to contribute to health and environmental problems. It is estimated that over 95 percent of all man-made NOx is produced by burning various fuels [1]. To protect the health of humans and the environment, many countries have enacted strict laws to limit the amount of penalty-free NOx emission. In Canada, according to the Canadian Environment Quality Guidelines [2], the release of NOx from an industrial furnace must be within the following limits:

1 hour:	400-1000 $\mu g/m^3$ (NOx/Flue gas)
24 hours:	200-300 $\mu g/m^3$ (NOx/Flue gas)
1 year:	60-100$\mu g/m^3$ (NOx/Flue gas)

To reduce NOx emission, many different techniques have been investigated, including changing the fuels used or adding additives [3], modification to the combustion chambers and fuel injectors, [4], as well as through feedback controls. A comprehensive review of existing techniques for NOx control can be found in two recent survey papers [5, 6].

Generally speaking, the NOx formed from industrial furnaces can be attributed to three distinct chemical kinetic processes: thermal NOx, fuel NOx, and prompt NOx.

[1] The work contained in this chapter was submitted to J. of Combustion Science and Technology in January 2004

However, the prompt NO and fuel NO are usually in very small quantities and only thermal NOx is considered in this work. In gas- or oil-fired industrial furnaces, the majority of NOx is NO, and the concentration of NO_2 is negligible in comparison to that of NO.

It is well understood that the thermal NOx relate closely to the hottest zones inside the furnace [7]. A desirable combustion environment must be maintained to reduce the formation of thermal NOx in the furnace and to steer away from favorable conditions for NOx formation. A significant amount of research has been done to design low NOx burners by optimizing the detail design of the furnace, such as dimensions, locations of fuel/air injection, and the operating condition, e.g. temperature, pressure etc. For example, it has been shown that the flue gas recirculation (FGR) is an effective way to reduce NOx emissions in industrial furnaces [8]. However, this scheme works well only at a low excess oxygen concentration. A slight deviation from this condition could result in a significant increase in the amount of NOx generated. Therefore, the optimal operation is as important, if not more, as the optimal design of a furnace.

It is easy to understand that the design parameters will be fixed once the furnace is constructed. However, the operating conditions may be subject to many operational uncertainties. To ensure that the furnace operate at the desired condition, users must rely on active combustion control systems.

A combustion control system maintains the furnace operation at the desired conditions by manipulating the external control variables based on the operational information of the furnace in real-time. The main objective is to minimize any excursion of the furnace operating variables from their desired values when subjected to disturbances and hence to reduce the potential hottest zones to reduce the NOx formation. Clearly, this is a regulation problem from a control system point of view. The solution to this problem can be achieved through some feedback control strategies.

In the current research, the furnace input variables that can be manipulated are: (a) the mass flow rate of the combustion air; (b) the temperature of the combustion air; and (c) the pressure head of the flue gas recirculation fan. The control system relies on the real-time measurements of two furnace outputs: oxygen (O_2) and the NO concentrations at the furnace outlet.

Other potentially undesirable substances in addition to NOx have to be considered. The most notable ones are CO and CO_2. Care must be taken so as not to get into a situation where NOx is minimized at the expense of the other undesirable emissions. These issues have to be carefully considered at the furnace design stage, which is beyond the scope of the present research. Assuming that the desired operating condition is determined through appropriate furnace design and analysis, the objective of the current research is to show how to maintain furnace operation at the design conditions through feedback controls.

It is imperative to have sufficient knowledge about the relationships between the manipulated furnace inputs and the measured furnace outputs in order to design an effective feedback control system. Unfortunately, a furnace is a highly nonlinear system and the fluid flow, heat transfer and combustion processes are also very complex. Even though full-scale Computational Fluid Dynamic (CFD) models have been constructed based on principles of fluid flow, heat transfer and combustion processes for open-loop studies, such models cannot be used directly for the design of closed-loop feedback controllers.

A novel approach is developed in chapter to circumvent such a difficult situation. Since the main issue dealt with in this study is to maintain the desired operating condition for the furnace, it is possible to represent the nonlinear furnace by linear dynamic models around the desired operating condition. These linear models are then be used in the feedback control system design. To construct accurate linear dynamic system models, detailed CFD solutions must be found and dynamic system identification techniques have to be employed.

In fact, CFD modeling is not new to furnace design and evaluation and is used in combustion optimization and NOx reduction technologies [9, 10, 11, 12, 13]. CFD plays two major roles in the current investigation: (1) linear dynamic model construction; and (2) full-scope performance evaluation of the designed feedback control systems in a nonlinear furnace environment.

A considerable amount of research has been carried out on the use of feedback control systems to reduce NOx emission. Interested readers can refer to [5, 6, 14, 15] and reference thereafter for details on this subject. The main contribution of this paper is to show how CFD can be used effectively to design and evaluate optimal feedback controllers to maintain the desired furnace operating conditions and hence to achieve NOx reduction.

Since the controller relies on the real-time information of the furnace, the availability of sensors to provide on-line measurements for the concept to be viable must be considered. So far as the current research is concerned, sensors and transducers for O_2

are readily available. As for on-line NOx measurement, significant progress has been made recently [16]. Several manufacturers have announced the availability of sensitive NOx analyzers using the chemiluminescent method. The measurement delay can be reduced to no more than one second and the minimum detectable concentration is as low as 0.02 ppm. The availability of such sensors will further enhance the practice value of the current investigation.

The paper is organized as follows: In Section 4.2, the configuration, the operating conditions of the FGR furnace used in this study are described with the problem statement. The construction of a linear dynamic model for the furnace that incorporates the operating conditions is covered in Section 4.3. The optimal control strategy is analyzed and the design is carried out in Section 4.4. The performance of the designed control systems is evaluated in Section 4.5 using both the linear dynamic models and the full-scope nonlinear CFD models. Finally, conclusions are discussed in Section 4.6.

4.2 The Furnace Configuration, Operating Condition and the Problem Statement

4.2.1 The furnace configuration

The furnace used in the current study is a reheating furnace with FGR as shown in Fig. 4.1. The dimensions of the furnace are $3.75\times1.4\times1.4$ m^3. The burner is located at the center of the left-side wall and the exhaust outlet is located at the center of the right-side wall as illustrated. A flue gas recirculation pipe 0.15 m in diameter is installed to circulate the flue gases from the rear top of the furnace back to the inlet. It re-enters the furnace from the center of the top-right side of the furnace as shown.

The dimensions of the mixing box at the inlet of the furnace are $0.3\times0.3\times0.8$ m^3. The combustion air and the recirculation flue gases enter the mixing box in the same direction so that they can be mixed symmetrically before entering the furnace to avoid any potential deviation of the flame in a particular direction inside the furnace. The stabilizer at the center of the right-side wall of the mixing box is simplified as a round plate of 0.07 m in diameter. A diffuser with an inlet diameter 0.2 m and an exit diameter 0.35 m is used between the mixing box and the furnace is shown in Fig. 4.1. The fuel and gases are injected into the diffuser through a concentric pipe with the inner diameter of 0.07 m and the outer diameter 0.2 m. The fuel is injected through the center pipe. The combustion air and flue gases are injected through the annular area between the two pipes.

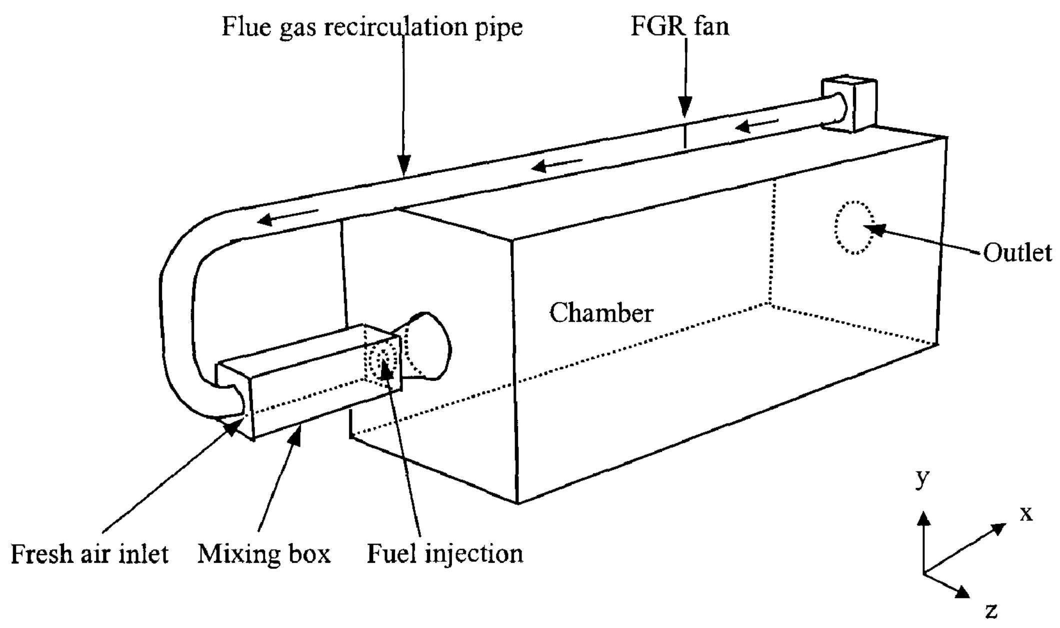

Figure 4.1 Configuration of the FGR furnace

The controllable furnace inputs are the flow rate, the temperature of the combustion air and the pressure head of the FGR fan. The actuators for these three variables are: air flow fan, pre-heater, and damper in the flue gas recirculation path. It is also assumed that the oxygen and NOx sensors are located at the immediate exhaust outlet.

4.2.2 A general strategy for determining desired operating conditions for NOx reduction

As in any dynamic system, different system inputs affect the system behaviors in different ways. Industrial furnaces are no exception. Based on an earlier study [17], it is concluded that the combustion air mass flux, which is mass flow rate per unit flow area, not only has a significant affect on the NO emission but also on the oxygen concentration at the furnace outlet. A simple strategy to determine the desired operating conditions for the furnace is to use the information from the oxygen concentration at the furnace outlet to determine the amount of mass flux of the combustion air at the furnace inlet for minimum NO emission. In fact, if the mass fraction of excessive air can be kept in the range of 2.5% to 2.8%, the corresponding NO emission due to the fluctuation of the combustion air mass flux can be limited to the range of 60 to 100 ppm [17]. After the combustion air mass flux is determined, the NOx emission can be further reduced through proper adjustments to the combustion air temperature and the pressure head of the FGR fan. The characteristics of the furnace are such that this kind of decoupled design is possible. Such a decoupled design also allows one to easily consider CO emission levels while minimizing NO because only the combustion air mass flow rate has a dominant effect on the CO emission in this furnace configuration. Through proper analysis and CFD simulations, the desired operating conditions of the furnace can be established.

The main objective of this paper is to design a real-time control system to maintain the furnace at the desired operating condition. Any further elaboration on the determination of such conditions here are beyond the scope of the current research.

4.2.3 The furnace operating condition

Based on the furnace control strategy outlined previously, the desired operating condition is determined and the corresponding parameters are summarized in Table 4.1. Since the furnace considered is a reheating furnace, the temperature at the furnace bottom wall is set at a constant value of 1100 K. It is assumed that the rest of the walls are insulated. The parameters of the fuel channel remain unchanged during normal operation. The furnace can be controlled through the flow rate and the temperature of the combustion air. As shown, their nominal values are 0.135 kg/s and 700K, respectively. The pressure head of the FGR fan, which is nominally set at 33.8 Pa, can also be adjustable.

Table 4.1 The normal furnace operating conditions

Fuel (propane, C_3H_8)	Flow rate	0.0075 kg/s
	Temperature	300 K
	Heating value	345 kW
Input combustion air	Flow rate	0.135 kg/s (or 1.849 kg/m^2·s)
	Temperature	700 K (or 426.85°C)
Heat output	190 kW from the bottom of the furnace	
Pressure head of the FGR fan	33.8 Pa	
Flue gas recirculation rate	0.012 kg/s	
Temperature at the bottom wall	1100 K	
Temperature at the FGR pipe	700K	

4.3 Construction of Linear Dynamic Model

To design an appropriate feedback controller for the furnace that maintains the desired operating condition, it is important to have causal relationships between the furnace inputs and the corresponding outputs. The full-scale mathematical model that describes the fluid flow, heat transfer and combustion process in the furnace can be derived by applying the mass, momentum and energy conservation laws. The resulting equations are nonlinear partial differential equations. These equations not only describe the input and output relations of the furnace, but also the fluid flow, heat transfer, and combustion variables internal to the furnace. These equations are very useful in the performance of the analysis and evaluation of the furnace characteristics and design parameters. Unfortunately, they are not suitable for feedback control system synthesis. Even though fluid flow, heat transfer and combustion process are highly nonlinear and the internal variables depend on the space, the furnace input and output characteristics around an operating point can still be approximated using a space-independent linear dynamic process, for which linear dynamic equations can be obtained. Based on these equations, the design process for the feedback controller can be simplified considerably.

4.3.1 Full-scale mathematical model for the furnace

Based on the fluid flow, heat transfer, and combustion process in the furnace, the following mathematical model is obtained. It consists of Favre-averaged conservation equations and a series of secondary models. The Favre-averaged conservation equations of mass, momentum and energy are given as [18, 19]:

$$\frac{\partial \rho}{\partial t}+\frac{\partial}{\partial x_i}\left(\tilde{\rho}\overline{u_i}\right)=0 \tag{4.1}$$

$$\frac{\partial}{\partial t}\left(\tilde{\rho}\overline{u_i}\right)+\frac{\partial}{\partial x_j}\left(\tilde{\rho}\overline{u_i}\,\overline{u_j}\right)=\frac{\partial}{\partial x_j}\left[\mu\left(\frac{\partial \overline{u_i}}{\partial x_j}+\frac{\partial \overline{u_j}}{\partial x_i}\right)-\left(\frac{2}{3}\delta_{ij}\mu\frac{\partial \overline{u_l}}{\partial x_l}\right)-\frac{\partial \tilde{P}}{\partial x_i}+\frac{\partial}{\partial x_j}\left(-\tilde{\rho}\overline{u_i' u_j'}\right)\right] \tag{4.2}$$

$$\frac{\partial}{\partial t}\left(\tilde{\rho}\bar{h}\right)+\frac{\partial}{\partial x_i}\left(\tilde{\rho}\overline{u_i h}\right)=\frac{\partial}{\partial x_i}\left(\frac{\mu_t}{\sigma_h}\frac{\partial \bar{h}}{\partial x_i}\right)+\overline{S_h} \tag{4.3}$$

where x_i is the position vector, u_i is velocity vector, ρ is density, P is pressure, μ is molecular viscosity, μ_t is turbulent viscosity, h is static enthalpy, and σ_h is the turbulent Prandtl number. The source term, S_h, in Eq. (4.3) consists of sources of enthalpy due to chemical reaction and radiation. The quantities with an overbar are the Favre-averaged values. The quantity with a tilde represents the Reynolds-averaged value. The prime denotes the fluctuation about the Favre average.The Reynolds stresses, $-\tilde{\rho}\overline{u_i' u_j'}$, in Eq. (4.2) must be modeled in order to solve it. The Bousinesq hypothesis is used to relate the Reynolds stresses to the mean velocity gradients as follows:

$$-\tilde{\rho}\overline{u_i' u_j'}=\mu_t\left(\frac{\partial \overline{u_i}}{\partial x_j}+\frac{\partial \overline{u_j}}{\partial x_i}\right)-\frac{2}{3}(\tilde{\rho}k+\mu_t\frac{\partial \overline{u_i}}{\partial x_i})\delta_{ij} \tag{4.4}$$

$$\mu_t=\tilde{\rho}C_\mu\frac{k^2}{\varepsilon} \tag{4.5}$$

where k and ε are the turbulent kinetic energy and its dispassion rate, respectively. The values of k and ε are obtained from the solution of their transport equations. For the standard k-ε model [20], k and ε transport equations are expressed as,

$$\frac{\partial}{\partial t}(\tilde{\rho}k)+\frac{\partial}{\partial x_i}\left(\tilde{\rho}\overline{u_i}k\right)=\frac{\partial}{\partial x_i}\left(\frac{\mu_t}{\sigma_k}\frac{\partial k}{\partial x_i}\right)+G_k-\tilde{\rho}\varepsilon \tag{4.6}$$

$$\frac{\partial}{\partial t}(\tilde{\rho}\varepsilon)+\frac{\partial}{\partial x_i}\left(\tilde{\rho}\overline{u_i}\varepsilon\right)=\frac{\partial}{\partial x_i}\left(\frac{\mu_t}{\sigma_\varepsilon}\frac{\partial \varepsilon}{\partial x_i}\right)+C_1\frac{\varepsilon}{k}G_k-C_2\tilde{\rho}\frac{\varepsilon^2}{k} \tag{4.7}$$

where $G_k=\mu_t\left(\frac{\partial \overline{u_j}}{\partial x_i}+\frac{\partial \overline{u_i}}{\partial x_j}\right)\frac{\partial \overline{u_i}}{\partial x_i}$, $C_1=1.44$, $C_2=1.92$, $C_\mu=0.09$, $\sigma_k=1.0$ and $\sigma_\varepsilon=1.3$.

As near wall boundary conditions, values of k and ε at the first grid node are obtained using semi-empirical formulae known as standard wall functions [21]. Wall functions are used to bridge the viscosity-affected region between the wall and the fully turbulent region.

The effect of turbulent fluctuations on the combustion is accounted for with an assumed-shape probability density function (PDF), the β-PDF [22, 23]. The discrete transfer radiation model (DTRM) [24, 25] is employed for the calculation of the radiation heat transfer. The assumption of gray radiation is acceptable for all inner surfaces of the furnace. The weighted-sum-of-gray-gases model [26, 27] is used to calculate the absorption coefficient. The chemistry model is based on the chemical equilibrium concept which assumes that the chemical reaction is rapid enough for chemical equilibrium to always exist at the molecular level is employed to specify the instantaneous thermo-chemical state of the combustion mixture. The liquid fuel injection is modeled using a discrete phase model. The turbulent dispersion of liquid fuel droplets and other forces on the liquid fuel phase are neglected because the liquid fuel droplets last for a very short period of time and exist only in a very small region near the inlet of the furnace. The mean NO concentration is obtained by solving its transport equation based on the flow field and combustion solution from the main combustion simulations. The temperature PDF approach [28] is used to account for the effect of turbulence on the NO formation.

4.3.2 Linear dynamic model of the furnace

Although the knowledge of the internal furnace variables are of interest in furnace design and analysis, these variables cannot be incorporated into the control system design process directly. From a control system point of view, it is more important to focus on input and output relations of the furnace. The furnace is modeled in this study using a three-input and two-output system as illustrated in Fig. 4.2. The input variables are the mass flux (mass flow rate per unit flow area) of the combustion air, m_{air}, and the temperature of the combustion air, T_{air}, at the furnace inlet, and the pressure head of the FGR fan, P_{fan}. The measurable output variables are the mole fraction of NO, y_{NO}, and the mass fraction of O_2, f_{O2}, at the furnace outlet.

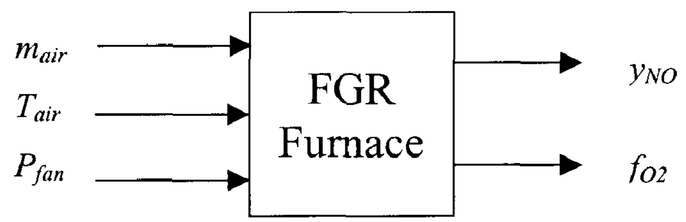

Figure 4.2 The input and output representation of the FGR furnace

It is important to note that the above variables are in the form of deviation from the values at the desired furnace operating condition. The relationships among these variables can be represented in terms of the transfer functions between appropriate inputs and the corresponding outputs.

The construction of these transfer functions requires the results from CFD simulations of the furnace. To obtain the linearized relationships among those input and output variables, low amplitude sinusoidal signals at different frequencies are added to the corresponding furnace inputs, and the resulting variations of the furnace outputs obtained by CFD simulations are recorded. Through proper analysis of these input and output values, the transfer functions between the furnace inputs and outputs are obtained by using least-squares based system identification techniques. Interested readers are referred to [29] for details. The transfer functions are shown as follows:

$$G(s)_{O2} = \frac{8.3875s^2 + 36.594s + 46.590}{s^5 + 3.1926s^4 + 27.868s^3 + 37.260s^2 + 78.147s + 10.000} \tag{4.8}$$

$$G(s)_{air\,mass} = \frac{-0.7532s^6 + 5.6356s^5 - 21.589s^4 + 423.76s^3 + 494.10s^2 + 2930.0s + 320.37}{s^6 + 4.3640s^5 + 62.070s^4 + 136.12s^3 + 402.91s^2 + 408.38s + 25.090} \tag{4.9}$$

$$G(s)_{air\,temp} = \frac{-23.6270s^3 - 133.77s^2 + 2398.2s + 20890}{s^4 + 39.556s^3 + 900.74s^2 + 3972.1s + 7478.8} \tag{4.10}$$

$$G(s)_{fan} = \frac{7.1681s - 63.801}{s^3 + 4.6133s^2 + 25.700s + 22.654} \tag{4.11}$$

where $G(S)_{O2}$ represents the relationship between the mass flux of the combustion air at the furnace inlet and the mass fraction of oxygen at the furnace outlet. $G(s)_{air\,mass}$ is the transfer function from the mass flux of the combustion air at the furnace inlet to the mole fraction of NO at the furnace outlet. $G(s)_{air\ temp}$ is the transfer function from the temperature of the input combustion air to the mole fraction of NO at the furnace outlet. $G(s)_{fan}$ is the transfer function between the pressure head of the FGR fan and the mole fraction of NO at the furnace outlet.

$$\begin{bmatrix} f_{O2} \\ y_{NO} \end{bmatrix} = \begin{bmatrix} G(s)_{O2} & 0 & 0 \\ G(s)_{air\,mass} & G(s)_{air\,temp} & G(s)_{fan} \end{bmatrix} \begin{bmatrix} m_{air} \\ T_{air} \\ P_{fan} \end{bmatrix}$$

It is important to point out that, since the mass fraction of the oxygen at the furnace output does not depend on the temperature of the combustion air or the pressure head of the FGR fan, the transfer functions $G(s)_{12}$ and $G(s)_{13}$ are zero. Therefore, there are four non-zero transfer functions that represent the input and the output variables of the furnace around the operating conditions.

4.4 Design of Feedback Control System

Although the desired operating conditions for the furnace with minimal NOx emission are determined using CFD simulations, a practical furnace is always subject to disturbances during its operation. In order to keep the furnace operating condition close to the designed ones, the furnace inputs have to be regulated continuously to reduce any deviations. The main objective of the controllers is to maintain the mass fraction of oxygen and the mole fraction of NOx at their designed values.

Even though the furnace is a multi-input and multi-output system, the non-dependence of the oxygen output from the combustion air temperature and the pressure head of the FGR fan has made the decoupled controller design possible. To be more precise, the oxygen feedback loop can be designed independent of that of the NO feedback loops. The measured oxygen level at the furnace outlet can be used to maintain the mass flow of the combustion air at a desired level, while also ensuring that other system variables such as the CO emission level satisfy the desired levels. The remaining two furnace inputs can then be used to further reduce the NO emission.

There are many control schemes that can achieve the intended control functions. One of the simplest and most popular controller structures is the PID type. Thus, the controllers with PID structure have also been selected for use in this work. The transfer function of a PID controller takes the following form:

$$G(s)=K_P+K_I/s+K_Ds \tag{4.12}$$

where K_P, K_I, and K_D are controller parameters. The input to the controller is the derivation between the desired and the measured furnace outputs; in this case, one is the oxygen and the other is NO. The controller generates appropriate signals to regulate the corresponding furnace inputs. Because there are three furnace input variables, the control system consists of three separate controllers. The overall structure of the control system is shown in Fig. 4.3. Due to the dynamic nature of the furnace from combustion air temperature and the pressure head of the FGR fan to NO output, derivative actions are not required. Therefore, the control system consists of one PID and two PI controllers. There are a total of seven parameters that need to be selected to achieve the desired dynamic performance.

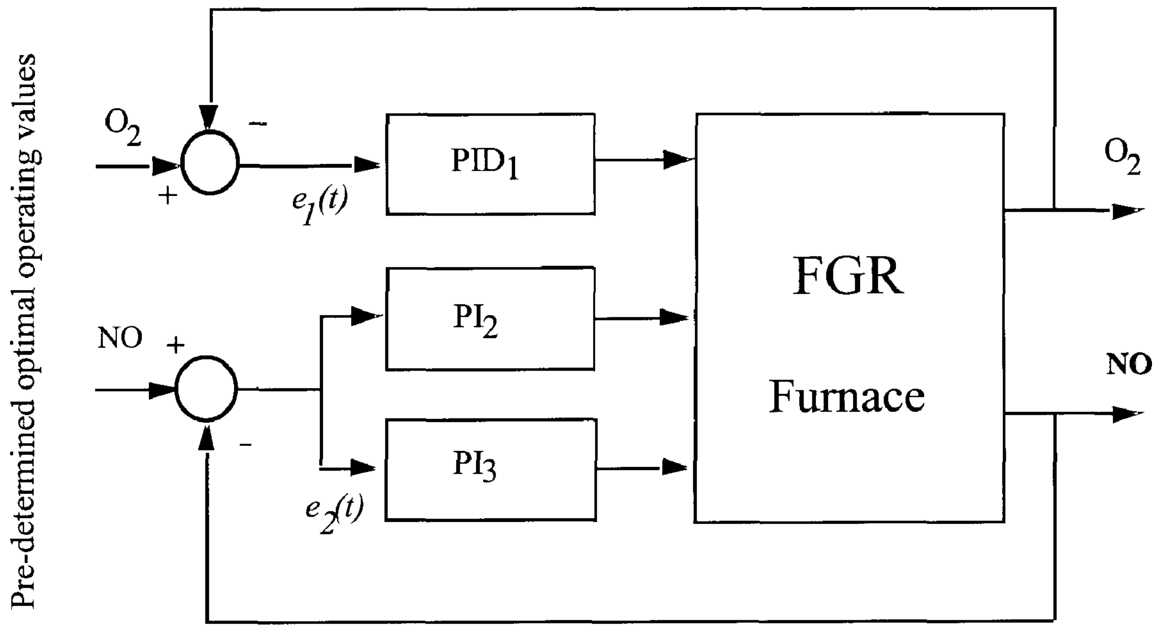

Figure 4.3 Configuration of the control system

These parameters in this study are chosen through an off-line nonlinear optimization technique based on simulated closed-loop system responses. The optimization problem can be formulated as follows:

$$\min(f(K_P, K_I, K_D)) = e_1^2(t_1) + e_1^2(t_2) + \cdots\cdots e_1^2(t_m)$$

$$\min(f(K_P, K_I)) = e_2^2(t_1) + e_2^2(t_2) + \cdots\cdots e_2^2(t_m) \tag{4.13}$$

where $e_1(t_i)$ and $e_2(t_i)$ represent the deviations of O_2 and NO from their desired value at time step i, respectively. Therefore, this optimization has a clear physical significance.

The resulting controller parameters are shown in Table 4.2. Even though the solution to the optimization process in Eq. (4.13) may not be globally optimal, the simulation results indicate that the designed control system performs satisfactorily. The step responses of the three closed-loop systems, which are generated with Simulink in MATLAB, are illustrated in Figs. 4.4-4.6. The results indicate that the feedback control system has excellent transient and steady state responses (less than 15% overshot and less than 1 second of 90% settling time). There is a negative response in Figure 4.5 at the rising time, which is mathematically caused by the transfer function and has no physical meaning. The performance of these controllers is evaluated again in the next section using results of full-scale CFD simulations of the furnace in next section.

Table 4.2 Parameters for the designed controllers

Transfer function	PID controller	K_P	K_I	K_D
$G(s)_{O2}$	PID_1	1.6143	0.2693	0.0795
$G(s)_{air\ temp}$	PI_2	0.4630	1.2894	0
$G(s)_{fan}$	PI_3	0.4784	0.5836	0

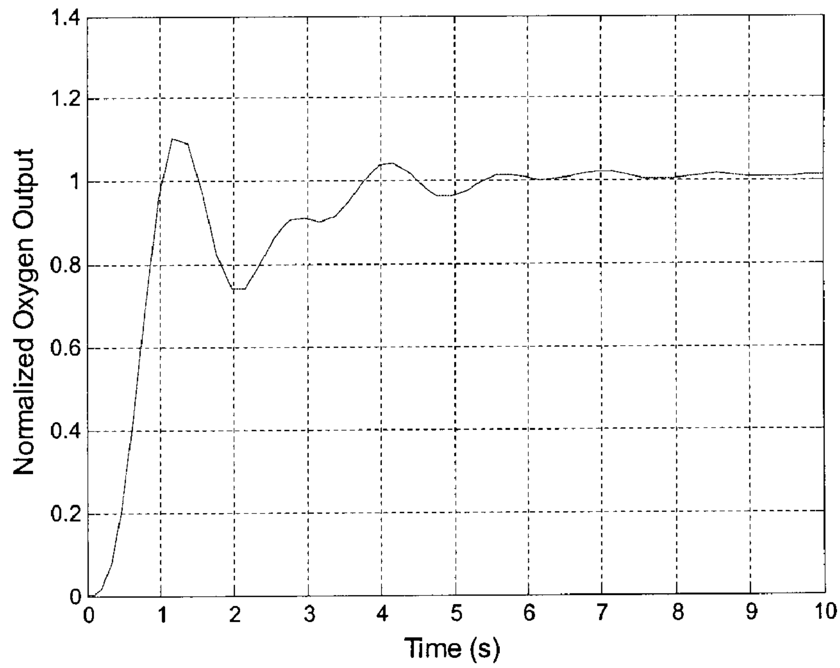

Figure 4.4 The step response of the O_2 output controlled by the controller PID_1

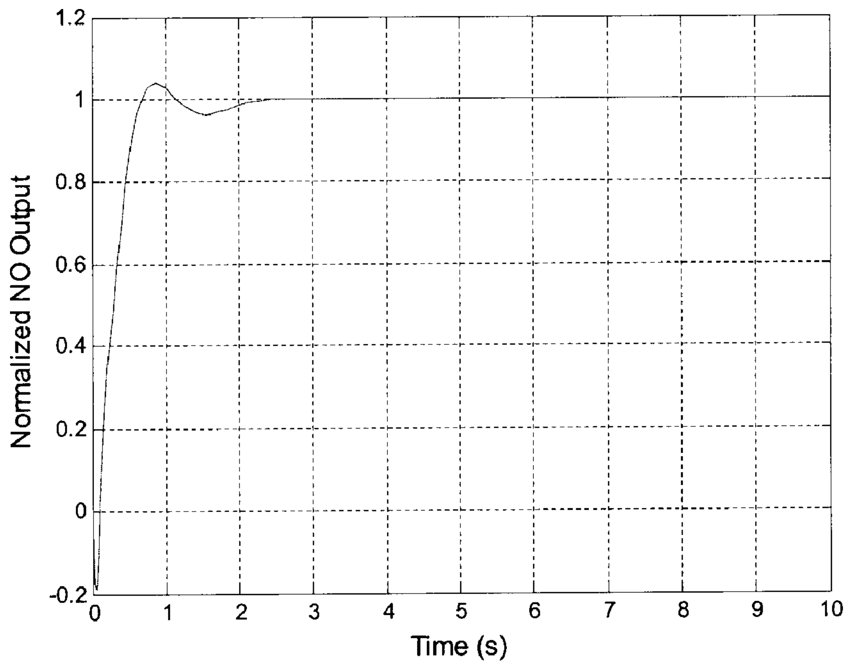

Figure 4.5 The step response of the NO output controlled by the controller PI_2

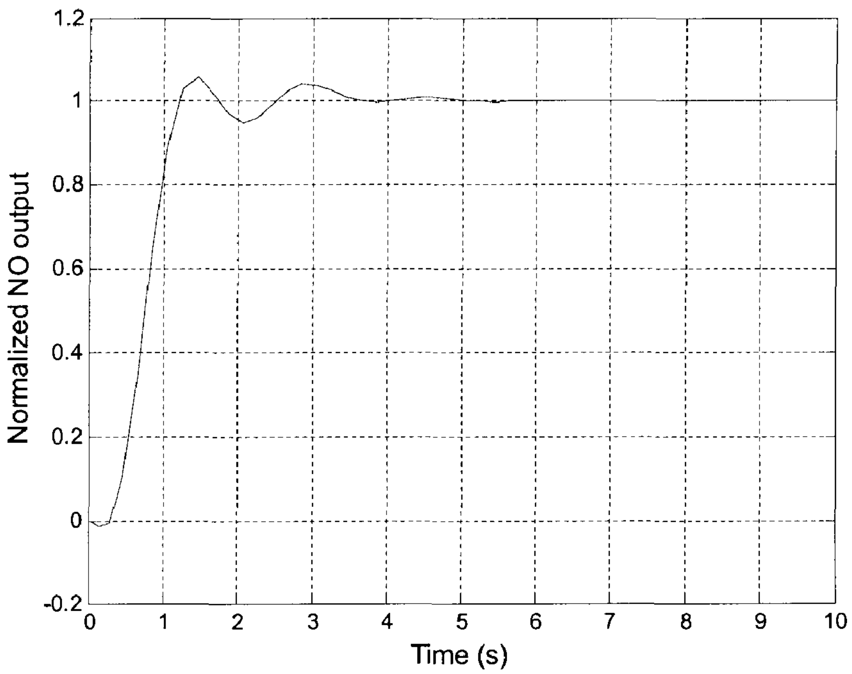

Figure 4.6 The step response of the NO output controlled by the controller PI_3

4.5 Validation of the Designed Control System by Nonlinear CFD Simulations

Difficulties in design of the controllers directly based on the nonlinear partial differential governing equations for the fluid flow, heat transfer and combustion process in the furnace necessitate that the design is carried out based on the linearized dynamic model for the furnace representations. Even though the simulations in the linear domain confirm the effectiveness of the designed controllers, it is still crucial to validate their performance in a full-scale nonlinear environment. This can be carried out by invoking the PID control algorithms within the CFD simulation process in a step-by-step manner. Specifically, the oxygen concentration and NO mole fraction at the furnace outlet are calculated at every time step. These output variables are then used to adjust the furnace input variables, i.e. the mass flow rate and the temperature of the combustion air, and the pressure head of the FGR fan, for the subsequent time step.

All the signals dealt with in Section 4.4 are deviations of the furnace variables from their desired values in the full-scope simulation. The inputs to the furnace are, therefore, the superposition of the control signals on the values at the desired operating conditions as follows:

$$(m_{air})_{inlet}=1.849+m_{air}=1.849+1.849\times pid_1(t_{K-1}) \qquad [Kg/m^2.s] \qquad (4.14)$$

$$(T_{air})_{inlet}=426.85+T_{air}=426.85+426.85\times pi_2(t_{K-1}) \qquad [\,^{\circ}C\,] \qquad (4.15)$$

$$(P_{fan})_{inlet}=33.8+P_{fan}=33.8+33.8\times pi_3(t_{K-1}) \qquad [Pa] \qquad (4.16)$$

In which,

$$pid_1(t_K)=1.6143e_1(t_K)+0.2693[E_1(t_{K-1})+e_1(t_K)\times\Delta t]+0.0795\frac{e_1(t_K)-e_1(t_{K-1})}{\Delta t} \qquad (4.17)$$

$$pi_2(t_K)=0.4630e_2(t_K)+1.2894[E_2(t_{K-1})+e_2(t_K)\times\Delta t] \qquad (4.18)$$

$$pi_3(t_K)=0.4784e_2(t_K)+0.5836[E_2(t_{K-1})+e_2(t_K)\times\Delta t] \qquad (4.19)$$

In which, $e_1(t_K)=0.05-f_{O2}(t_{K-1})/0.02674$

$e_2(t_K)=0.05-y_{NOx}(t_{K-1})/74.9$

E_1, E_2 are accumulated errors. Δt is the sampling interval. It is important to point out that the concept of time steps in CFD is different from that of the sampling interval in control system simulations. The time step in a CFD simulation is the discretizing step for the governing fluid flow and heat transfer equations. These steps must be small enough to obtain accurate numerical solutions for the partial differential equations. On the other hand, the sampling interval in a control system is the discrete time step that the controller takes to generate the control inputs to the furnace. The CFD time step is much smaller than the control sampling interval in most cases. Normally, there are several discretizing steps within a single sampling interval. However, for the sake of easy plotting, the plotting interval of the CFD simulation results is given as 0.2 seconds.

The results of the full scale CFD simulations are shown in Figs. 4.7 and 4.8 (asterisk lines) when subjected to a 5% change from the desired oxygen and the NOx levels. For comparison, the corresponding simulation results based on the linear dynamic models are also included (solid lines). It is noted that this 5% change is just a way to perturb the system and to examine the performance of the control systems in regulating the system response. In a practical situation, the perturbations can have many different origins.

It can be seen that the results from the full-scope nonlinear simulation are in good agreement with those obtained based on linear models. It is important to mention that in Figs. 4.7 and 4.8, the relative scale is chosen to zoom in the difference between the two simulation results. In fact, the steady state difference between the linear and nonlinear models is less than 5% for both outputs.

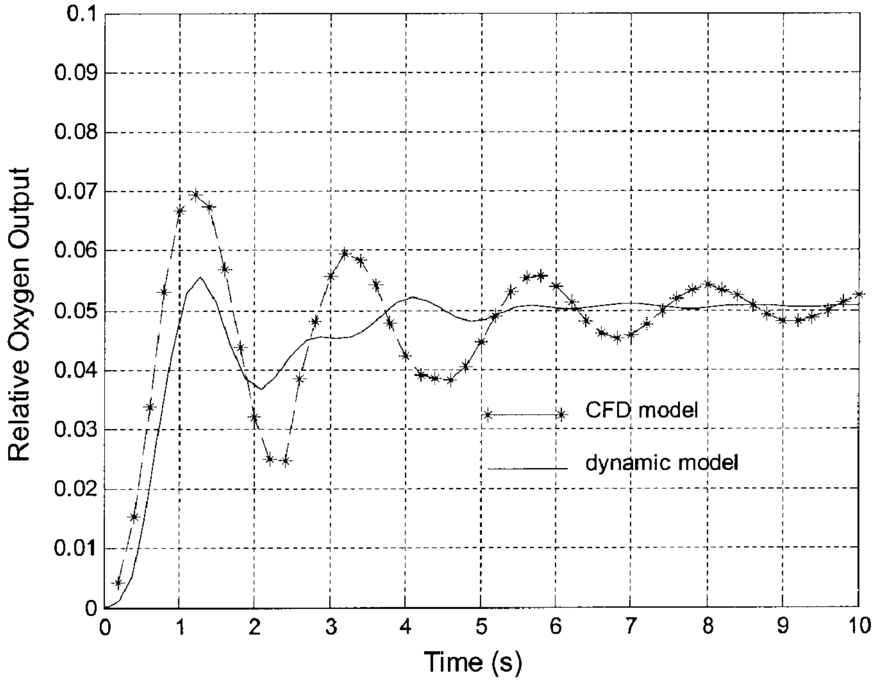

Figure 4.7 The step responses of O_2 based on the linear and the nonlinear CFD models

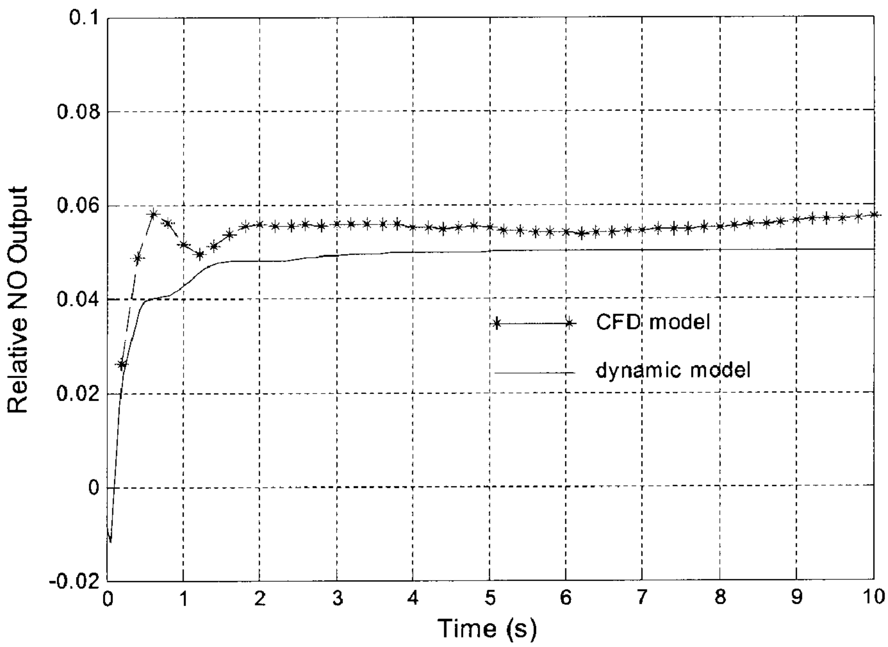

Figure 4.8 The step responses of NOx based on the linear and the nonlinear CFD models

There are several potential sources of error that contribute to the above discrepancies. The major source of error is in the derivation of the linear models based on the nonlinear CFD equations. Theoretically, the characteristics of a furnace are those of a space-dependent dynamic system. It is often known as "distributed parameter" system. The dimensions of its corresponding linear equation are of an infinite order. However, in the current study, the highest order of the linear system is only six. Hence, some dynamics of the furnace are left out in this modeling process.

The second source of error is due to the time dependent (and iteration dependent) numerical solutions of the CFD equations with PID controllers embedded between the sampling intervals. At the beginning of each iteration, newly generated controller outputs are incorporated as the new inputs to the furnace, which can cause potential numerical inconsistency between subsequent simulation steps.

The third source of error is probably due to the negligence of the influence of the mass flow rate of the combustion air to the NO using the decoupled control design strategy. Even though the design process has been significantly simplified without considering the coupling terms, such simplification does have some negative effects on the overall accuracy of the linear model simulations.

Finally, one has to face the fact that no matter how closely a nonlinear system can be represented by a linear one, it is always an approximation. A general observation from Fig. 4.7 indicates that the controller synthesizes system based on the linear models tends to overestimate the damping of the actual system.

In closing, it is also important to emphasize that the linear models and the corresponding controllers discussed here are for the specific furnace operating conditions. If the operating conditions change for any reason, the controllers will likely need to be modified as well. Fortunately, for industrial reheating furnaces, there are only a finite number of operating conditions that need to be considered. Therefore, it is possible to synthesize a set of feedback controllers that correspond to each operating condition, and to use gain-schedule techniques to switch among them.

4.6 Conclusions

NOx formation in an industrial FGR furnace has been analyzed in this paper. Recognizing the fact that NOx is particularly sensitive to the oxygen content of the combustion air input, a control strategy has been chosen to use the measured oxygen content in the exhaust to control the air mass flow of the combustion air at the furnace inlet first. The measured NOx signal is then used to adjust the temperature of the combustion air and the pressure head of the FGR fan to further reduce the amount of NOx at the exhaust. However, the design of such feedback controllers cannot be easily carried out in the nonlinear domain. This chapter shows that it is possible to represent the nonlinear characteristics of a FGR furnace by a multi-input and multi-output linear dynamic system around a certain chosen operating point in terms of transfer functions. Based on these transfer functions, a feedback control system can be synthesized to provide continuous regulation to the furnace so that the variation of the furnace never deviates significantly from the desired operating point in the presence of disturbances. A novel method based on off-line nonlinear optimization has been used to select the most appropriate controller parameters. Finally, the control system designed has been evaluated by embedding it to the CFD based nonlinear furnace simulations. Excellent results have been obtained.

References

1. Hayhurst, A. N. and Vince, I. M., 1980, "Nitric Oxide Formation From Nitrogen Flames", Progress in Energy and Combustion Science, vol. 6 (1), pp. 35-51.
2. Canadian Environment Quality Guidelines, 2003, www.ccme.ca, Page 7.
3. Jiang, Q., Zhang C., and Jiang J., 2004, "Reduction of Nitric Oxide in a Regenerative Industrial Furnace with the Addition of Methanol in the Fuel", Accepted by ASME J. of Energy Resources Technology.
4. Micklow, Folsom, B. A., Courtney, C. W., Heap, M. P., 1980, "Effects of LBG Composition and Combustor Characteristics on Fuel NOx Formation", Journal of Engineering for Power, Transactions ASME, vol. 102, no. 2, pp. 459-467.
5. Docquier, N. and Candel, S., 2002, "Combustion Control and Sensors: A Review", Progress in Energy and Combustion Science, vol. 28, pp. 107-150.
6. Muzio, L. J. and Quartucy, G. C., 1997, "Implementation NOx Control: Research to Application", Progress in Energy and Combustion Science, vol. 23, pp. 233-266.
7. Dupont, V., Porkashanian, M., Williams, A., and Wolley, R., 1993, "Reduction of NOx Formation in Natural Gas Burner Flames", Fuel, vol. 72, No. 4, pp. 497-503.
8. Lewandowski David A., 2000, "Design of Thermal Oxidation System For Volatile Organic Compounds", Lewis Publishers.

9. Falcitelli, M., Pasini, S., Tognotti, L., 2002, "Modelling Practical Combustion Systems and Predicting NOx Emissions with an Integrated CFD Based Approach", Computers and Chemical Engineering, vol. 26, NO. 9, pp. 1171-1183.

10. Adams, B., Cremer, M., Valentine, J., Bhamidipati, V., O'Connor, D., Vierstra, S., 2002, Letcavits, J.J., "Use of CFD Modeling for Design of NOx Reduction Systems in Utility Boilers", Proc.2002 International Joint Power Generation Conference, Scottsdale, AZ, United States, pp. 695-702.

11. Ilbas, M., Bowen, P., O'Doherty, T., and Syred, N., 1995, "CFD Modelling of a Low NOx Combustor Fired by Natural Gas and Gas-oil", Proc. Conference on Combustion & Emission Control, London, UK, pp. 189- 198.

12. Fiveland, W. A. and Laitham, C. E., 1995, "Use of Numerical Modeling in the Design of a Low-NOx Burner for Utility Boilers", Proc. Combustion Technologies for a Clean Environment, Ed. Maria da Graça Carvalho, pp. 111-130.

13. Zhang, C., Ishii, T., Hino, Y. and Sugiyama, S., 2000, "The Numerical and Experimental Study of Non-premixed Combustion Flames in Regenerative Furnaces", ASME Trans. Journal of Heat Transfer, 122, pp. 287-293.

14. Matsumura, S., Ogata, K., Fujii, S., Shioya, H. and Nakamura, H., 1995, "Modeling and DeNOx Control System for Fossil-fuel-fired Power Plants", Proc. IFAC Control of Power Plants and Power Systems, Cancum, Mexico, pp.19-24.

15. Delabroy, O., Haile, E., Lacas, F., Candel, S., Pollard, A, Sobiesiak, A., and Becker, H. A. , 1998, "Passive and Active Control of NOx in Industrial Burners", Experimental Thermal and Fluid Science, vol. 16, pp. 64-75.

16. www.k2bw.com, 2003.

17. Jiang, Q., Zhang, C. and Jiang, J., 2003, "A Sensitivity Study of NOx Emission to the Change in the Input Variables of a FGR Industrial Furnace", Proc. 2003 ASME Summer Heat Transfer Conference, July 21-23, Las Vegas, Nevada, USA, Fire and Combustion, Paper No. HT2003-47315.

18. Jones, W. P. and Whitelaw, J. H., 1982, "Calculation Methods for Reacting Turbulent Flows: A Review", Combustion and Flame, vol. 48, pp.1-26.

19. Peters, A. A. F. and Weber, R., 1995, "Mathematical Modeling of a 2.25 MW_t Swirling Natural Gas Flame, Part1: Eddy Break-up Concept for Turbulent Combustion; Probability Density Function Approach for Nitric Oxide Formation," Combustion Science and Technology, vol. 110-111, pp.67-101.

20. Launder, B. E. and Spalding, D. B., 1972, Lectures in Mathematical Models of Turbulence, Academic Press, London, England.

21. Launder, B. E. and Spalding, D. B., 1974, "The Numerical Computation of Turbulent Flow", Computer Methods in Applied Mechanics and Engineering, vol. 3, pp. 269-289.

22. Bilger, R. W., (1980) Turbulent Reacting Flows, Springer-Verlag, Berlin.

23. Janicka, J. and Kollmann, W., 1982, "A Numerical Study of Oscillating Flow Around a Circular Cylinder", Combustion and Flame, vol. 44, pp. 319-336.

24. Carvalho, M. G., Farias, T. and Fontes, P., 1991, "Predicting Radiative Heat Transfer in Absorbing, Emitting, and Scattering Media Using the Discrete Transfer Method", Fundamentals of Radiation Heat Transfer, ASME HTDS, vol. 160, pp. 17-26.

25. Shah, N. G., 1979, "A New Method of Computation of Radiant Heat Transfer in Combustion Chambers", Ph.D. Thesis, Imperial College of Science and Technology, London, England.

26. Siegel, R. and Howell, J. R., 1992, Thermal Radiation Heat Transfer, Hemisphere, Washington D.C.

27. Coppalle, A. and Vervisch, P., 1983, "The Total Emissivities of High-Temperature Flames", Combustion Flame, vol. 49, pp. 101-108.

28. Janicka, J. and Kollmann, W., 1982, "A Numerical Study of Oscillating Flow Around a Circular Cylinder", Combustion and Flame, vol. 44, pp. 319-336.

29. Jiang, Q., Zhang, C. and Jiang, J., 2003, "Dynamic Model Construction of an Industrial Flue Gas Recirculation (FGR) Furnace for Real-Time NOx Emission Control", Proc. 2003 International Joint Power Conference, Atlanta, Georgia, June 16-19, Fuel, Combustion and Emission Issues, Paper NO. IJPGC2003-40110.

CHAPTER FIVE

Conclusions

5.1 Summary of the Work

The objectives of this thesis are to construct on-line real-time dynamic feedback controllers to reduce the NOx emission in an FGR industrial furnace. At the beginning of this research, a simplified FGR furnace is designed whose dimensions, dynamical head of FGR fan, and arrangement of mixing box are optimized by the CFD results using code FLUENT. Based on the results at the steady state, the dynamic relationship between the inputs and outputs is investigated by imposing low amplitude sinusoidal signals of different frequencies at the inputs around the operating point. Then, the dynamic model is constructed by a linear least squares method in the form of a series of transfer functions which are validated by the CFD simulations. Finally, nonlinear optimization is used to obtain optimal PID controllers to minimize any deviations of the furnace from the operating point, and the controllers are validated by the results of CFD simulation.

5.2 Conclusions

The research in this thesis resulted in several conclusions given below:

- It is found that the combustion air and the recirculation flue gases should enter the mixing box in the same direction as the fuel injection. In this way, the flue gases and the combustion air can be mixed symmetrically before entering the furnace thus avoiding potential deviation of the flame in a particular direction inside the FGR furnace.

- FGR is an effective way to reduce NOx emissions. Compared with standard industrial furnaces emissions can be reduced by 87%.
- The NOx output is very sensitive to the direction of fuel injection. The simulation results show that direct injection (zero cone angle) is the best way, and most of the NOx is produced just behind of the far flame front.
- NOx will change dramatically if the combustion air fluctuates at very low frequency. The NOx output will triple the value at the operating point if the mass flow of combustion air makes only a 10% positive drift from the operating point. The NOx output is not as sensitive to the temperature of combustion air as it is to flow rate of the combustion air. A drift of the pressure head of the FGR fan will cause the least effect on the NOx output. The fluctuations of the flow rate and temperature of combustion air have little effect on the heat output from the furnace. Only the drift of flow rate of the combustion air will cause obvious fluctuations of excess oxygen at the outlet of the furnace.
- The dynamic model can be described as three inputs and two outputs. The inputs to this model consist of the pressure head of the FGR fan, the temperature of the combustion air, and the flow rate of the combustion air. The outputs are NOx mole fraction and excess oxygen ratio. All relationships between inputs and outputs can be described using the transfer functions except for the relationship between NOx and combustion air flow rate.
- The CFD simulations have been shown that the optimally designed PID and PI controllers can indeed minimize the deviation of the furnace from its desired operating conditions and hence can prevent any unnecessary NOx formation.

5.3 Future Work

- It is suggested to design and build an experimental FGR furnace with measurement equipments and control devices. More funds are needed to support this significant investigation.
- The control model needs to be validated against the experimental data.
- Fuel nozzles with different cone angles are to be tested for NOx emission release.
- The flue gases usually contaminate the detectors. It is suggested that a carbon filter be installed in the FGR pipe and the detectors be set just behind of the carbon filter.

APPENDIX A

Frequency Response Plots for Transfer Functions (3.12) – (3.15)

A.1 The Transfer Function $G(s)_{O2}$

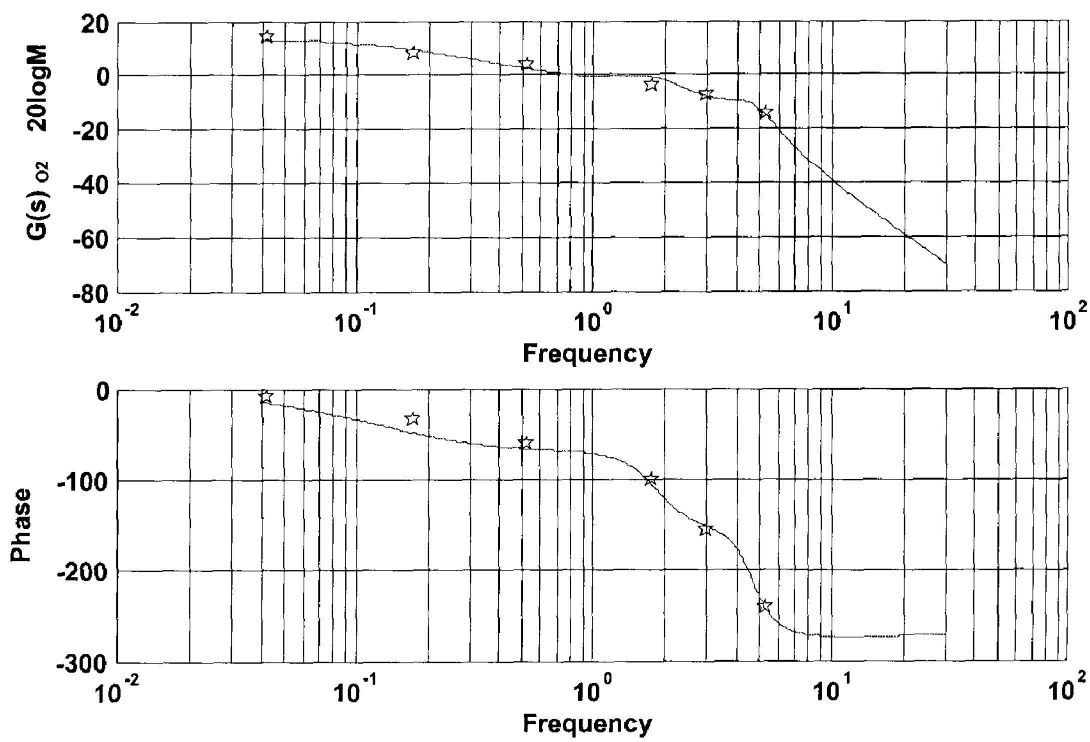

A.2 The Transfer Function $G(s)_{air\ mass}$

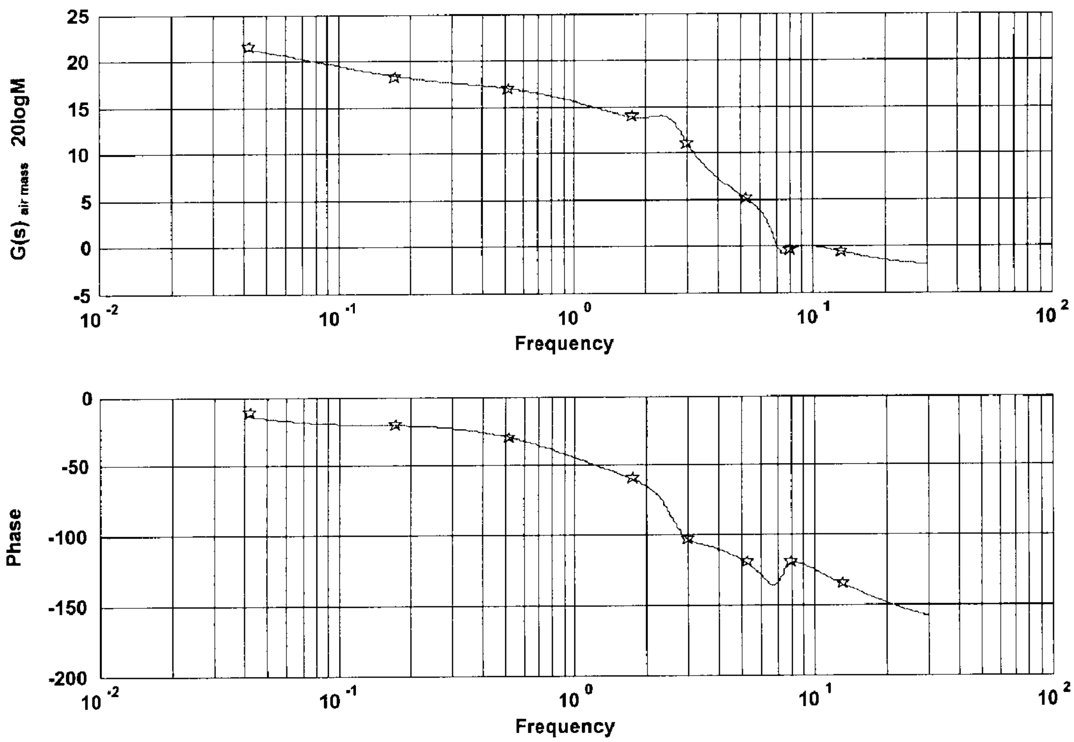

A.3 The Transfer Function $G(s)_{air\ temp}$

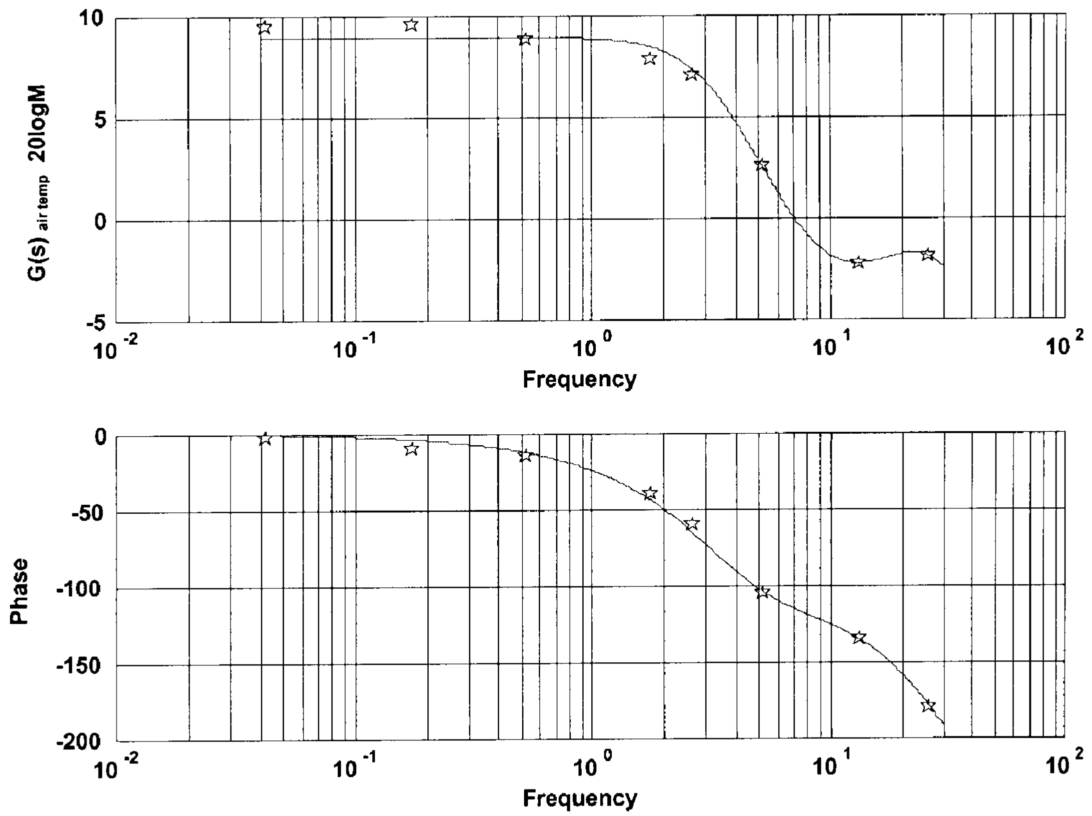

A.4 The Transfer Function $G(s)_{fan}$